# Thermal Decomposition of Pyrite and Limestone in Fluidized Bed( Dissertation_全文 )

AUTHOR(S):

Asaki, Zenjiro

# THERMAL DECOMPOSITION OF PYRITE AND LIMESTONE IN FLUIDIZED BED

by

ZENJIRO ASAKI

# THERMAL DECOMPOSITION OF PYRITE AND LIMESTONE IN FLUIDIZED BED

by

ZENJIRO ASAKI

Submitted to Kyoto University

in December, 1969

in Partial Fulfillment of the Requirements for

the Degree of Doctor of Engineering

## ABSTRACT

This research work was undertaken in order to study the rate of thermal decomposition of pyrite and limestone particles in the fluidized bed. The overall decomposition rate of these particles in the fluidized bed is thought to be affected by the fluidization quality and by the heat transfer characteristics of the fluidized bed.

Prior to the thermal decomposition study of pyrite and limestone particles, therefore, the mean, $\mu_c$, and the variance, $\sigma_c^2$, of the local particle concentration in the fluidized bed were studied by using a capacitance probe method. The particle concentration in the bubbles and the dense phases, $C_L$ and $C_U$, and the frequency, f, the vertical thickness, y, and the rise velocity, $u_b$, of bubbles were obtained from the traces on an oscillogram of the output signal from the probe. From the surveys on the regression of $\sigma_c^2$ upon $C_L$, $C_U$, f, y and $u_b$, it was revealed that $\sigma_c^2$ is a measure representing the nonuniformity in a fluidized bed in terms of the difference in particle concentration between bubble and dense phases.

The overall heat transfer coefficient between the reactor wall and the fluidized bed, $h_c$, was measured

at the temperature of 500° to 800°C. And the radiative heat transfer coefficient, $h_r$, was calculated by Stefan-Boltzmann's law. By subtracting $h_r$ from $h_c$, the film coefficient of heat transfer, $h_w$, was obtained. Measured $h_w$ was found to be in good coincidence with those by the previous workers obtained at lower temperatures where the radiative heat transfer can be omitted.

The particles of pyrite and limestone were decomposed in the fluidized bed. The fluidized bed temperature was maintained at 650° to 750°C for pyrite and at 825° to 875°C for limestone. From the batch process experiment, it was found that the overall decomposition rate of these particles is determined by the rate of heat transfer from the reactor wall to the fluidized bed. The film coefficient of heat transfer, $h_w$, estimated from the rate constant coincides well with that obtained in this work. It was clarified by the previous workers that the overall rate of thermal decomposition of limestone at a temperature below 900°C is controlled by the rate of interfacial reaction when a small amount of limestone is decomposed in a large space of furnace and this seems to be somewhat different from the result obtained in this work. The rate of heat transfer from the surroundings to the unit surface area of limestone particles present in fluidized bed was

found to be extremely lower than that in the case where a small amount of limestone is decomposed. This may be the reason why the heat transfer controlling model is applied to the thermal decomposition of limestone particles in fluidized bed at a temperature below 900°C.

For the continuous process experiment, two rate equations, Eqs. (4.19) and (4.22), were derived by assuming the complete mixing and the upward piston flow of the particles in the fluidized bed. In the thermal decomposition of pyrite, the flow rate of nitrogen gas was kept at about three times that of the minimum fluidization. The mean fraction of decomposed pyrite in the overflow deviates from Eq. (4.19) and it approaches to Eq. (4.22) at higher feeding rates of pyrite particles because of the possible segregation of particles at the surface of fluidized bed. On the other hand, this deviation becomes minor at lower feeding rates because the difference in the fraction decomposed between the bulk and the surface of fluidized bed is so trivial.

In the experiment of thermal decomposition of limestone, the flow rate of air was kept at a relatively higher value of 8.5 times that of the minimum fluidization. Eq. (4.19) was found to be satisfactory at higher feeding rates of limestone particles because the overflow pipe is buried within the bulk of fluidized

bed where the particles are completely mixed with each other. At lower feeding rates, on the other hand, the mean fraction of decomposed limestone in the overflow deviates from Eq. (4.19) because of the possible segregation of particles at the level of overflow pipe.

# TABLE OF CONTENTS

Table of contents (cont.)

Table of contents (cont.)

# LIST OF FIGURES

List of figures (cont.)

List of figures (cont.)

List of figures (cont.)

# LIST OF TABLES

## ACKNOWLEDGEMENTS

The author is very grateful to his thesis supervisor, Professor Yoshio Kondo, for the encouragement and counsel given throughout the course of this work.

The auther is also thankful to Mr. S. Yamazaki (Nippon Light Metal Co.), Mr. K. Harada(Nippon Light Metal Co.), Mr. M. Fukuda(Kobe Steel Making Co.), Mr. T. Nagase(Nippon National Railway), Mr. Y. Awakura (Graduate student, Kyoto University), Mr. Y. Fukunaka (Graduate student, Kyoto University) and Mr. S. Tagawa (Ube Industry Co.) for their earnest assistances provided in the experimental works of this study.

The appreciation of the author extends to Assistant Professor S. Nishimura for his thoughtful encouragement and help during this investigation.

The author expresses his thanks to Mr. M. Satake and Miss M. Watanabe for their help in drawing many illustrations and in preparing the manuscript. Thanks are also extended to his wife, M. Asaki, for her job of typing this thesis.

# CHAPTER 1 INTRODUCTION

The first commercial fluidized bed reactor was built in Germany in 1921 (1). It was installed in the Winkler gas generator. Since then, the fluidizing technique has been widely applied to the various industrial processes, such as classification and drying of the particles, catalytic cracking of petroleum, synthesis of hydrocarbon, and so on.

In metallurgical industry, the fluidizing technique is being applied to the roasting of sulfide ores (2,3), to the reduction of oxide ores (4,5), calcination (14,15), and so on. Previously, sulfide ores were roasted in the flash roasters and in the multiple hearth roasters such as Herreshoff and Wedge furnaces. However, these roasters were replaced and more than 60 fluidized bed roasters are being operated in Japan (6). The features of the fluidizing technique mentioned below are thought to cause this evolution; its extensive adaptability exploits various applications in the chemical and metallurgical industries. On the other hand, however, there still remains many problems to be clarified in order to better understand and to improve the fluidizing

techniques.

Features of fluidized bed reactor in metallurgical processes where solid particles are treated can be summarized as follows:

1) Fluidization permits the ready charge and discharge of bed with solid particles. This enables the continuous operation and reveals a possibility of controlling the residence time of solid particles in the bed.

2) Because of the high effective thermal conductivity in the bed and of the high heat transfer coefficient between the reactor wall and the bed, temperature profile throughout the bed becomes much more uniform than that realized in the fixed bed. And thus, this feature made it possible to control the bed temperature precisely even when a large amount of heat is evolved or consumed during the reaction occurring in the fluidized bed.

3) Since the solid particles of smaller size can be treated with higher efficiency, the fluidized bed is profitable for the treatment of flotation concentrate.

4) The size of particles fed to the fluidized bed is usually smaller than that fed to the fixed bed type reactors, and consequently, the effective surface area of particles is larger and the resistance

to heat- and mass-transfer within particles can be omitted. This may also be profitable for the chemical reactions.

And, on the other hand, the following items can be mentioned which are sometimes thought to be disadvantageous for the fluidized bed.

1) Because of the vigorous agitation of particles within the bed, complete mixing of particles can be realized in a well-fluidized bed. Under this condition, some of the unreacted particles happen to be included in the overflow and some of the reacted particles happen to remain in the bed for a long time. This may lower the overall fraction of reacted product in the overflow.

2) When the fine particles are fed into the fluidized bed, an amount of particles is often carried out of the bed by fluidizing gas. This is known as elutriation. In order to avoid this elutriation, some installations are required for recovering the fine carry-over. The residence time of these fine particles carried out by the gas is much shorter than that of the overflow particles. This may also lower the overall fraction of reacted product.

Thus, it is indispensable for designing the fluidized bed reactor, for obtaining the optimum conditions of operation and for improving the technique, to study

not only the reaction rate and the heat- and mass-transfer rate but also the behavior of the particles in the bed.

Among the chemical reactions carried out in the fluidized bed reactor in metallurgical industry, oxidation, reduction and thermal decomposition of mineral particles are thought to be important.

The purpose of this work is to study the thermal decomposition. Thermal decomposition of solid particles is represented by,

$$(\text{Solid}) \longrightarrow (\text{Solid}) + (\text{Gas})$$

It is usually an endothermic reaction. This reaction is composed of the following three sequential steps:

1) Transport of heat from the surroundings to the reaction interface within particles.
2) Thermal decomposition which occurs at the interface.
3) Escape of the gas evolved at the interface to the surroundings.

Rate determining step of this reaction may be varied by the conditions. In the case that the thermal decomposition of the particles is carried out at higher temperature and the decomposed product is porous, the reaction rate at the interface is relatively high because of its higher activation energy, and the diffusion rate of gas evolved at the interface through the

shell of decomposed product is rather high because of its porosity. Consequently, it is reasonable to presume that the overall rate of the decomposition is mainly controlled by the rate of heat transfer from the surroundings to the interface. It is of basic interest in pyro-metallurgical processes to clarify the overall rate of the thermal decomposition of particles in the fluidized bed.

Pyrite and limestone particles were chosen as the feed for the fluidized bed. Interest in the thermal decomposition of pyrite with inert gas stream increased recently, because of possible elimination of arsenic from pyrite in processing highly purified iron oxide pellets and of producing elemental sulfur from pyrite instead of sulfuric acid. The thermal decomposition of limestone, on the other hand, has been studied by many workers (9-13) and basic information on its mechanism is easily available. From this, the thermal decomposition study of limestone particles in the fluidized bed is destined not only to study its kinetics but also to clarify the characteristics of high temperature fluidized bed.

It is known that the enthalpy changes in the thermal decomposition of pyrite and limestone are about 37 and 43 kcal/mole, respectively, and that the decomposed products of these materials are very porous (7-9).

And thus, the overall rate of thermal decomposition of these solid particles at higher temperature is revealed to be determined by heat transfer rate from the surroundings to the decomposing interface within particles (8,9).

When the fluidization tube is heated from the outside and the heat is supplied to the bed through the reactor wall, the heat transfer rate between the reactor wall and the fluidized particles in the bed plays a very important role. Moreover, this heat transfer rate is affected by the fluidization characteristics. Therefore, the fluidization characteristics and the heat-transfer rate are indispensable for understanding the endothermic reaction in a fluidized bed whose overall rate is controlled by heat-transfer rate. This is the reason why the fluidization characteristics and the heat transfer rate were studied in this work prior to the kinetic studies on the thermal decomposition of pyrite and limestone perticles in a fluidized bed.

Fluidization quality is a complex function of concentration and properties of the fluidized particles, bed geometry, and properties and flow rate of the fluidizing gas. In Chapter 2 of this paper, mean, $\mu_c$, and variance, $\sigma_c^2$, of local particle concentration in a fluidized bed were chosen as the measures of fluidization quality and they were studied in relation to the fluidizing conditions, such as the bed height and the

flow rate of gas. $\sigma_c^2$ is a measure representing the nonuniformity of local particle concentration in the bed. The correlationship between $\sigma_c^2$ and fluidization characteristics, such as, the size, the frequency, and the rise velocity of gas bubbles and the particle concentration in the bubble and dense phases were also pursued.

In Chapter 3, the heat transfer coefficient between the reactor wall and the fluidized bed was studied at the temperature range of 500° to 800°C. Although many works have been published on the heat transfer phenomena in the fluidized bed, most papers pursued the heat transfer coefficient at lower temperature below 200°C where the radiative mechanism of heat transfer can be omitted in comparison with those by conduction and convection. Heat transfer coefficient obtained in this work was compared with those measured at lower temperatures. And the correlationship between the heat transfer coefficient and the fluidization characteristics studied in Chapter 2 was also discussed.

Finally, in Chapters 4 and 5, the thermal decomposition rate of pyrite and limestone particles in a fluidized bed was studied. Assuming that the heat transfer rate from the surroundings to the fluidized particles controls the overall decomposition rate, the rate equations for the batch process and for the

continuous process were derived. These rate equations were evaluated by comparing them with the experimental results. And the heat transfer coefficient estimated from the rate constant was compared with that obtained in Chapter 3. Moreover, the decomposition rate of limestone in the fluidized bed was discussed by comparing it with the results obtained by the previous workers.

## References to Chapter 1


1) Leva,M.: "Fluidization", 1959, p. 5, McGraw-Hill Book Company Inc., New York

2) Takagi,Y., T.Komiyama, I.Kagihara and K.Tarumi : Kagaku Kikai (Japanese), 1952, vol. 16, No. 5, pp. 138-148

3) Yagi,S., D.Kunii, K.Nagano and H.Mineda : Kagaku Kikai (Japanese), 1952, Vol. 16, No. 9, pp. 288-293

4) Kivnick,A. and N.Hixson : Chem. Eng. Progr.,1952, Vol. 48, No. 8, pp. 394-400

5) Feinman,J. and T.D.Drexler : A.I.Ch.E.Journal, 1961, Vol. 7, No. 4, pp. 584-587

6) Minamoto,K. and H.Manabe : Ryusan (Japanese), 1967, Vol. 20, No. 11, pp. 255-264

7) Schwab,G.M. and J.Philinis : J. Am. Chem. Soc., 1947, Vol. 69, pp. 2588-2596

8) Nishihara,K. and Y.Kondo : Mem. Fac. Eng., Kyoto Univ., 1958, Vol. 20, pp. 258-306

9) Satterfield,C.N. and F.Feakes : A.I.Ch.E.Journal, 1959, Vol. 5, No. 1, pp. 115-122

10) Furnas,C.C. : Ind. Eng. Chem., 1931, Vol. 23, No. 5, pp. 534-538

11) Edmond,P.H., I.B.Cutler and M.E.Wadsworth : J.Am. Cer.Soc., 1958, Vol. 41, No. 1, pp. 70-74

12) Narsimhan,G. : Chem. Eng. Sci., 1961, Vol. 16, pp. 7-20

13) Hashimoto,H. : Kogyo Kagaku Zasshi (Jananese), 1961, Vol. 64, No. 7, pp. 1162-1169

14) Leva,M. : "Fluidization", 1959, p. 10, McGraw-Hill Book Co., Inc., New York

15) Grimmett,E.S. : A.I.Ch.E.Journal, 1964, Vol. 10, No. 5, pp. 717-722

# CHAPTER 2 PARTICLE CONCENTRATION AND THE NONUNIFORMITY IN FLUIDIZED BED

## 2.1 Introduction

It was clarified by many research works (1-3) on the gas fluidized bed that the bulk of excessive gas stream above its minimum fluidization passes through the bed in the form of bubbles and that the fluidized bed is essentially composed of two phases, bubble and dense phases. This nonuniformity of fluidized bed affects the rate and mechanism of heat- and mass-transfer and of chemical reaction occurring in the bed. It is also recognized that the movement of particles in the bed is chiefly caused by the ascending bubbles through the bed (5-7). Many of the recent works were directed to the study on the behavior of bubbles, such as their size, rise velocity and frequency, particle concentration in bubble and dense phases and cross-flow of gas and solid particles between the two phases (2-7).

Behavior of particles in a fluidized bed is thought to affect the rate of heat transfer to the particles. Thus, the overall rate of reaction, such as thermal decomposition, which is usually controlled by the heat transfer rate, is affected by the fluidizing conditions, such as bed height, particle size, flow rate of gas and so on. However, many reports which concentrated on the behavior of bubbles limited the local movement of particles around a single bubble (7-11). And reports on the overall movement of particles in the fluidized bed are scarcely available. (19)

Some of the earlier works pursued the correlationship between the nonuniformity of fluidized bed and the fluidizing conditions ; Morse and Ballou (12) measured the local particle concentration in a fluidized bed by means of the capacitance probe method and calculated the uniformity index proposed by themselves. Their uniformity index was defined in a form of,

$$\text{uniformity index} = \frac{\text{variation in density}}{\text{frequency of density fluctuation}} \times 100$$

Variation of density in this equation was calculated by measuring the area between the curve and a base

line representing the average density on a oscillogram and by dividing this area by the average density. They studied the correlationship between the uniformity index and the fluidizing conditions, such as particle size distribution, flow rate of gas, bed height and type of distributor. Shuster and Kisliak (13) obtained the same uniformity index by measuring the pressure fluctuation across the horizontal section of fluidized bed by using a thin flat aluminum diaphragm to which wire strain gauges were attached. Dotson (14) also discussed the nonuniformity of fluidized bed by using similar index which was obtained by measuring the local particle concentration in the bed. Although these uniformity indices proposed by different workers can be applied to the qualitative evaluation of nonuniformity in fluidized bed, correlationship between these indices and the fluidization charactristics, such as the behavior of bubbles and the particle concentration in bubble and dense phases, could not be obtained in a clear form.

The local particle concentration in a fluidized bed varies with time and it can be represented by two measures, its mean and variance. The latter measure of particle concentration is proposed to represent the nonuniformity of fluidized bed. It is intended in

this work, therefore, to measure the mean and variance of local particle concentration in a fluidized bed, and to correlate them with the fluidizing conditions of bed height and flow rate of gas. Efforts are also directed to combine these measures with fluidization characteristics which include the size, rise velocity and frequency of bubbles and the particle concentration in bubble and dense phases in the fluidized bed.

## 2.2 Experimental

### 2.2.1 Apparatus

Fig. 2.1 demonstrates a schematic illustration of the fluidization apparatus. The fluidization column was made of 106 mm I.D. and 1218 mm long transparent Panlite resin tube. The distributor consists of a 300-mesh brass screen sandwitched between two 1.0 mm thick aluminum plates perforated with 1.0 mm D. holes spaced on a 7.0 mm trianglar pitch. The flow rate of air is metered through rotameters or through an orifice meter.

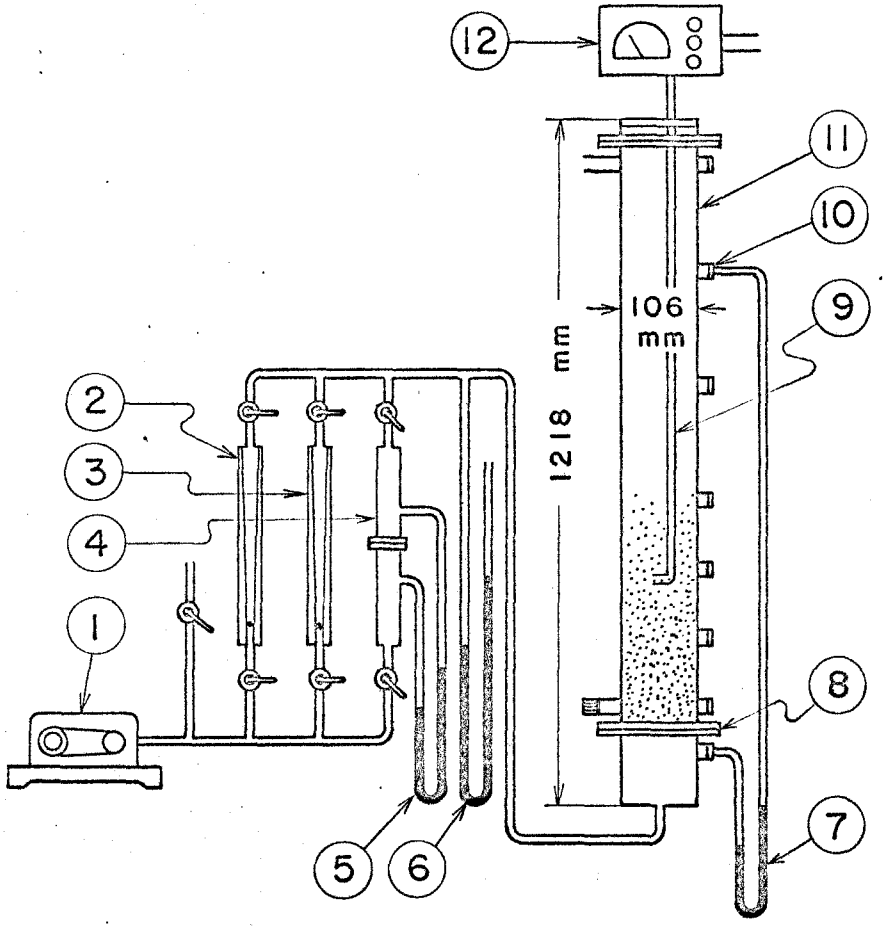


1. Two-impeller type rotary blower
2. Rotameter ( 40-200 $cm^3/sec$ )
3. Rotameter (200-1000 $cm^3/sec$)
4. Orifice meter (1000-5000 $cm^3/sec$)
5. 6. 7. Manometer
8. Distributor
9. Probe
10. Pressure tap
11. Fluidization tube
12. Oscillator and detector

Fig.2.1 Apparatus

Details of capacitance probes are shown in Fig. 2.2. The tips of lower and upper probes were designed to be separated 24 mm from each other. The tips are essentially 1.5 mm D. brass wire condenser and their cross-sectional areas are sufficiently small so as to minimize the disruption of the fluidized bed in the vicinity. By means of an oscillator and detector circuit shown in Fig. 2.3, the change of capacitance of the probes are linearly converted into D.C. signals and their traces on a 2-channel synchroscope are filmed. The scanning speed of the synchroscope was chosen at 0.1 second per cm. The D.C. signal is also transmitted to an integrator and a vacuum tube thermocouple to measure their mean and variance, respectivily. The time constant of the integrator was chosen at 10 seconds.

### 2.2.2 Material

Spherical glass beads of two different sizes were used as fluidized material. Most of the measurements were performed on the glass beads whose size distribution and physical properties are summarized in Fig. 2.4 (A). The size distribution of other glass beads is illustrated in Fig. 2.4 (B).

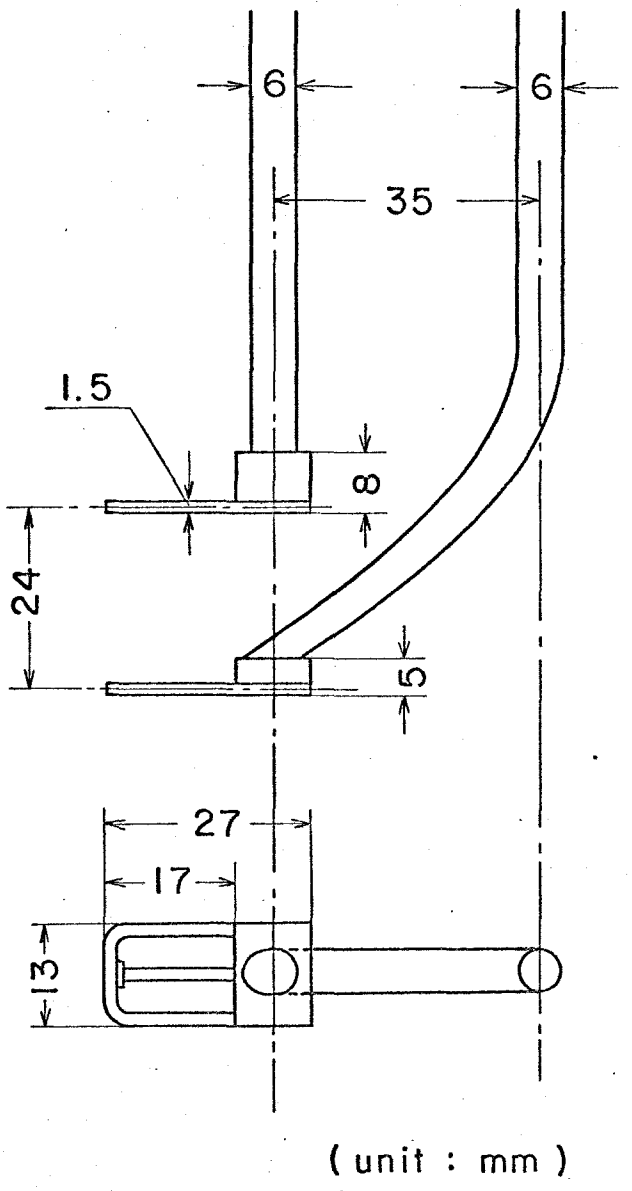


Fig. 2.2 Tips of capacitance probe

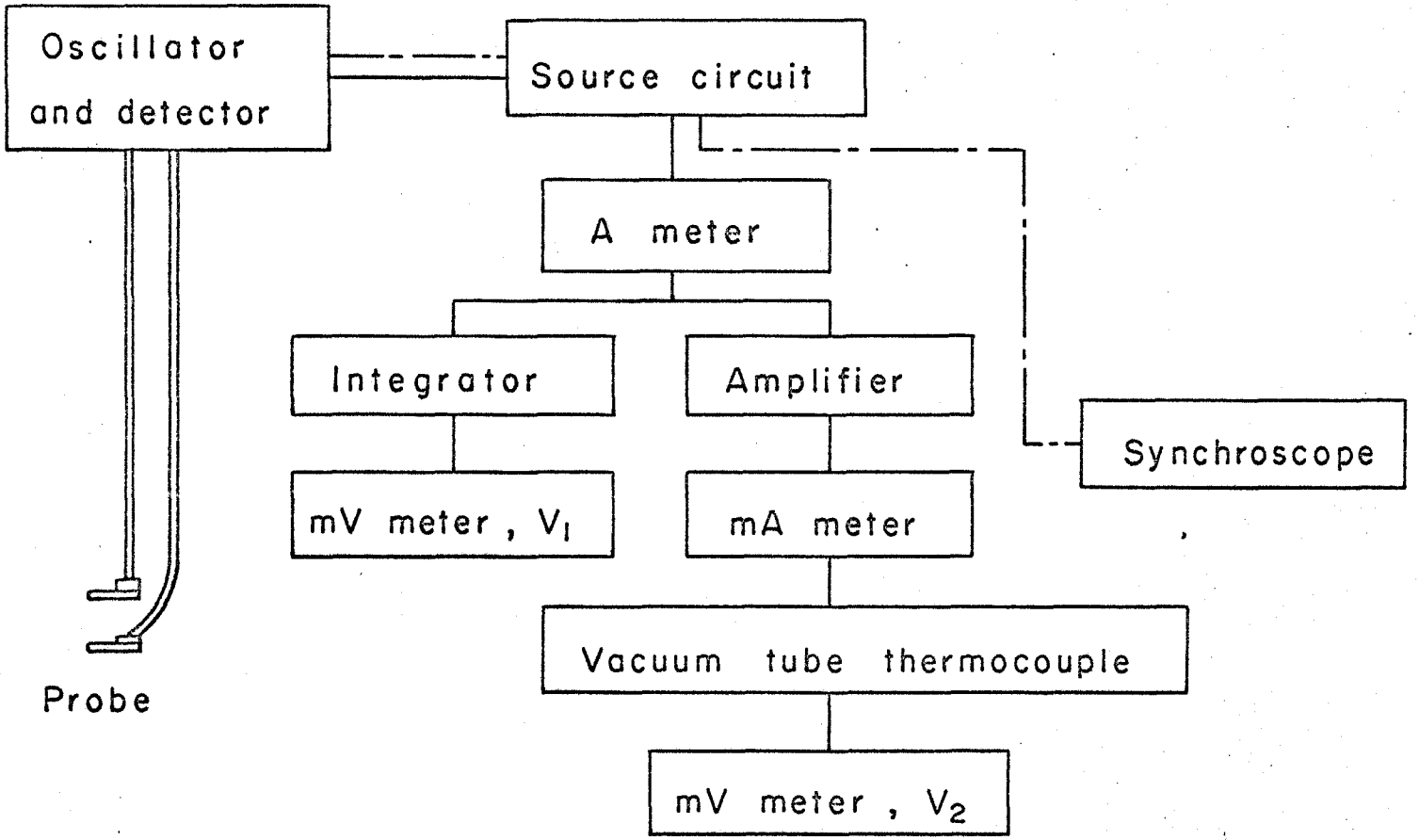


Fig. 2.3 Block diagram of circuit

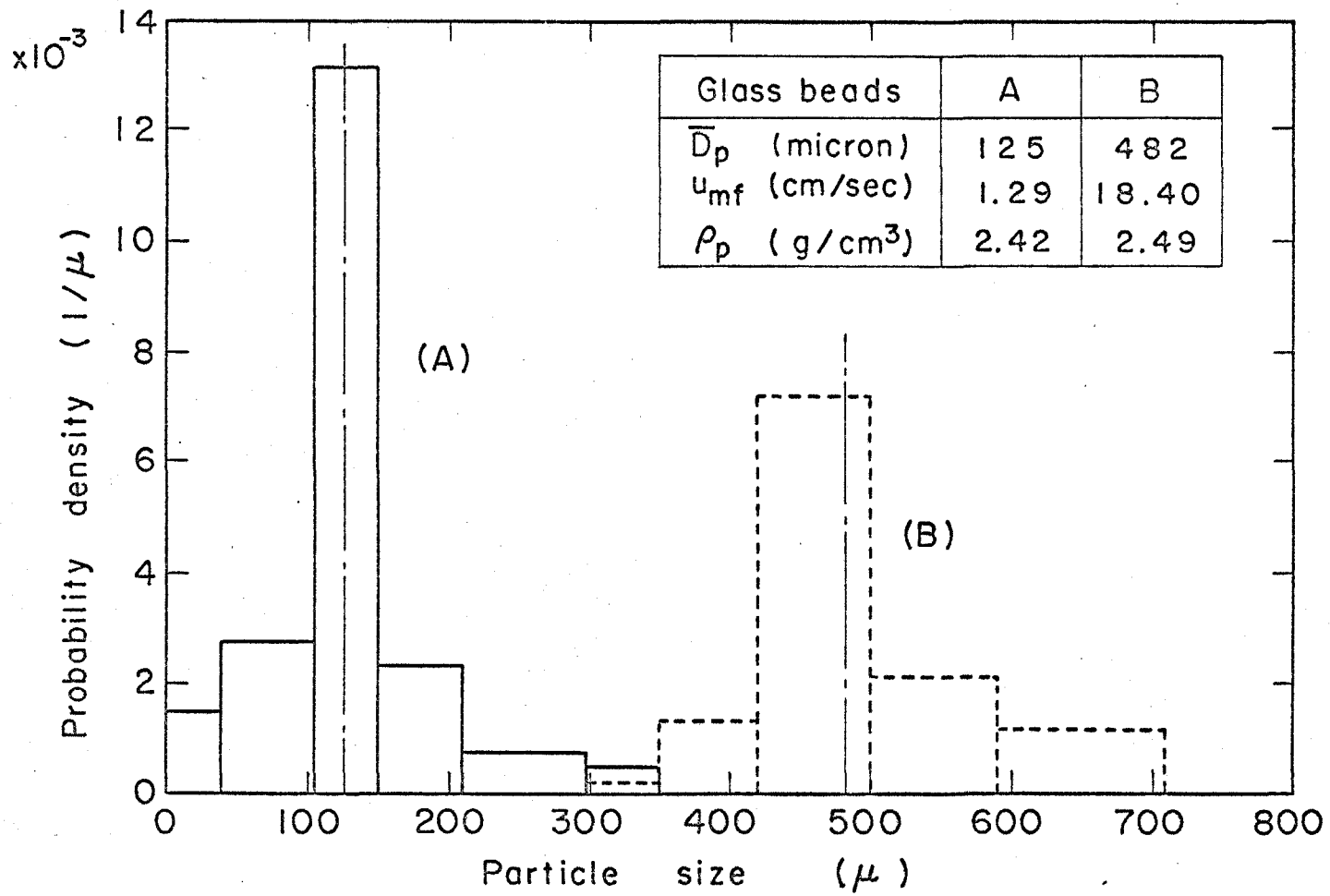


Fig. 2.4 Size distribution and physical properties of glass beads

### 2.2.3 Measures representing the fluidization characteristics

Mean, $\mu_v$, and variance, $\sigma_v^2$, of the D.C. signal, v, are defined by the following equations.

$$\mu_v = \frac{1}{\theta}\int_0^\theta v\,d\theta \tag{2.1}$$

$$\sigma_v^2 = \frac{1}{\theta}\int_0^\theta (v-\mu_v)^2 d\theta = \frac{1}{\theta}\int_0^\theta v^2 d\theta - \mu_v^2 \tag{2.2}$$

$\mu_v$ in Eq. (2.1) is obtained as output voltage, $v_1$, from the integrator. The first term on the right-hand side of Eq. (2.2) is obtained as output voltage, $v_2$, from the vacuum tube thermocouple. Mean, $\mu_c$, and variance, $\sigma_c^2$, of particle concentration in dimensionless form are calculated as $\mu_v$ and $\sigma_v^2$ divided by $\mu_s$ and $\mu_s^2$, respectively;

$$\mu_c = \frac{\mu_v}{\mu_s} \tag{2.3}$$

$$\sigma_c^2 = \frac{\sigma_v^2}{\mu_s^2} \tag{2.4}$$

where $\mu_s$ is the output voltage from the integrator at zero air velocity.

An example of oscillogram of the signals from the detector is shown in Fig. 2.5. Peaks in these osillograms represent the passage of bubbles through the probe tip. The average peak and valley heights of traces

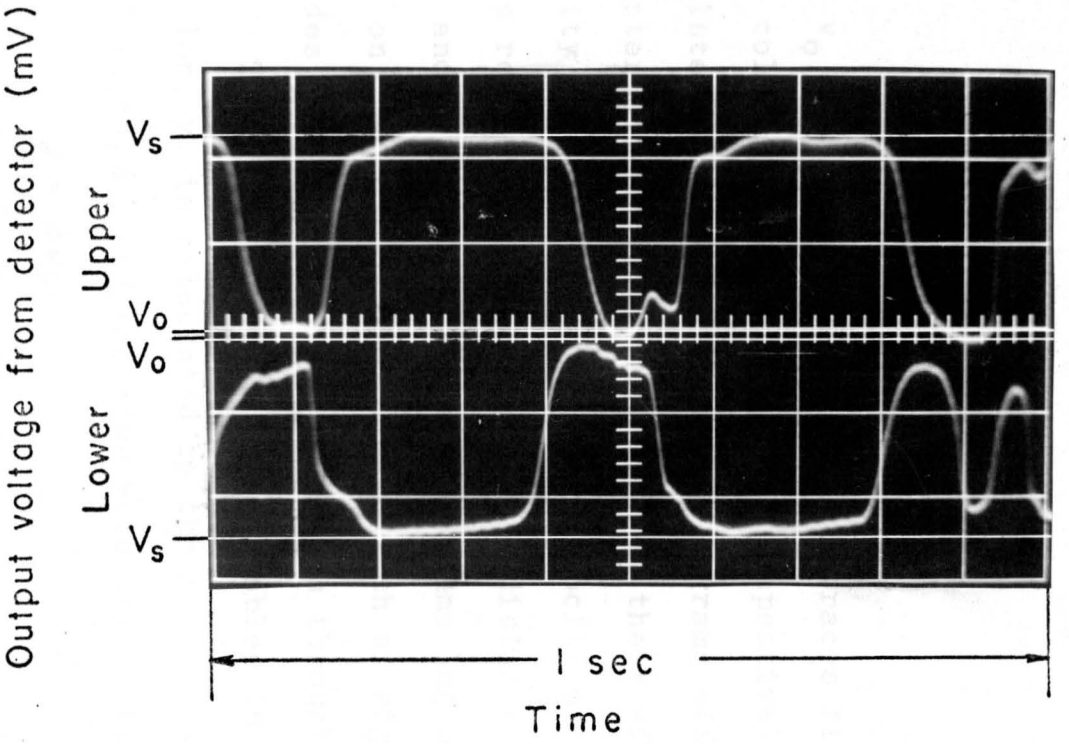


Glass beads : A , u = 11.34 cm/sec

$L_c / D_t$ = 1.0 , Probe height = 27.0 cm

Fig. 2.5 An example of oscillogram

are represented by $v_L$ and $v_U$, respectively, and they are converted into dimensionless particle concentrations by,

$$C_L = \frac{v_L - v_o}{v_s - v_o} \tag{2.5}$$

and

$$C_U = \frac{v_U - v_o}{v_s - v_o} \tag{2.6}$$

where $v_o$ and $v_s$ are the heights of traces filmed on empty column and on settled bed, respectively.

Interpretation of these osillograms offers the characteristics of bubbles, such as their size, rise velocity and frequency. Rise velocity of bubbles, $u_b$, is represented by the ratio of distance between lower and upper probes to average time lag of signal waves on the osillogram. The width of signal wave provides the passing time of bubbles through the probe tip. The average thickness of bubbles in vertical direction, y, is calculated by the average width of signal waves, $\delta$, and the rise velocity of bubbles, as,

$$y = \delta u_b \tag{2.7}$$

The frequency of bubbles, f, is determined by counting the number of signal waves and dividing them by the time elapsed.

### 2.2.4 Experimental conditions

The bed height and flow rate of air were chosen as the independent factors. The levels of these factors are listed in Table 2.1. Effects of particle size were also partially tested.

Table 2.1 The factors and their levels at which experiments were carried out

| | |
|---|---|
| Glass beads A | ($\bar{D}_p$= 125$\mu$, $u_{mf}$= 1.29 cm/sec) |
| Relative bed height: | $L_c/D_t$= 1.0, 2.5, 4.0 (-) |
| Air velocity | : u = 1.70, 3.40, 5.67, 11.34,20.86, 28.91, 40.14 (cm/sec) |
| Glass beads B | ($\bar{D}_p$= 482$\mu$, $u_{mf}$= 18.40 cm/sec) |
| Relative bed height: | $L_c/D_t$= 2.0, 3.0 (-) |
| Air velocity | : u = 22.68, 27.44, 31.75, 43.65 (cm/sec) |

### 2.2.5 Experimental procedure

The fluidization column was charged with a prescribed amount of glass beads and the height of the

settled bed, $L_c$, was measured by decreasing gradually the flow rate of air to zero from a flowing rate above its minimum fluidization velocity. Prior to making a run, the electric circuit shown in Fig. 2.3 was energized and allowed to be warmed up. Output voltages of the integrator and the vacuum tube thermocouple were then adjusted to zero with the probe tip placed above the bed surface. A prescribed amount of air was blown in and the probe tip was immersed into the bed. Output voltages of integrator and vacuum tube thermocouple, $v_1$ and $v_2$, were measured five times at 60 seconds' intervals, and their means were used to calculate $\mu_v$ and $\sigma_v^2$ shown in Eqs. (2.1) and (2.2). On the other hand, traces on 2-channel synchroscope were filmed three times at 30 seconds' intervals from which $C_L$, $C_U$, $u_b$, y and f were obtaind.

$\mu_s$ was measured by placing the probe tip 5 cm below the surface of settled bed which was established after gradually decreasing the flow rate of air to zero.

## 2.3 Experimental Results

### 2.3.1 Mean of particle concentration

Mean, $\mu_c$ , of particle concentration in a fluidized bed of $L_c/D_t = 4.0$ and $u = 5.67$ cm/sec is illustrated in Fig. 2.6. Examining this and many other similar illustrations indicates the following:

1) $\mu_c$ around the central axis of the bed is lower than those in the vicinity of column wall.

2) In the lower part of the bed, $\mu_c$ increases towards its maximal value with elevating probe level, and it remains unvaried in its upper part or it decreases slightly in the case of higher air velocities.

Thus, it may be said that the bubbles tend to rise around the central axis of the bed and that the fluidized particles are floating above the distributor because of low $\mu_c$ at the bottom of the bed. Fig. 2.7 illustrates the relationship between the mean of $\mu_c$'s in the upper part of the bed, $\bar{\mu}_{cm}$ , and the excessive superficial air velocity, $(u-u_{mf})$. It is seen in this figure that the effects of $L_c/D_t$ and $D_p$ are scarcely followable and that $\bar{\mu}_{cm}$ decrases linearly with increase

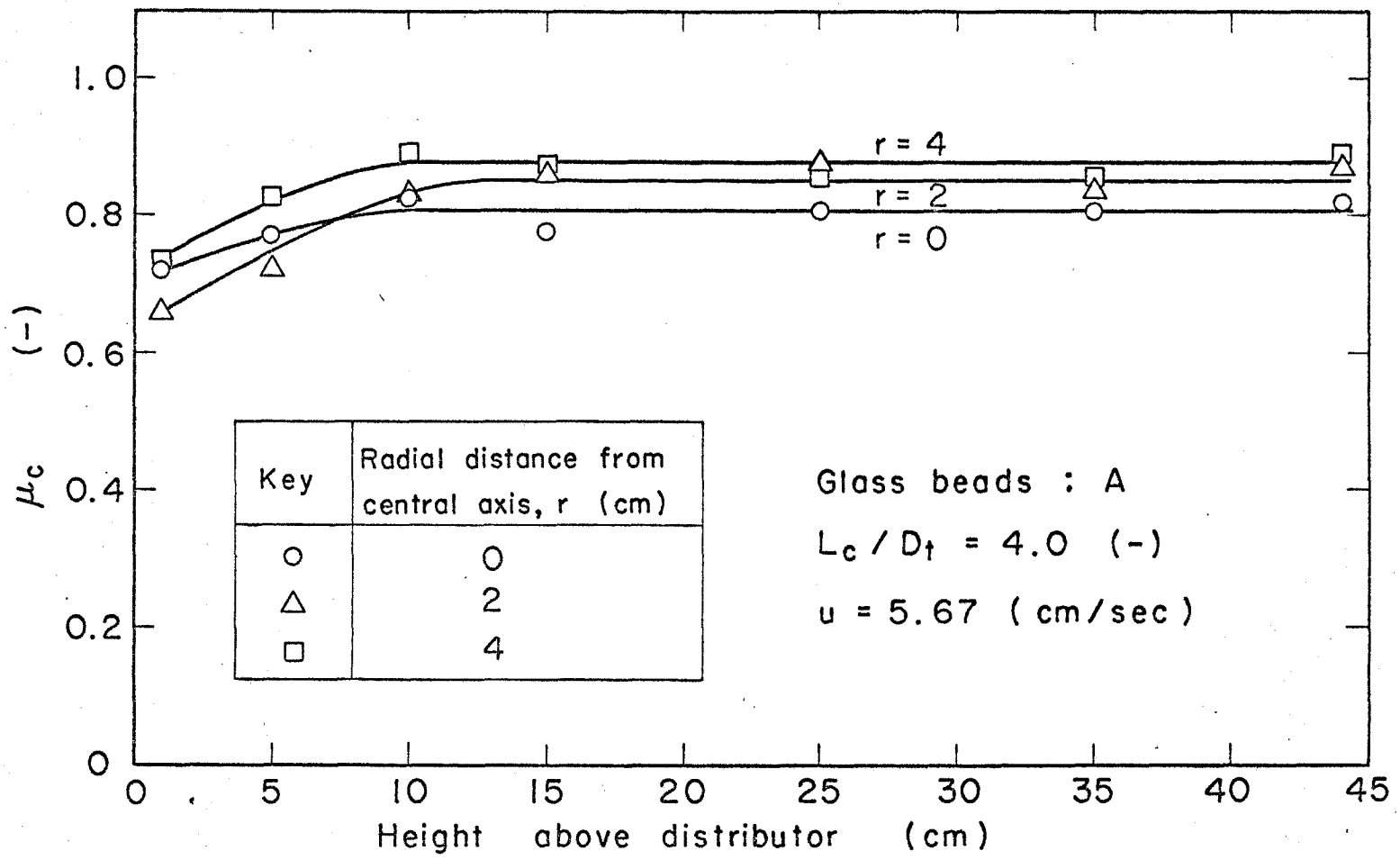


Fig. 2.6 An example of mean of particle concentration

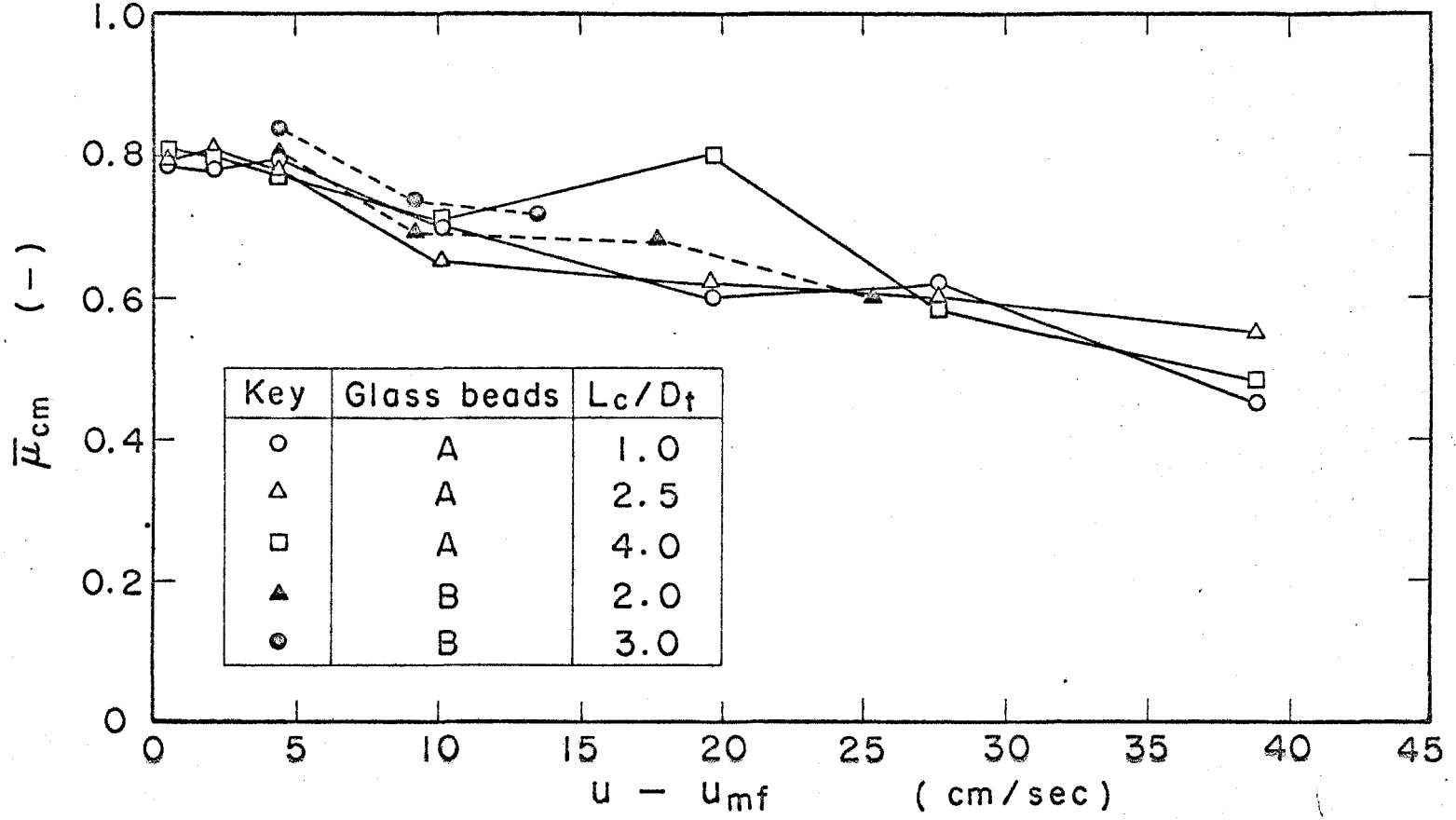


Fig. 2.7 Effect of excess air velocity on $\bar{\mu}_{cm}$

of $(u-u_{mf})$. This tendency coincides with the results obtained by Bakker and Heertjes (15).

### 2.3.2 Variance of particle concentration

An example of variance, $\sigma_c^2$, of particle concentration in a fluidized bed is shown in Fig. 2.8. By examining this and many other similar illustrations, it is revealed that:

1) $\sigma_c^2$ around the central axis is higher than those near the column wall.
2) $\sigma_c^2$ increases with the probe level up to a considerably higher portion of the bed and it varies scarcely there.

Though $\sigma_c^2$ varies in the lower part of the bed, its variation becomes so slight in the upper part, and their mean, $\bar{\sigma}_{cm}^2$, in this part is thought to represent the fluidization quality under the fluidizing conditions concerned. Fig. 2.9 represents the effect of $(u-u_{mf})$ on $\bar{\sigma}_{cm}^2$. Though the measuring precision of $\bar{\sigma}_{cm}^2$ is rather poor probably because of the two variables present in Eq. (2.2), it may be seen in this figure that $\bar{\sigma}_{cm}^2$ increases with the $(u-u_{mf})$ up to about 10 cm/sec and that further increase in air velocity seems to yield a significant effect of $L_c/D_t$ on $\bar{\sigma}_{cm}^2$ ;

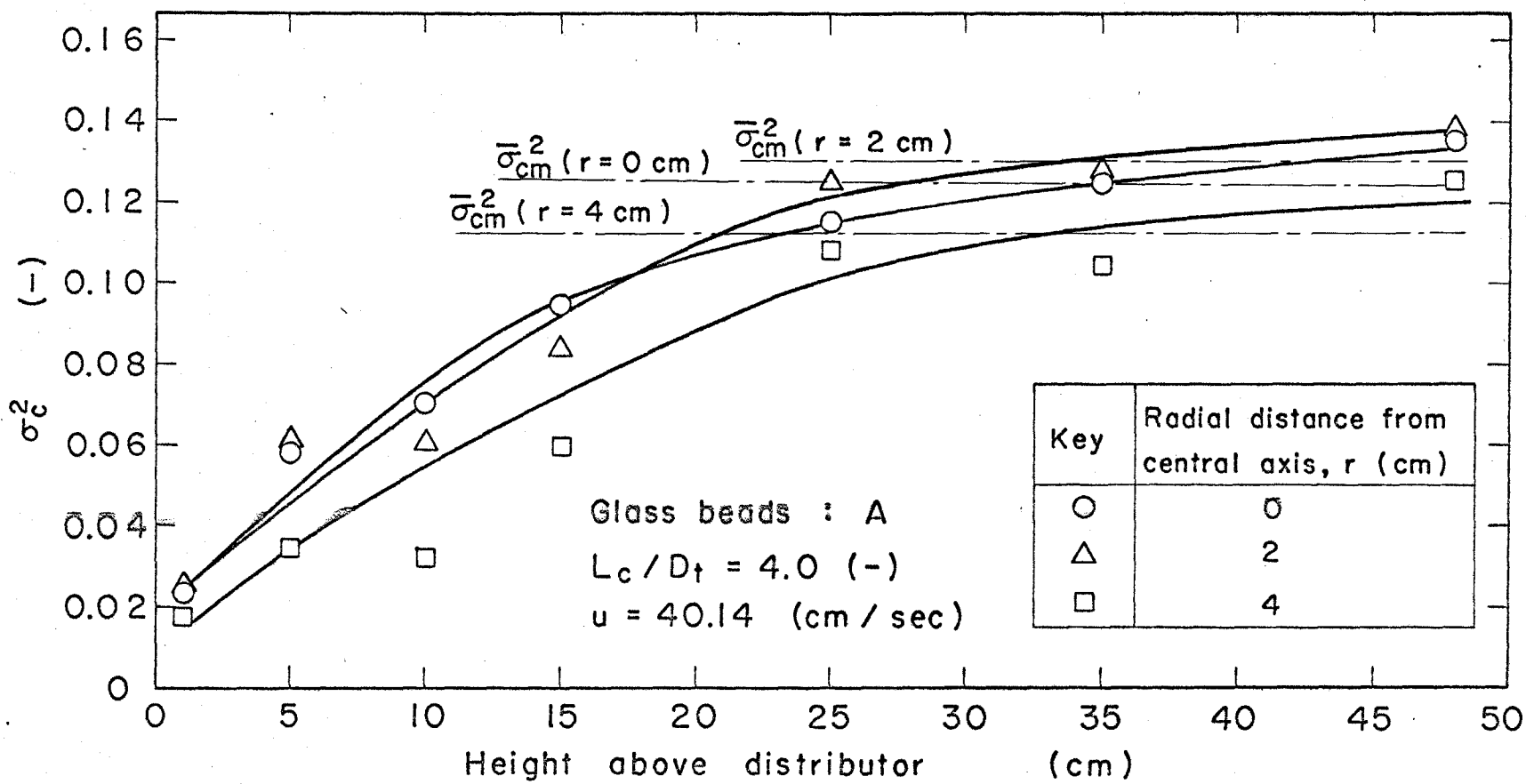


Fig. 2.8 An example of variance of particle concentration

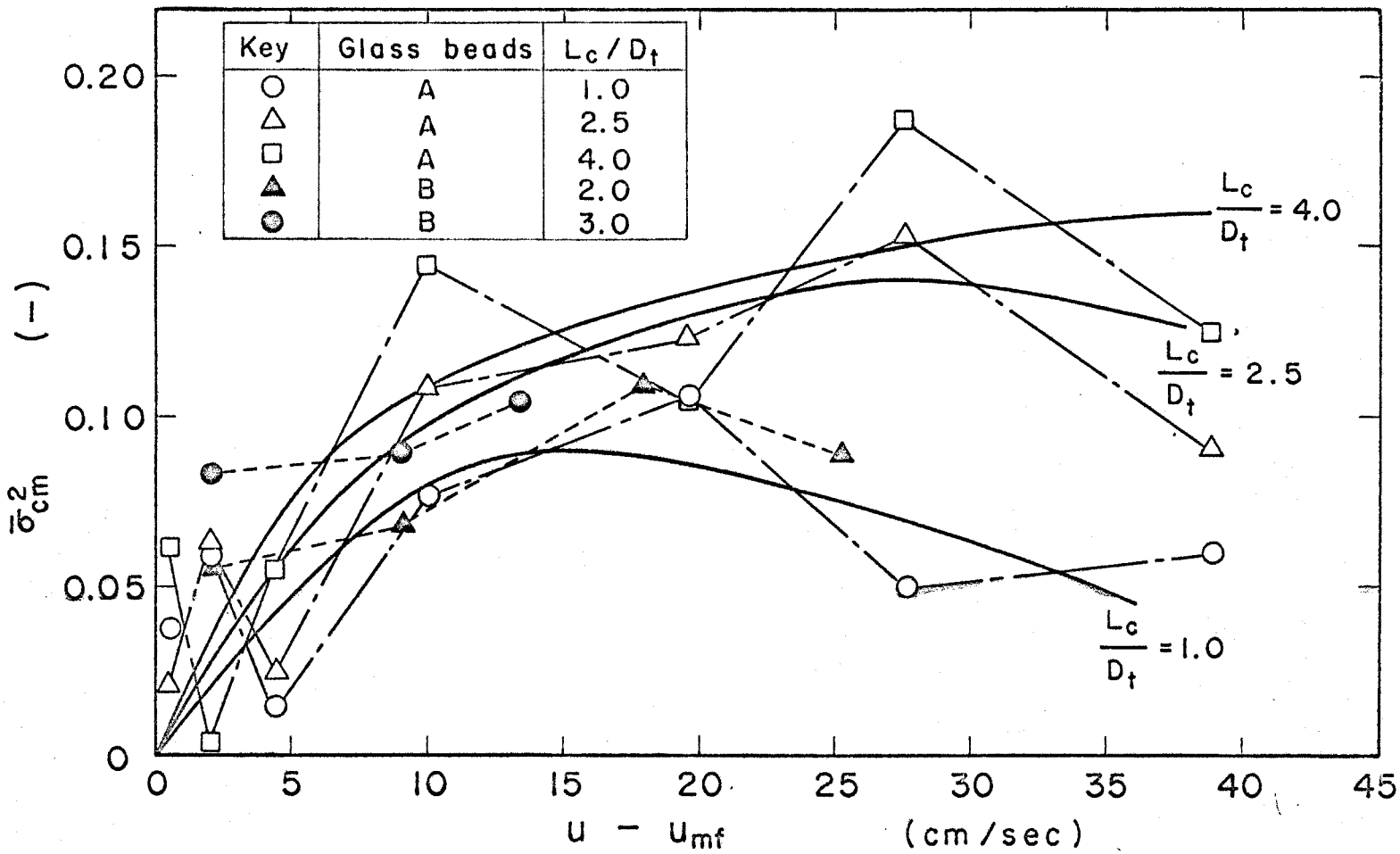


Fig. 2.9 Effect of excess air velocity on $\bar{\sigma}^2_{cm}$

especially, at the lower bed height of $L_c/D_t = 1.0$, $\bar{\sigma}_{cm}^2$ tends to decrease.

To confirm this, a statistical technique of analysis of variance was employed. Data with glass beads A shown in Fig. 2.9 were analysed, regarding them as a factorially designed experiment with two factors. $L_c/D_t$ and $(u-u_{mf})$ were chosen as the factors with their number of levels being 3 and 7, respectively. The result is shown in Table 2.2. It reveals, over the range analysed, that the effect of air velocity

Table 2.2 Analysis of variance (1)

| s.v. | s.s. | d.f. | m.s. | Fo |
|---|---|---|---|---|
| $L_c/D_t$ | 0.004707 | 2 | 0.002353 | 1.764 |
| $u-u_{mf}$ | 0.035338 | 6 | 0.005889 | 4.414* |
| Error | 0.016011 | 12 | 0.001334 | |
| Total | 0.056056 | 20 | | |

$F(2, 12 ; 0.05) = 3.89$, $F(6, 12 ; 0.05) = 3.00$

* : significant at 5 % significance level.

on $\bar{\sigma}_{cm}^2$ is statistically significant and that the effect of $L_c/D_t$ is not detected. It was mentioned above that the effect of $L_c/D_t$ becomes evident at higher air velocities. Another analysis of variance was tried in order to verify it ; the two lower levels of air veloc-

ity, $(u-u_{mf}) = 0.41$ and 2.11 cm/sec, were discarded and only the data at five higher levels were employed. The result is summarized in Table 2.3. This demon-

Table 2.3 Analysis of variance (2)

| s.v. | s.s. | d.f. | m.s. | Fo |
|---|---|---|---|---|
| $L_c/D_t$ | 0.011082 | 2 | 0.005541 | 5.724* |
| $u-u_{mf}$ | 0.016109 | 4 | 0.004027 | 4.160* |
| Error | 0.007748 | 8 | 0.000968 | |
| Total | 0.034939 | 14 | | |

$F(2, 8 ; 0.05) = 4.46$ , $F(4, 8 ; 0.05) = 3.84$

* : significant at 5 % significance level.

strates that, in the range thus limited, the effects of both factors are significant at 5 % significance level.

From these statistical analyses, it can be said that $\bar{\sigma}_{cm}^2$ is affected chiefly by the air velocity and that the bed height also becomes another significant factor at higher air velocity, or, $\bar{\sigma}_{cm}^2$ increases with $L_c/D_t$ at higher air velocity.

### 2.3.3 Frequency, vertical thickness and rise velocity of bubbles

(A) Bubble frequency

Bubble frequency, f, measured in the fluidized bed of u = 5.67, 11.34, 20.86 and 28.91 cm/sec and $L_c/D_t$ = 1.0 and 4.0 is shown in Fig. 2.10. Effects of bed height and air velocity upon f are not detectable, and only the probe level was found to affect f over the range investigated; f decreases when the probe level is raised.

(B) Vertical thikness of bubbles

Data of vertical thickness of bubbles, y, are shown in Fig. 2.11. At smaller excess air velocities above the minimum fluidization, that is, at $(u-u_{mf})$ = 0.41 and 2.11 cm/sec, y keeps almost unvaried during the passage of bubble through the bed. y tends to increase with probe level when additional air velocity is supplied. These tendencies of y are consistent with those found by Toei et al. (16). When y is larger than about 10 cm, it is thought that slugging occurs in the fluidized bed because y exceeds the diameter of fluidization column. The tendencies of f decreasing with probe level and of y increasing with probe level at higher air velocity may be attributed to coalescing bubbles

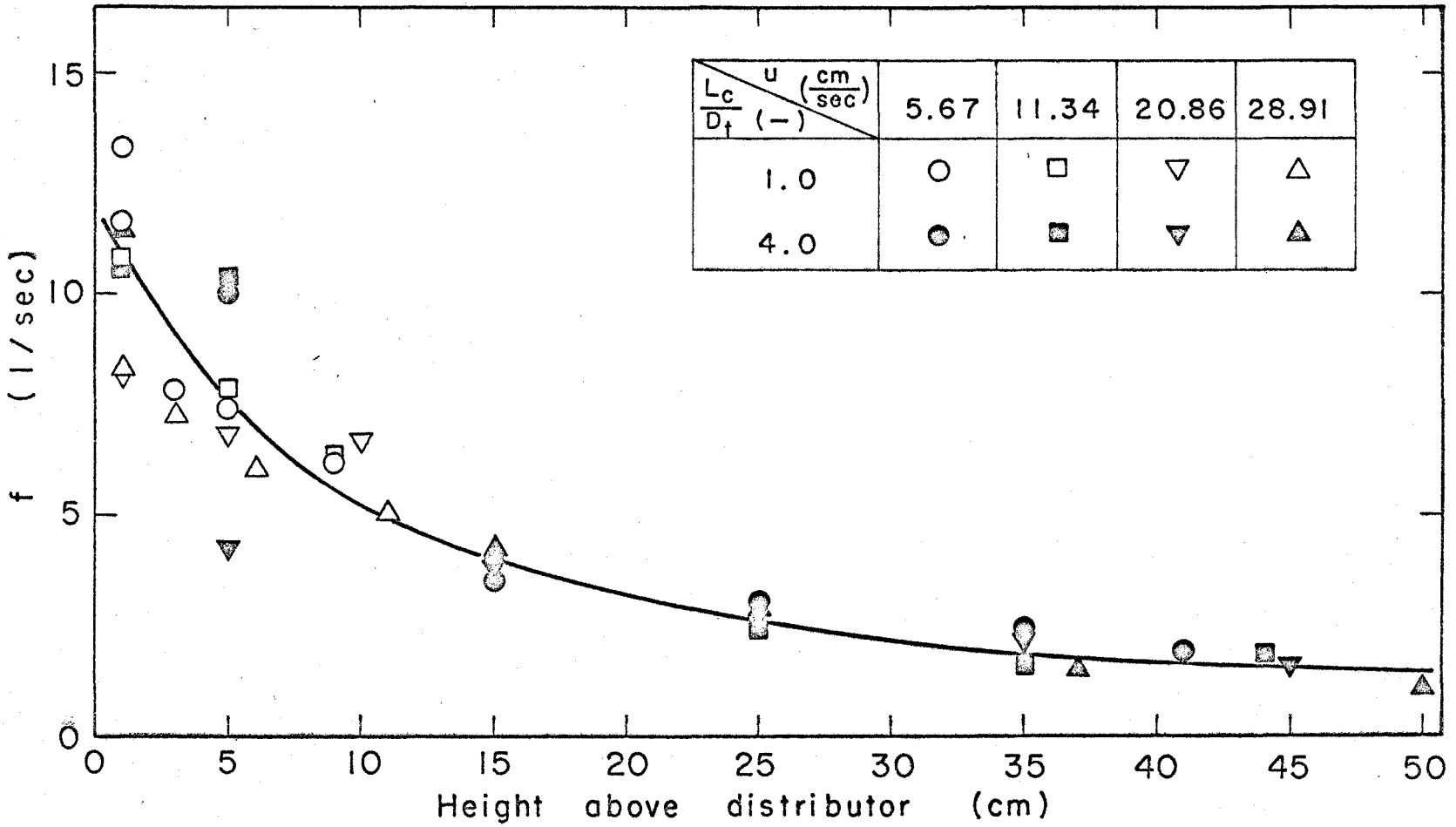


Fig. 2.10 Bubble frequency

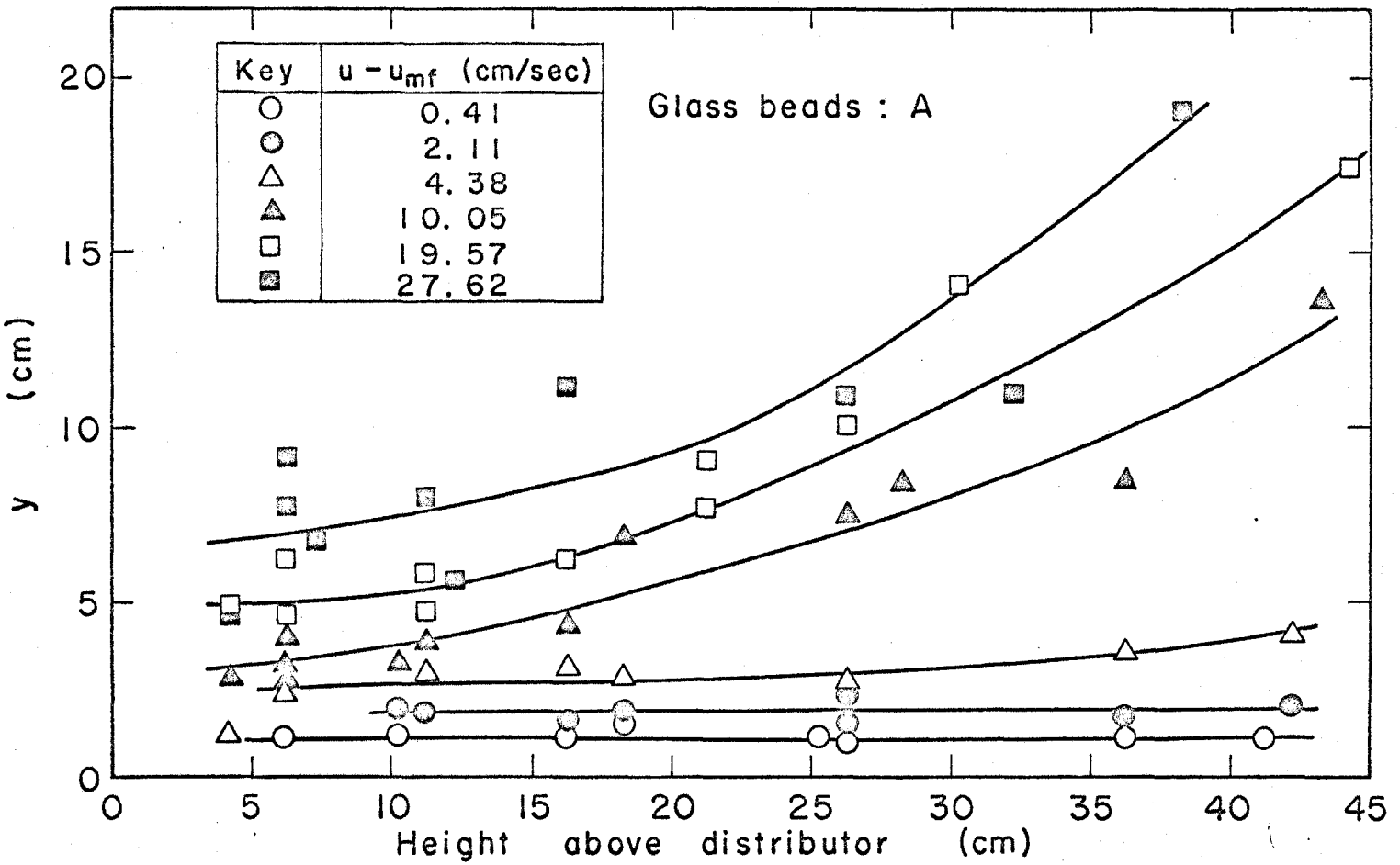


Fig. 2.11 Vertical thickness of bubble

during ascending through the bed.

At $(u-u_{mf})$ above 10 cm/sec, y increases remarkably with the probe level, and it may be of interest that $\bar{\sigma}_{cm}^2$ increases also with $L_c/D_t$ in this range of air velocity. Fig. 2.12 represents the correlationship between $\bar{\sigma}_{cm}^2$ and y in the upper part of fluidized bed. It is seen in this figure that $\bar{\sigma}_{cm}^2$ increases with y in the upper part of the bed when y is less than about 10 cm and that $\bar{\sigma}_{cm}^2$ decreases with further increase of y. This tendency will be discussed in 2.4 in relation with the particle concentration difference between bubble and dense phases.

(C) Rise velocity of bubbles

Rise velocity of bubbles, $u_b$, in the fluidized bed of $u = 5.67$ cm/sec and $L_c/D_t = 1.0$, 2.5 and 4.0 are summarized in Fig. 2.13. Though they appear dispersed owing to various error sources, it seems to be reasonable from this figure that the bed height has no significant effect on $u_b$ and that the bubbles rise through the bed at a fixed velocity. Logarithm of their mean, $\bar{u}_b$, are plotted against logarithmic air velocity in Fig. 2.14. From this, $\bar{u}_b$ is found to be determined by air velocity and the following empirical

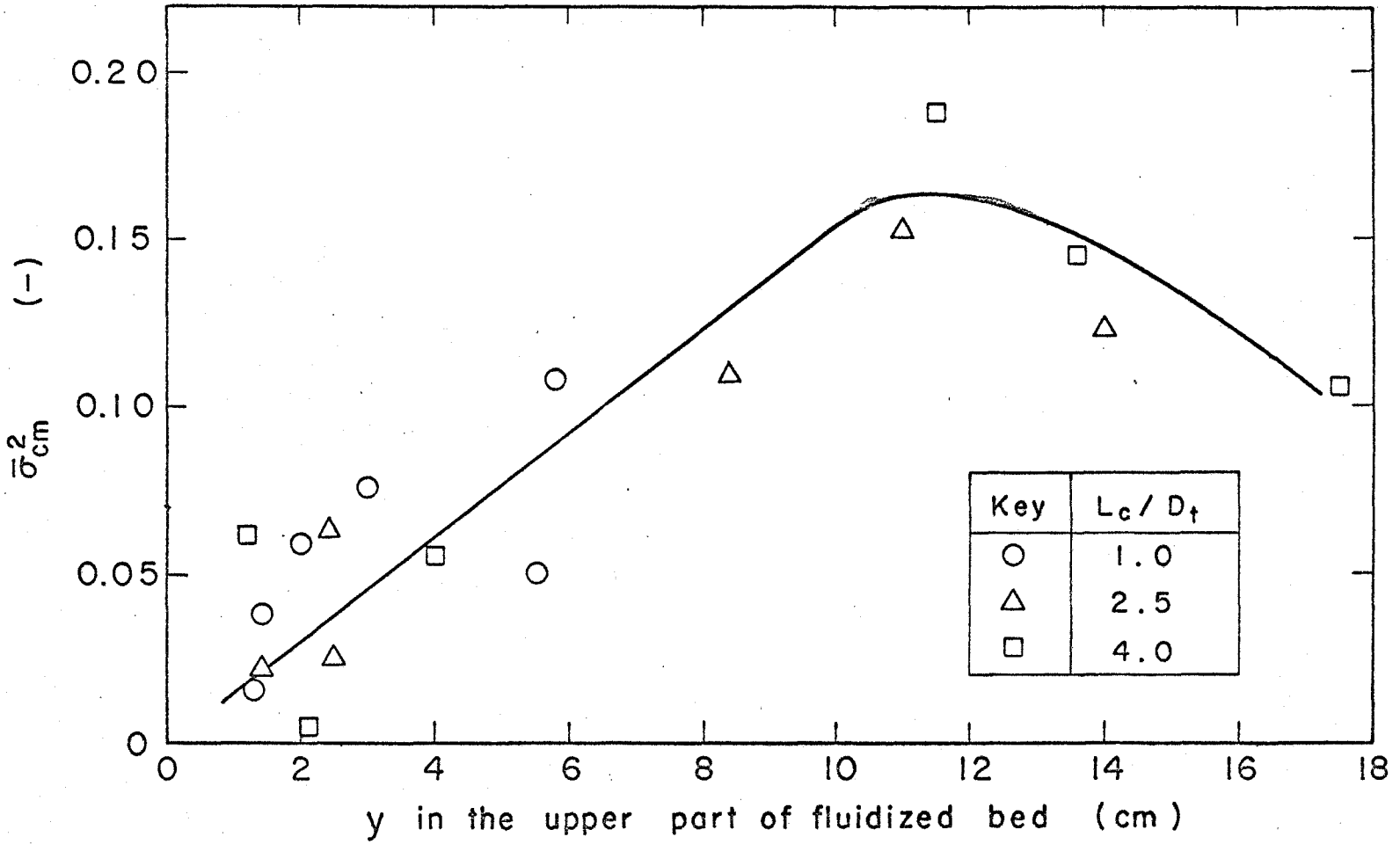


Fig.2.12 Correlationship between $\bar{\sigma}^2_{cm}$ and y in the upper part of fluidized bed

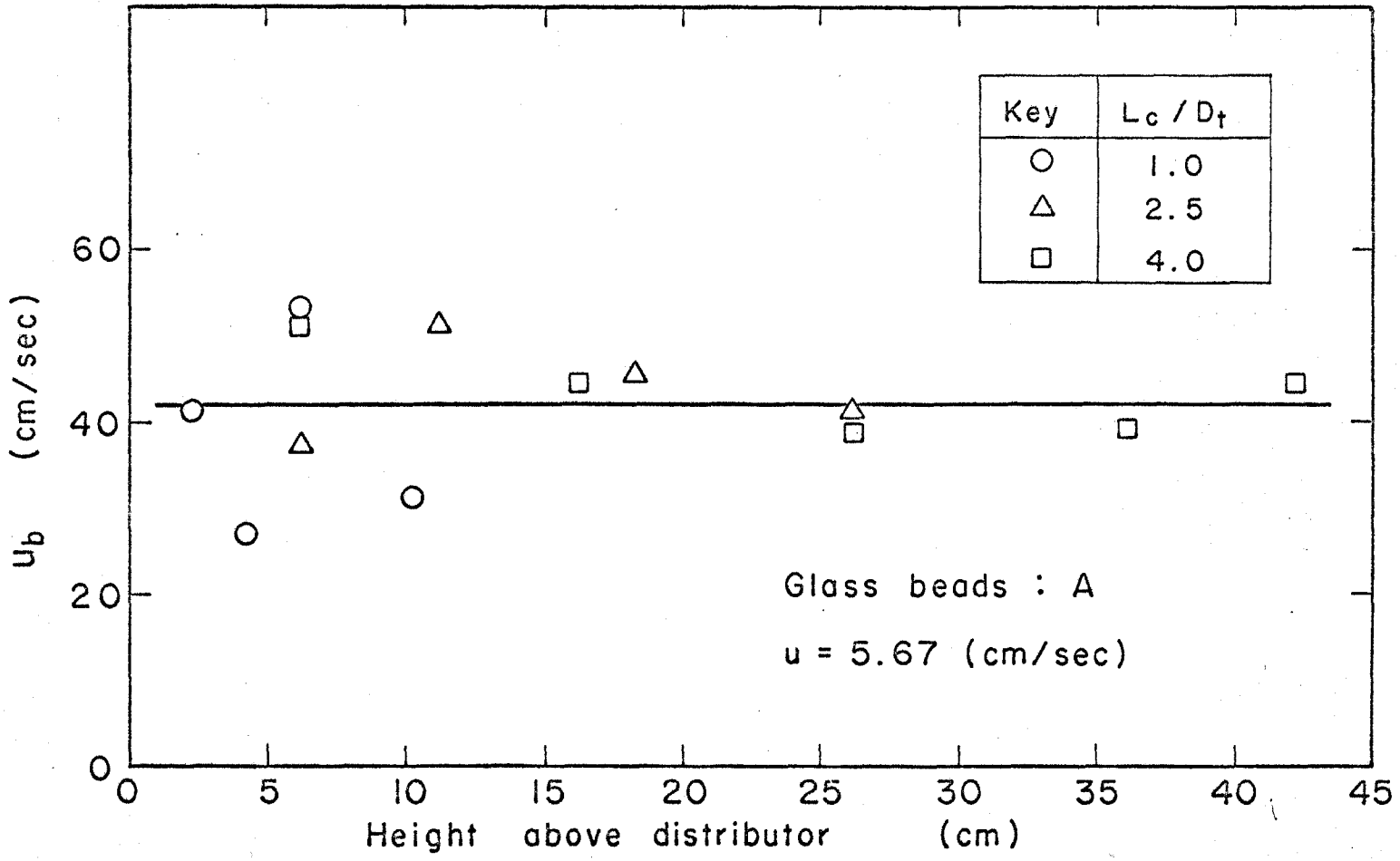


Fig.2.13 Rise velocity of bubbles

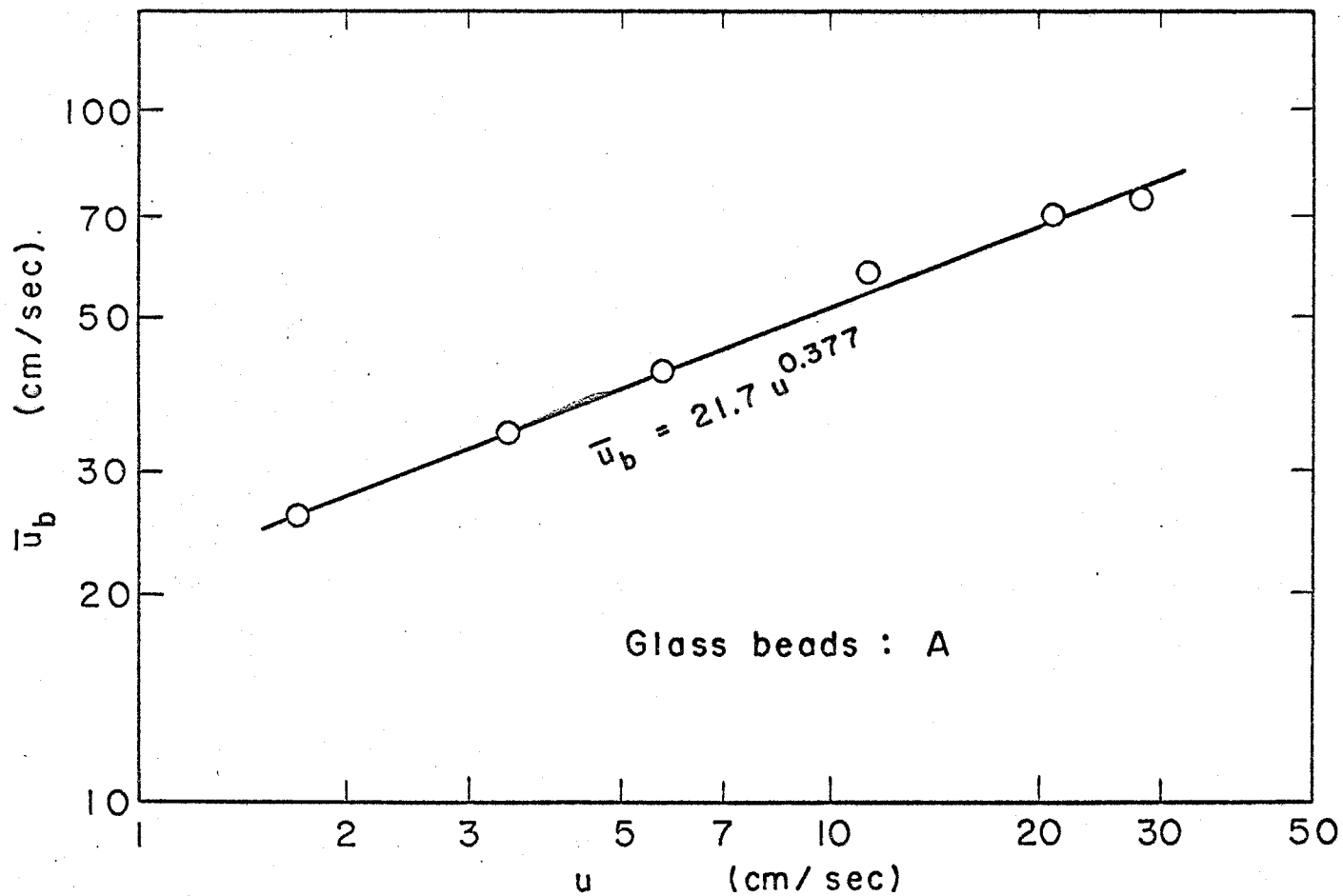


Fig. 2.14 Correlationship between u and $\bar{u}_b$

equation can be obtained.

$$\bar{u}_b = 21.7\ u^{0.377} \qquad (2.8)$$

The correlationship between $u_b$ and y is illustrated in Fig. 2.15 and it is seen in this figure that $u_b$ agrees well with the equation, $u_b = 0.732\sqrt{gy}$, obtained by Toei et al. (16).

### 2.3.4 Particle concentration in bubble and dense phases

Fig. 2.16 illustrates an example of dimensionless particle concentration, $C_L$ and $C_U$, calculated by Eqs. (2.5) and (2.6), respectively.

It was observed by Toei et al. (17) that the fluidized particles rain through the ascending bubble either in the form of smaller aggregates or of individual particles when a bubble passes through the probe tip. On the other hand, when the probe tip is immersed in the dense phase, the particle concentration measured may be affected by the presence of the tip and the measured concentration is supposed to be different from those in its vicinity. It is thought, therefore, that $C_L$ and $C_U$ measured may deviate from the true particle concentration in bubble and dense phases, respec-

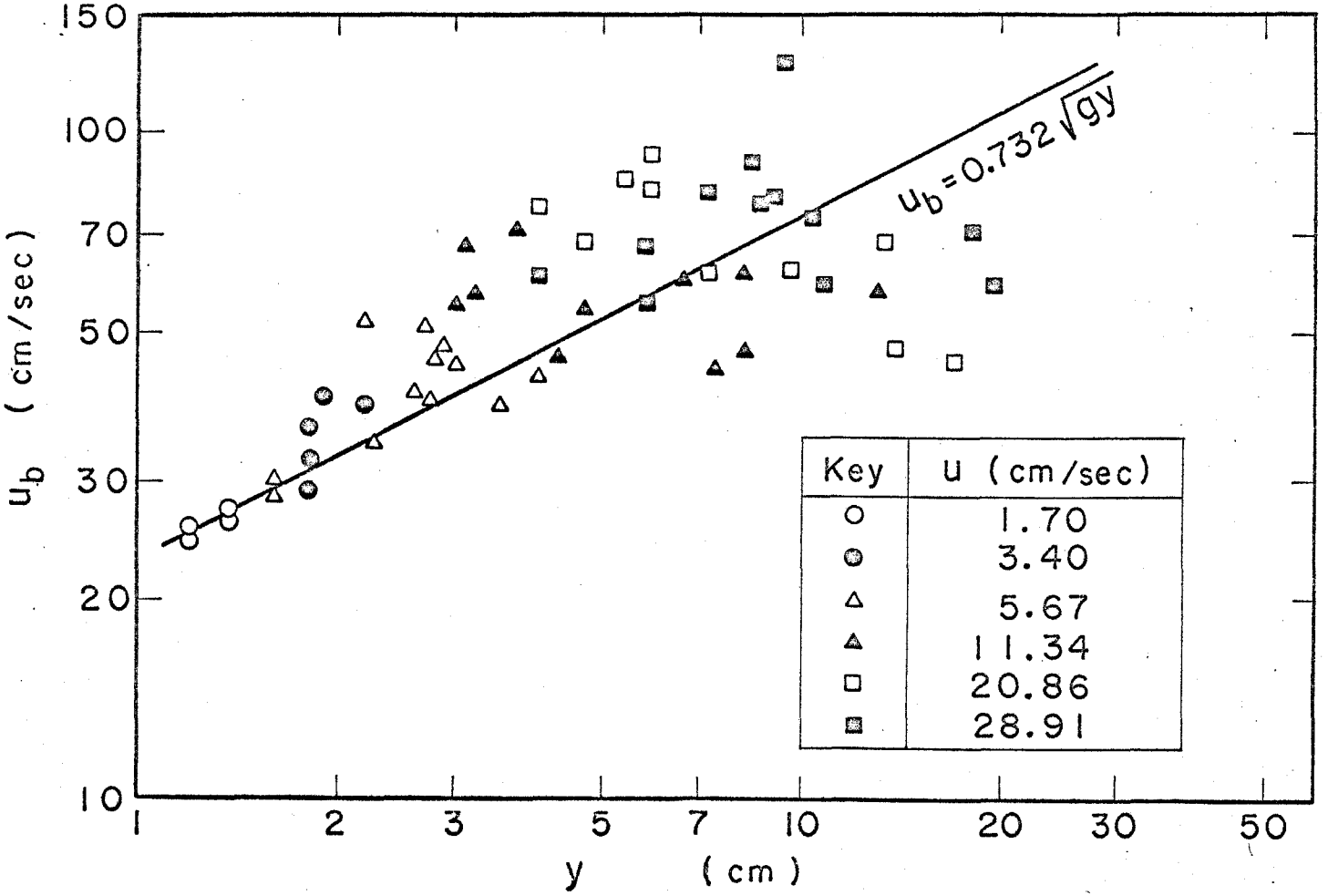


Fig. 2.15 Correlationship between y and $u_b$

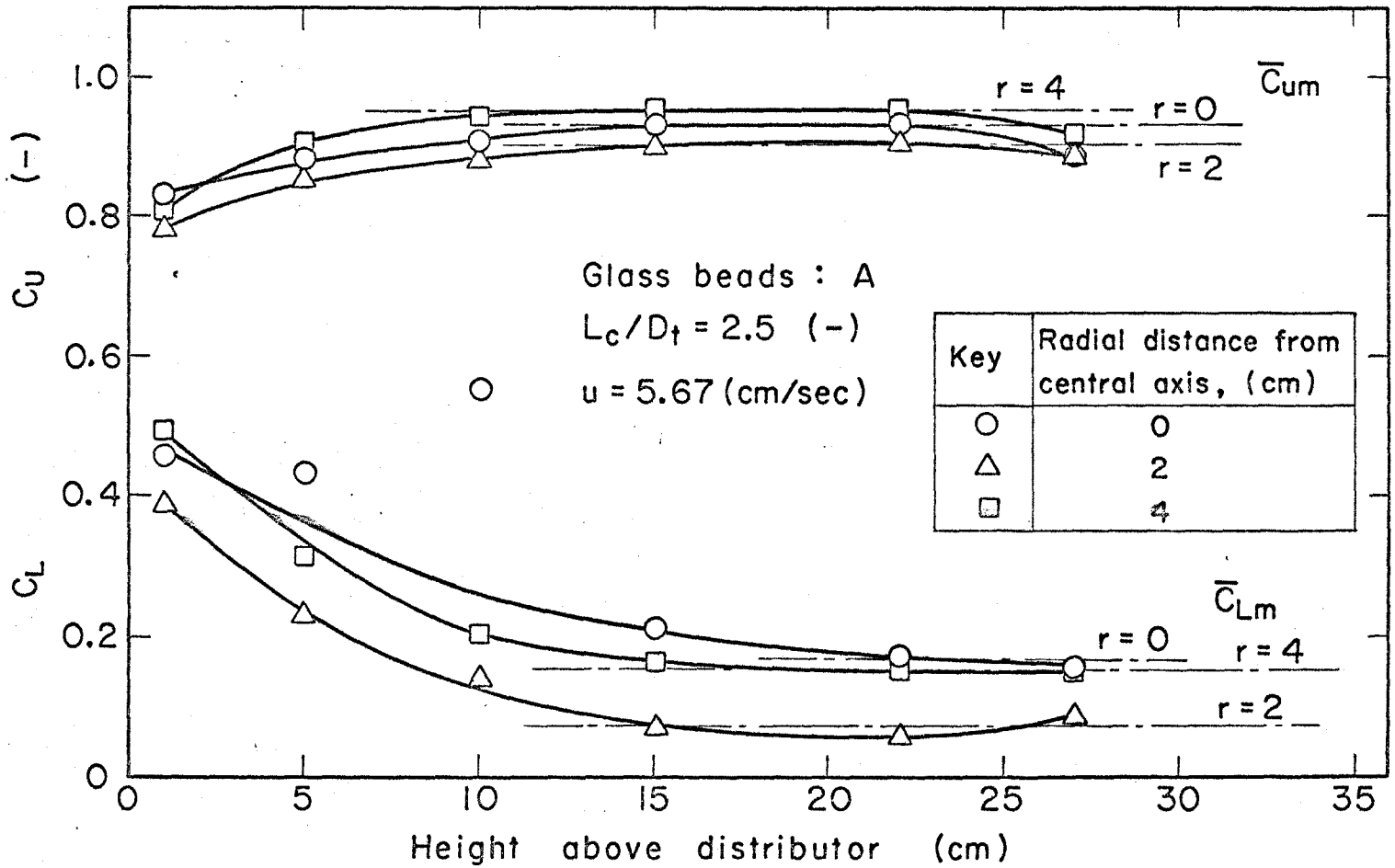


Fig. 2.16 An example of $C_L$ and $C_U$

tively. However, they can be used as a measure, or relative value, representing particle concentration in these phases.

The difference between $C_L$ and $C_U$ was found minor at the bottom of the bed, and the difference becomes evident with increase of probe level ; $C_L$ and $C_U$ converge to their specific values of $\bar{C}_{Lm}$ and $\bar{C}_{Um}$, respectively. These $\bar{C}_{Lm}$ and $\bar{C}_{Um}$ are plotted in Fig. 2.17 against $(u-u_{mf})$. As shown in this figure, the effects of bed height and particle size on $\bar{C}_{Lm}$ and $\bar{C}_{Um}$ are not evident. Over the range studied, $\bar{C}_{Um}$ was found to be nearly equal to 1.0 ; it is very close to that measured in the settled bed. In the ranges of $(u-u_{mf})$ below 2 cm/sec and above 30 cm/sec, however, $\bar{C}_{Um}$ is below 1.0. These results are consistent with those obtained by Lanneau (18).

## 2.4 Discussion

Mean, $\mu_c$ , and variance, $\sigma_c^2$ , of local particle concentration in the fluidized bed were proposed as the parameters representing fluidization quality, and their relationship to the fluidizing conditions was studied. Moreover, the fluidization characteristics, such as bubble frequency, f, bubble thickness, y, rise

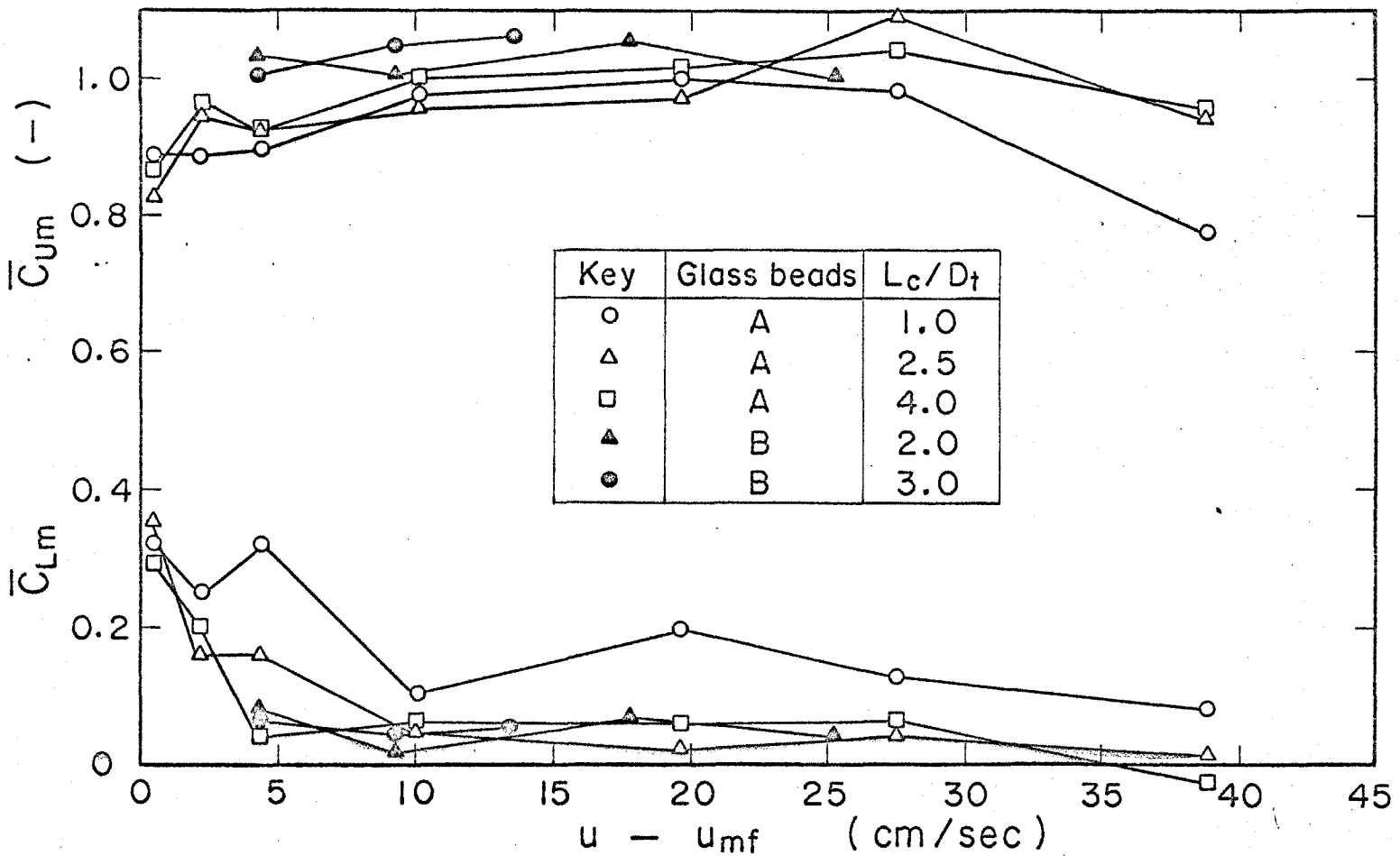


Fig. 2.17 Effect of excess air velocity on $\overline{C}_{Lm}$ and $\overline{C}_{Um}$

velocity of bubble, $u_b$, and the relative particle concentration in bubble and dense phases, $C_L$ and $C_U$, were also measured. It is intended in this section to correlate $\mu_c$ and $\sigma_c^2$ with the fluidization characteristics above mentioned.

$\mu_c$ defined by Eqs. (2.1) and (2.3) is expected to be a linear function composed of a product of particle concentration in bubble phase, $C_b$, multipied by time fraction of bubble phase covering the probe tip and another product of particle concentration in dense phase, $C_d$, multiplied by time fraction of dense phase covering the tip. A measure representing the former time fraction is $yf/u_b$, and that of the later is $(1-yf/u_b)$.

On the other hand, $\sigma_c^2$ defined by Eqs. (2.2) and (2.4) is supposed to be zero when the local particle concentration remains unchanged during the measuring time. In addition, $\sigma_c^2$ is a function of difference in particle concentration between bubble and dense phases, $(C_d - C_b)$.

Keeping these features of $\mu_c$ and $\sigma_c^2$ in mind, the following equations for $\mu_c$ and $\sigma_c^2$ were introduced where the oscillogram of particle concentration is replaced by a rectangular wave of Fig. 2.18.

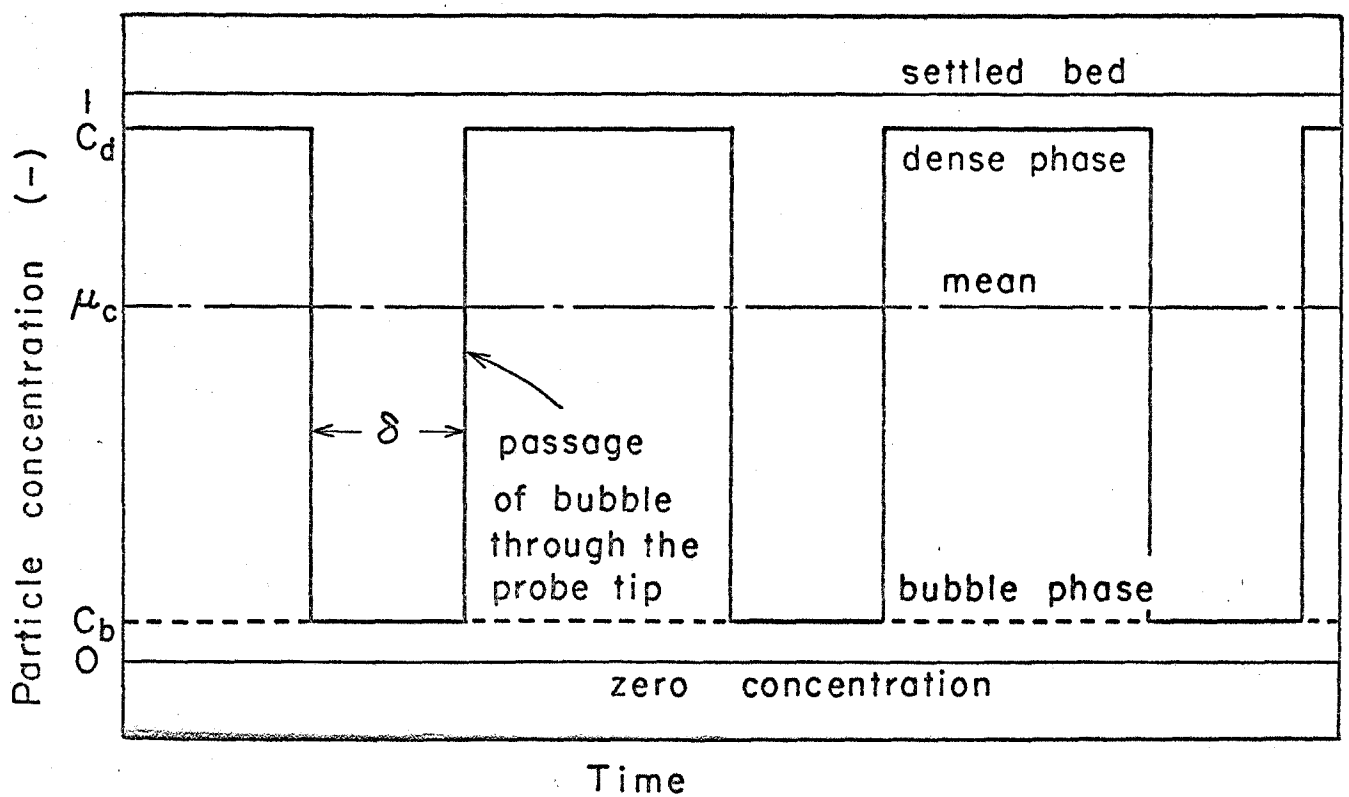


Fig. 2.18 Schematic oscillogram

$$\mu_c = \frac{1}{\theta}\int_0^{\theta} C\,d\theta$$

$$= \delta f C_b + (1-\delta f) C_d$$

$$= \frac{yf}{u_b} C_b + \left(1 - \frac{yf}{u_b}\right) C_d \qquad (2.9)$$

$$\sigma_c^2 = \frac{1}{\theta}\int_0^{\theta} (C-\mu_c)^2 d\theta$$

$$= \frac{1}{\theta}\int_0^{\delta f\theta} (C_b-\mu_c)^2 d\theta + \frac{1}{\theta}\int_{\delta f\theta}^{\theta} (C_d-\mu_c)^2 d\theta$$

$$= \delta f (1-\delta f)(C_d - C_b)^2$$

$$= \frac{yf}{u_b}\left(1 - \frac{yf}{u_b}\right)(C_d - C_b)^2 \qquad (2.10)$$

$\mu_c$ and $\sigma_c^2$ were calculated with Eqs. (2.9) and (2.10) by using y, $u_b$, f, $C_L$ and $C_U$ in place of $C_b$ and $C_d$, respectively. They were compared with measured $\mu_c$ and $\sigma_c^2$ in Figs. 2.19 and 2.20. In Fig. 2.19, it is seen that $\mu_c$ thus calculated are consistent with the measured values of $\mu_c$. However, the calculated values of $\sigma_c^2$ deviate from measured $\sigma_c^2$; calcuslted $\sigma_c^2$ in Fig. 2.20 are several times larger than the measured $\sigma_c^2$. This deviation arises from overestimating the terms $(C - \mu_c)^2$ in Eq. (2.10) by replacing the smooth oscillograms by rectangular waves. The consistency

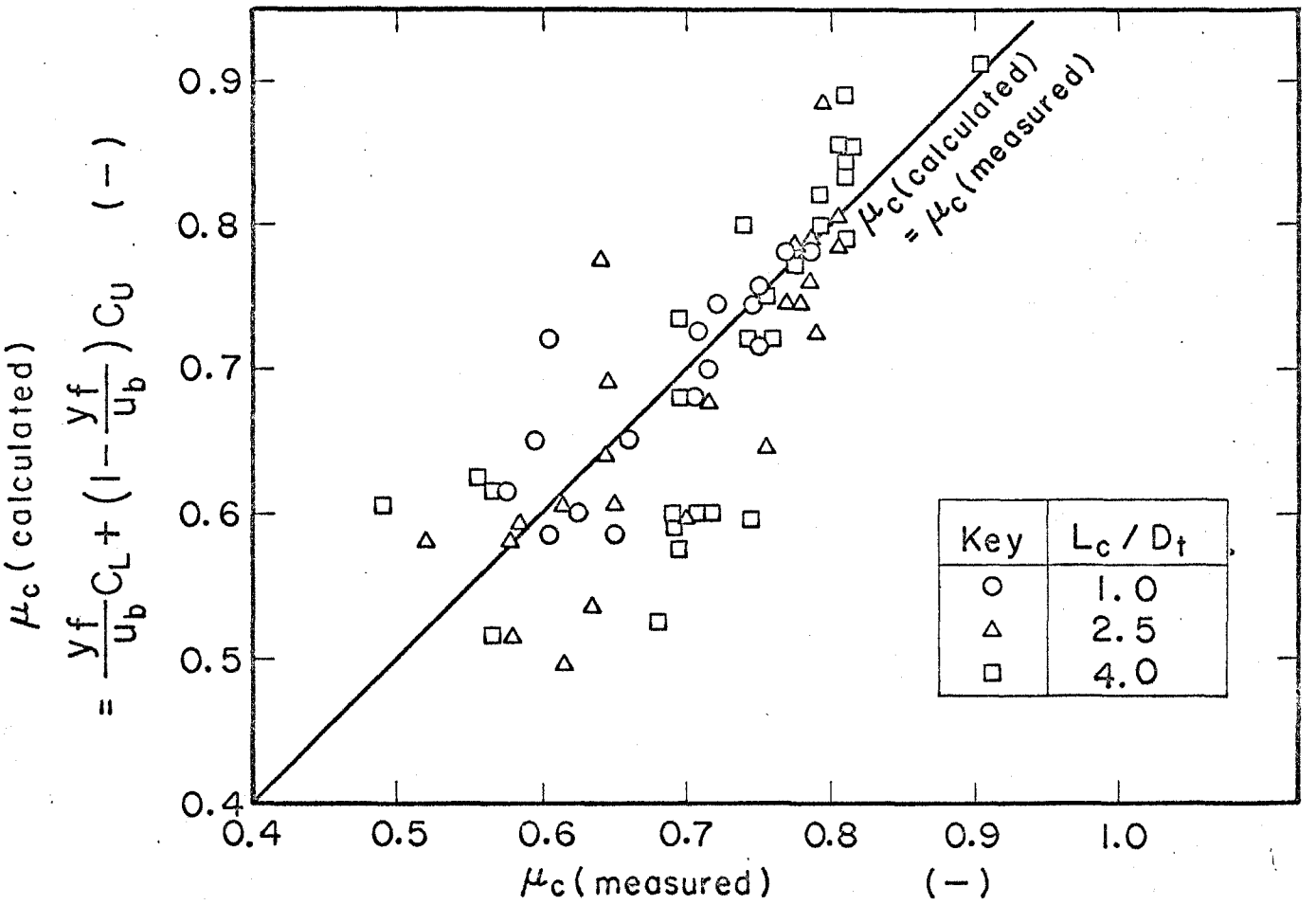


Fig. 2.19 Correlationship between measured and calculated $\mu_c$

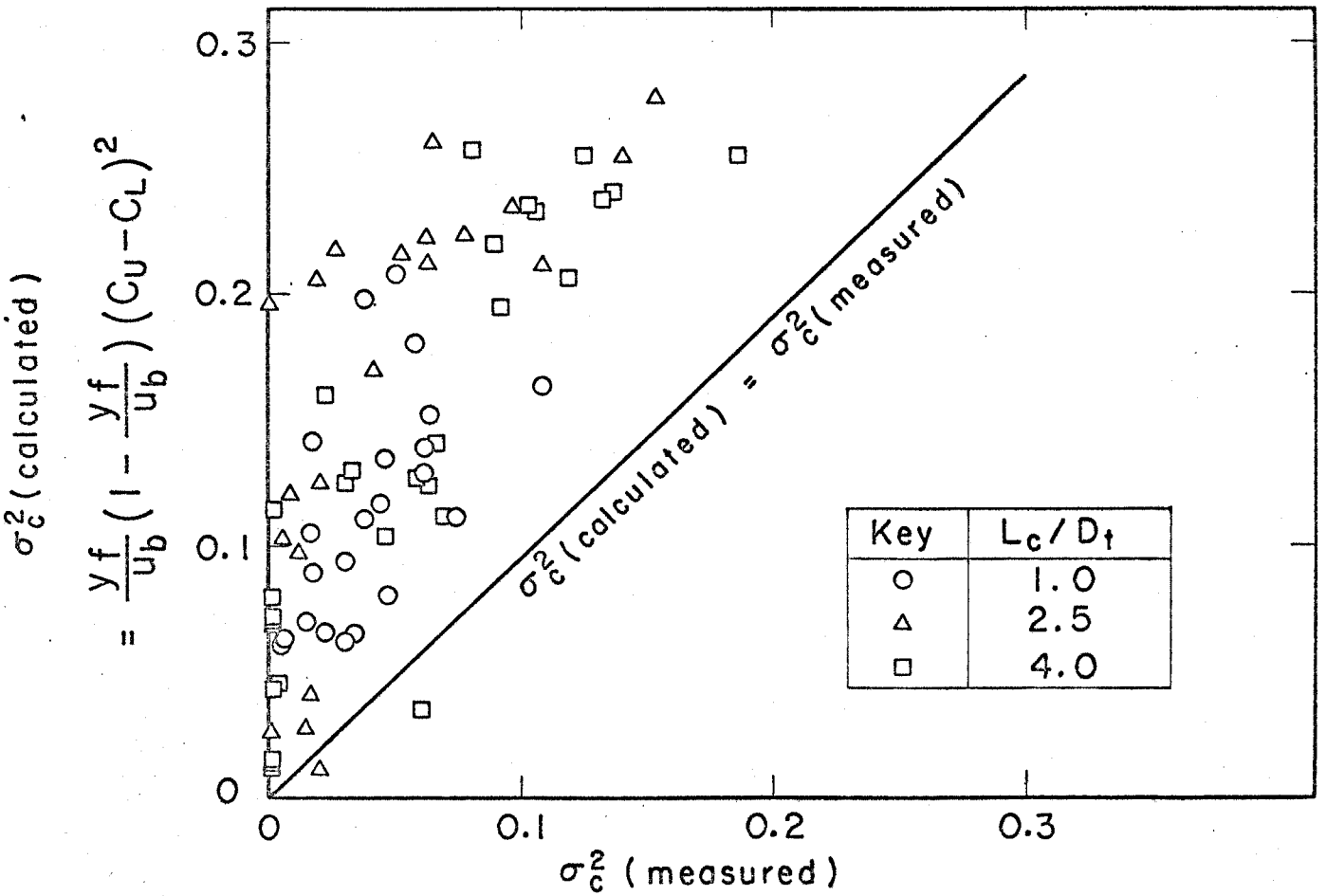


Fig. 2.20 Correlationship between measured and calculated $\sigma_c^2$

of calculated $\mu_c$ with the measured values, on the other hand, are understood because both side deviations, positive and negative, of rectangular wave from the oscillogram cancel themselves.

To pursue further $\sigma_c^2$, a measure of nonuniformity, a function of $C_L$, $C_U$, y, $u_b$ and f in the following form is presumed;

$$\sigma_c^2 = A\left\{\frac{yf}{u_b}\left(1-\frac{yf}{u_b}\right)\right\}^B (C_U - C_L)^C \qquad (2.11)$$

In trying to estimate the constants A, B and C in this equation the least squares method was used; data of 55 sets on $\sigma_c^2$, $C_U$, $C_L$, y, $u_b$, and f were applied and the resulting regression equation was,

$$\sigma_c^2 = 0.72\left\{\frac{yf}{u_b}\left(1-\frac{yf}{u_b}\right)\right\}^{0.46} (C_U - C_L)^{2.89} \qquad (2.12)$$

And hence, the statistical interpretation of Eq. (2.12) and its individual terms are to be discussed.

Total sum of squares of $\log\sigma_c^2$ and its degrees of freedom are,

$$\left.\begin{aligned} S_T &= \Sigma(\log\sigma_c^2)^2 - \frac{(\Sigma\log\sigma_c^2)^2}{55} = 12.4266 \\ \phi_T &= 55-1 = 54 \end{aligned}\right\} \qquad (2.13)$$

Residual sum of squares from the regression and its degrees of freedom are,

$$\left.\begin{aligned} S_E &= \Sigma\left[\log\sigma_c^2 - \log 0.72\left\{\frac{yf}{u_b}\left(1-\frac{yf}{u_b}\right)\right\}^{0.46}(C_U-C_L)^{2.89}\right]^2 \\ &= 8.3844 \\ \phi_E &= 55-3=52 \end{aligned}\right\} \quad (2.14)$$

and the sum of squares due to the regression and its degrees of freedom are,

$$\left.\begin{aligned} S_R &= S_T - S_E = 4.0422 \\ \phi_R &= \phi_T - \phi_E = 2 \end{aligned}\right\} \quad (2.15)$$

With these S and $\phi$ , F-ratio for testing the statistical significance of Eq. (2.12) is calculated as,

$$\left.\begin{aligned} F_o &= \frac{S_R/\phi_R}{S_E/\phi_E} = 12.54^{**} \end{aligned}\right\} \quad (2.16)$$

where

$$F(2, 52; 0.01) < F(2, 40; 0.01) = 5.18$$

Thus, $F_o$ is larger than its critical value of F(2, 52; 0.01) which means that Eq. (2.12) is statistically significant to represent $\sigma_c^2$.

Contributions of the terms of $\left\{\frac{yf}{u_b}\left(1-\frac{yf}{u_b}\right)\right\}$ and $(C_U - C_L)$ in Eq. (2.12) on $\sigma_c^2$ are tested by likelihood ratio test in the next step. The term $\left\{\frac{yf}{u_b}\left(1-\frac{yf}{u_b}\right)\right\}$ is a variable which changes with time fraction of bubble phase covering the probe tip, and the term $(C_U - C_L)$ represents the difference in particle concen-

tration between bubble and dense phases.

In order to test the significance of $\left\{\frac{yf}{u_b}\left(1-\frac{yf}{u_b}\right)\right\}$, B in Eq. (2.11) is presumed to be equal to zero. On this statistical hypothesis, residual sum of squares and its degrees of freedom are,

$$\left.\begin{aligned} S_{E(B=0)} &= \Sigma\left\{\log\sigma_c^2 - \log A(C_U-C_L)^C\right\}^2 \\ &= 8.4691 \\ \phi_{E(B=0)} &= 55-2=53 \end{aligned}\right\} \quad (2.17)$$

Sum of squares due to the term of $\left\{\frac{yf}{u_b}\left(1-\frac{yf}{u_b}\right)\right\}$ and its degrees of freedom are,

$$\left.\begin{aligned} S_B &= S_{E(B=0)} - S_E = 0.0847 \\ \phi_B &= \phi_{E(B=0)} - \phi_E = 1 \end{aligned}\right\} \quad (2.18)$$

and the F-ratio is

$$\left.\begin{aligned} F_o &= \frac{S_B/\phi_B}{S_E/\phi_E} = 0.53 \\ & F(1,52;0.05) > F(1,60;0.05) = 4.00 \end{aligned}\right\} \quad (2.19)$$

where

$F_o$ is less than its critical value and the contribution of $\left\{\frac{yf}{u_b}\left(1-\frac{yf}{u_b}\right)\right\}$ on $\sigma_c^2$ is not significant at 5 % significance level. A similar test on the term of $(C_U - C_L)$ was tried and it gave $F_o = 21.64$. The critical value is $F(1, 52; 0.05) < F(1, 40; 0.05) = 4.08$ and it can be said that the term $(C_U - C_L)$ is indispensable for $\sigma_c^2$.

Summarizing the above statistical analyses, it is

concluded that $\sigma_c^2$ represents the nonuniformity in a fluidized bed mainly in terms of particle concentration difference between bubble and dense phases. Fig. 2.21 represents the correlationship between $(\bar{C}_{Um} - \bar{C}_{Lm})$ and $\bar{\sigma}_{cm}^2$. From this figure, it is seen that $\bar{\sigma}_{cm}^2$ increases with the particle concentration difference between bubble and dense phases and that the effect of $L_c/D_t$ on $\bar{\sigma}_{cm}^2$ is scarcely followable in this figure. On the other hand, it was shown in Fig. 2.12 that $\bar{\sigma}_{cm}^2$ increases with y in the upper part of the fluidized bed when y is below about 10 cm. From these relationships between $\bar{\sigma}_{cm}^2$ and y and between $\bar{\sigma}_{cm}^2$ and $(\bar{C}_{Um} - \bar{C}_{Lm})$, it can be summarized that $\sigma_c^2$ increases when large bubbles of low particle concentration ascend through the fluidized bed. It can also be said from Figs. 2.12 and 2.21 that $\bar{\sigma}_{cm}^2$ is minor when the air velocity is considerably high and y is larger than about 10 cm in the upper part of the bed, because particle concentration difference between bubble and dense phases is rather small.

## 2.5 Summary

As a measure of nonuniformity in a fluidized bed,

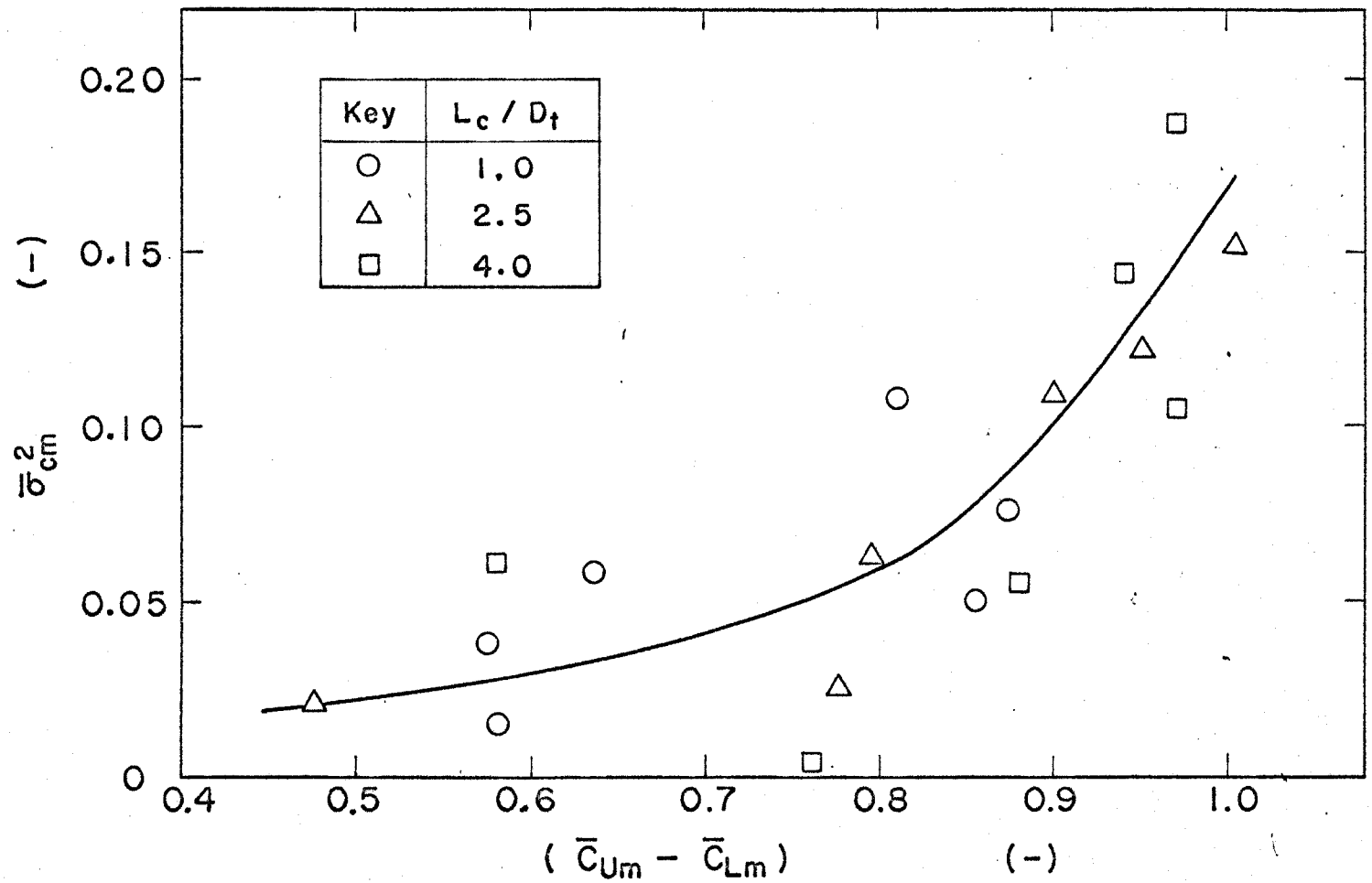


Fig.2.21 Correlationship between $(\overline{C}_{Um} - \overline{C}_{Lm})$ and $\overline{\sigma}^2_{cm}$

variance, $\sigma_c^2$, of local particle concentration in the bed was proposed. In addition to this, the mean local particle concentration, $\mu_c$, was also studied. They were measured with the capacitance probe method by using a vacuum tube thermocouple and an integrator, respectively. On the other hand, the change of capacitance of the probes was linearly converted into D.C. signal and its traces on a 2-channel synchroscope were filmed. From these oscillograms, the fluidization characteristics of the bed, such as rise velocity of bubble, $u_b$, vertical thickness of bubble, y, and bubble frequency, f, were measured. Moreover, the dimensionless particle concentration, $C_L$ and $C_U$, corresponding to the peak and valley height of traces on the oscillogram were measured and these concentrations were used as the measures representing the particle concentration in bubble and dense phases, respectively.

From the measurement of $\mu_c$, it was found that $\mu_c$ in the bulk of the bed remains at a constant value, $\bar{\mu}_{cm}$, which is determined by the fluidizing conditions. $\bar{\mu}_{cm}$ decreases with increasing excessive air velocity above the minimum fluidization. $\sigma_c^2$ increases with probe level and it becomes unvaried in the upper part of the fluidized bed. $\bar{\sigma}_{cm}^2$, mean of $\sigma_c^2$ in this part of the bed, increases with bed height and excessive air

velocity.

At the bottom of the fluidized bed, the particle concentration difference, $(C_U - C_L)$, is minor, and this suggests that the bubbles are just born there and are not yet grown in size. On rising the probe level, $C_L$ and $C_U$ converge to their specific values, $\bar{C}_{Lm}$ and $\bar{C}_{Um}$, respectively. $\bar{C}_{Um}$ were found at around 1.0, very close to those in the settled bed.

Effects of the bed height and of the probe level on the rise velocity of bubbles, $u_b$, were not followable and the bubbles rise through the bed at a fixed velocity. The mean $\bar{u}_b$ is determined chiefly by air velocity and the following empirical equation was obtained.

$$\bar{u}_b = 21.7\, u^{0.377}$$

Vertical thickness of bubble, y, increases with raising probe level at higher air velocity and bubble frequency, f, decreases with probe level. These tendencies of y and f can be attributed to the coalescence of bubbles during their rise through the bed.

Mean local particle concentration, $\mu_c$, is well represented by $C_L$, $C_U$, y, $u_b$ and f in the form of

$$\mu_c = \frac{yf}{u_b} C_L + \left(1 - \frac{yf}{u_b}\right) C_U$$

On the other hand, $\sigma_c^2$, a measure of nonuniformity in the fluidized bed, can not be explained by Eq. (2.10)

which assumes the rectangular waves. The regression of $\sigma_c^2$ is expressed by,

$$\sigma_c^2 = 0.72 \left\{ \frac{yf}{u_b}\left(1-\frac{yf}{u_b}\right)\right\}^{0.46} (C_U - C_L)^{2.89}$$

From statistical tests on this equation, it was found that $\sigma_c^2$ varies mainly with the term $(C_U - C_L)$ and the effect of term $\left\{\frac{yf}{u_b}\left(1-\frac{yf}{u_b}\right)\right\}$ on $\sigma_c^2$ is not significant. And it was also found that $\bar{\sigma}_{cm}^2$ increases with y in the upper part of the bed. From these results, it can be concluded that $\sigma_c^2$ represents the nonuniformity in the fluidized bed in the term of particle concentration difference between bubble and dense phases and that $\sigma_c^2$ increases when large bubbles of low particle concentration exist in the fluidized bed.

## Notation in Chapter 2

| | | | |
|---|---|---|---|
| f | : | bubble frequency | (1/sec) |
| u | : | air velocity | (cm/sec) |
| $u_b$ | : | rise velocity of bubble | (cm/sec) |
| $u_{mf}$ | : | u at minimum fluidization | (cm/sec) |
| v | : | output D.C. signal from detector | (mV) |
| $v_o$ | : | v from the empty column | (mV) |
| $v_L$ | : | v from bubble phase | (mV) |

| | | | |
|---|---|---|---|
| $v_U$ | : | v from dense phase | (mV) |
| $v_s$ | : | v from settled bed | (mV) |
| y | : | vertical thickness of bubble | (cm) |
| $C_b$ | : | particle concentration in bubble phase | (-) |
| $C_d$ | : | particle concentration in dense phase | (-) |
| $C_L$ | : | particle concentration corresponding to the peak height on oscillogram | (-) |
| $\bar{C}_{Lm}$ | : | mean of $C_L$ in the upper part of bed | (-) |
| $C_U$ | : | particle concentration corresponding to the valley height on oscillogram | (-) |
| $\bar{C}_{Um}$ | : | mean of $C_U$ in the upper part of bed | (-) |
| $D_t$ | : | internal diameter of fluidization column | (cm) |
| $L_c$ | : | settled bed height | (cm) |
| $S_E$ | : | residual sum of squares | (-) |
| $S_R$ | : | sum of squares due to regression | (-) |
| $S_T$ | : | total sum of squares | (-) |
| $\delta$ | : | width of peak on oscillogram | (sec) |
| $\theta$ | : | time | (sec) |
| $\mu_c$ | : | mean of particle concentration | (-) |
| $\bar{\mu}_{cm}$ | : | mean of $\mu_c$ in the bulk of bed | (-) |
| $\mu_s$ | : | v from settled bed (= $v_s$) | (mV) |
| $\mu_v$ | : | mean of v | (mV) |
| $\sigma_c^2$ | : | variance of particle concentration | (-) |
| $\bar{\sigma}_{cm}^2$ | : | mean of $\sigma_c^2$ in the upper part of bed | (-) |
| $\sigma_v^2$ | : | variance of v | ($mV^2$) |

$\phi_E$ : degrees of freedom of $S_E$ (-)

$\phi_R$ : degrees of freedom of $S_R$ (-)

$\phi_T$ : degrees of freedom of $S_T$ (-)

## References to Chapter 2


1) Harrison, D., J. F. Davidson and J. W. de Kock : Trans. Instn Chem. Engrs, 1961, Vol. 39, pp. 202-211

2) Toomey, R. D. and H. F. Johnstone : Chem. Eng. Progr., 1952, Vol. 48, No. 5, pp. 220-226

3) Yasui, G. and N. L. Johanson : A. I. Ch. E. Journal, 1958, Vol. 4, No. 4, pp. 445-452

4) Baumgarten, P. K. and R. L. Pegford : A. I. Ch. E. Journal, 1960, Vol. 6, No. 1, pp. 115-123

5) Toei, R., R. Matsuno, Y. Nagai, M. Ota and H. Ishii : Proceedings of Symposium on Chem. Eng., Tokyo, Soc. Chem. Eng. (Japan), 1965, No. 4, pp. 48-53

6) Mori, S., R. Shichi and I. Muchi : Proceedings of Symposium on Chem. Eng., Tokyo, Soc. Chem. Eng. (Japan), 1965, No. 4, pp. 31-36

7) Rowe, P. N. and B. A. Partridge : Symposium on the Interaction between Fluids and Particles, London, Instn Chem. Engrs, 1962, pp. 135-140

8) Rowe, P. N., B. A. Partridge, A. G. Cheney, G. A. Henwood and E. Lyall : Trans. Instn Chem. Engrs, 1965, Vol. 43, p. 271

9) Reuter, H. : Chemie-Ing. Techn., 1963, Bd. 35, s. 219

10) Jackson, R. : Trans. Instn Chem. Engrs, London, 1963, Vol. 41, p. 22

11) Matsuno, R. : Dr. Eng. thesis, Kyoto Univ., 1967

12) Morse, R. D. and C. O. Ballou : Chem. Eng. Progr., 1951, Vol. 47, No. 4, pp. 199-204

13) Shuster, W. W. and P. Kisliak : Chem. Eng. Progr., 1952, Vol. 48, No. 9, pp. 455-458

14) Dotson, J. M. : A. I. Ch. E. Journal, 1959, Vol.5, No. 2., pp. 169-174

15) Bakker, P. J. and P. M. Heertjes : Chem. Eng. Sci., 1960, Vol. 12, pp. 260-271

16) Toei, R., R. Matsuno, H. Ishii and H. Kojima : Proceedings of Symposium on Chem. Eng., Nagoya, Soc. Chem. Eng. (Japan), 1964, No. 3, pp. 32-38

17) Toei, R., R. Matsuno, H. Kojima, Y. Nagai, K. Nakagawa and S. Yu : Kagaku Kogaku (Japanese), 1965, Vol. 29, No. 11, pp. 851-857

18) Lanneau, K. P. : Trans. Instn Chem. Engrs, 1960, Vol. 38, pp. 125-143

19) Kondukov, N. B., A. N. Kornilaev, I. M. Skachko, A. A. Akhromenkov and A. S. Kruglov : Intern. Chem. Eng., 1964, Vol. 4, No. 1, pp. 43-47

# CHAPTER 3 HEAT TRANSFER RATE BETWEEN REACTOR WALL AND FLUIDIZED BED

## 3.1 Introduction

The rate of heat transfer in the fluidized bed plays an important role on various aspects of operation. When a large amount of heat is evolved or consumed within a fluidized bed along with the progress of reaction occurring in the bed, the corresponding amount of heat should be removed or supplied in order to maintain the fluidized bed at a fixed temperature. When a heat exchanger is to be equipped with a fluidized bed reactor, proper estimation of the heat transfer area is important. In some cases of roasting sulfide ore, on the other hand, an amount of water is added to the ore. An amount of heat which is evolved by the oxidation of sulfide ore is consumed by the evaporation of this water. And the temperature of the fluidized bed is controlled by adjusting the amount of water added to the ore. In this case, the simultaneous transport of heat and mass from the

fluidized particles to the gas phase becomes important.

Although many works (1, 4, 5, 22, 25) have been published which contributed to the heat transfer in the fluidized bed, the consistency among the results of those experimental works is rather poor, and this is thought to be due to the differences in their experimental conditions and the measurement.

Concerning the gas fluidized bed, the following two mechanisms of heat transfer are important:

a) Heat transfer between fluidized bed and the reactor wall.

b) Heat transfer between fluidized particles and gas.

Wen and Leva (2) tried to correlate the data of heat transfer between the fluidized bed and the reactor wall obtained by four groups of workers (3-6). Conventional plotting technique was applied on the assumption that heat is transferred through a laminar gas film whose thickness is influenced by the movement of solid particles along the wall. And the following dimensionless equation was derived.

$$\frac{h_w D_P}{k_g} = 0.16 \left(\frac{C_g \mu}{k_g}\right)^{0.4} \left(\frac{D_P \rho_g u}{\mu}\right)^{0.76} \left(\frac{\rho_P C_P}{\rho_g C_g}\right)^{-0.2} \left(\frac{\eta L_{mf}}{L_f}\right)^{0.36} \qquad (3.1)$$

where $\eta$ is defined by

$$\eta = \frac{u - \left(\begin{array}{c}\text{superficial gas velocity for} \\ \text{uniform expansion of bed}\end{array}\right)}{u}$$

In some cases, however, it is observed that the measured heat transfer coefficient deviates widely from that estimated from Eq. (3.1). Frantz (7) also endeavored to correlate the data of heat transfer between fluidized particles and gas obtained by Heertjes and Mckibbins (8) and by Walton, Olson and Levenspiel (9) by using the similar technique and derived the following expression;

$$\frac{h_p D_p}{k_g} = 0.015 \left(\frac{D_p G}{\mu}\right)^{1.6} \left(\frac{C_g \mu}{k_g}\right)^{0.76} \qquad (3.2)$$

In the case that a large amount of heat is consumed by the reaction occurring within the fluidized particles in the bed and that the required amount of heat is supplied to the particles through the fluidization tube wall, heat transfer rate between the tube wall and the fluidized bed becomes an important factor in the reaction rate. Thermal decomposition of pyrite and limestone particles in the fluidized bed which will be described in Chapters 4 and 5, respectively, can be regarded as the examples of such a reaction.

Consequently, quantitative knowledge on the heat transfer rate between the reactor wall and the fluidized bed is thought to be indispensable for the analysis of thermal decomposition rate of these mineral particles.

Fluidized bed reactors are operated in metallurgical processes at higher temperatures where the heat transfer by radiation can not be omitted. However, almost all of the works (1, 4, 5, 24) contributed to the heat transfer in fluidized bed were carried out at temperatures below 200°C where the radiative heat transfer can be omitted; heat is transferred by conduction and convection. It is required in this work, therefore, to grasp the heat transfer coefficient at higher temperatures in order to analyse the reaction rate in metallurgical processes.

In this chapter, the heat transfer coefficient between the fluidized bed and the tube wall was measured at the temperature between 500° and 800°C, and the results were compared with those obtained at lower temperatures by previous workers.

It is said that the major resistance to heat transfer exists in a laminar gas film on the wall and its thickness is influenced by the fluidization quality (2, 4, 5). And the correlationship between the

experimental results on heat transfer coefficient and on the fluidization characteristics discussed in Chapter 2 is also pursued.

## 3.2 Heat balance

Fig. 3.1 represents the heat flow diagram between the tube wall, the fluidized particles and the gas. Heat is supplied to the fluidized particles from the tube wall by conduction and radiation and, on the other hand, an amount of heat is transferred from the fluidized particles to the gas blown into the fluidized bed from the bottom. In addition to this, heat is supplied to the gas directly from the tube wall and thus the gas temperature is raised from $t_{go}$ at the bottom of the fluidized bed to $t_f$ in the upper part of the bed.

To obtain the heat balance between the tube wall, the fluidized particles and the gas, the following assumptions were made.

1) Heat transfer from the distributor and from the portion of the tube wall above the surface of the fluidized bed to the fluidized particles is neglected.

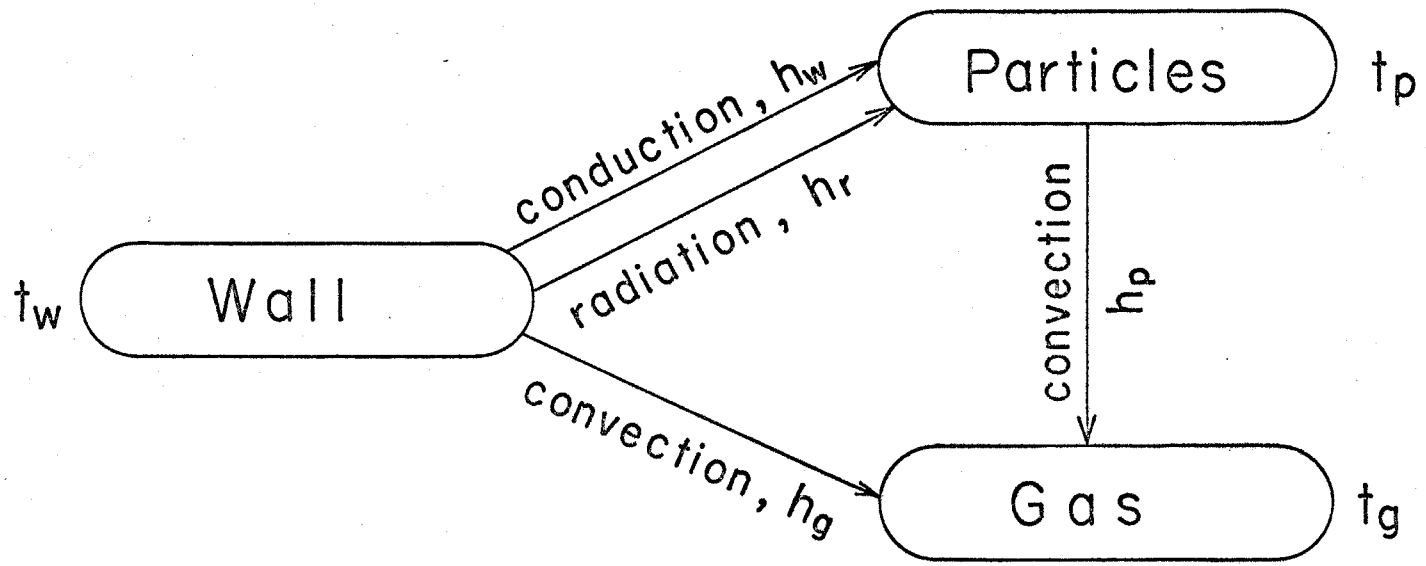


Fig. 3.1 Heat flow in fluidized bed

2) Size of fluidized particles is so small that the temperature profile within the particles is uniform.

3) Gas blown into the fluidized bed from the bottom is heated rapidly in the lower part of the bed and the gas and particles are in thermal equilibrium with each other in the upper part of the fluidized bed. Temperature at this portion of the bed is denoted by $t_f$ ($= t_g = t_p$).

4) Owing to the vigorous agitation of fluidized particles, temperature of the particles are uniform in both radial and axial directions throughout the bed.

Heat balance concerning the fluidized particles is represented by,

$$h_w F_w (t_w - t_p) + h_r F_r (t_w - t_p) - h_p \int_0^{L_f} A_p (t_p - t_g) dL = W C_p \frac{dt_p}{d\theta} \qquad (3.3)$$

And the heat balance concerning the gas is,

$$h_p \int_0^{L_f} A_p (t_p - t_g) dL + h_g F_g (t_w - t_g) - \int_{t_{go}}^{t_f} V \rho_g C_g dt = \frac{\pi}{4} D_t^2 L_f \varepsilon \rho_g C_g \frac{dt_g}{d\theta} \qquad (3.4)$$

At the steady state, Eqs. (3.3) and (3.4) are,

$$h_w F_w (t_w - t_p) + h_r F_r (t_w - t_p) - h_p \int_0^{L_f} A_p (t_p - t_g) dL = 0 \qquad (3.5)$$

$$h_p \int_0^{L_f} A_p (t_p - t_g) dL + h_g F_g (t_w - t_g) - \int_{t_{go}}^{t_f} V \rho_g C_g dt = 0 \qquad (3.6)$$

Concerning the left-hand side in Eq. (3.6), the magnitude of the second term is compared with that of the first term. $h_g$ represents the heat transfer coefficient between the tube wall and the gas. Because no information on $h_g$ in the fluidized bed is available, the film coefficient of heat transfer between the wall of an empty tube and the flowing gas through the tube, h, was estimated instead of $h_g$. Maximal values of air velocity and of bed temperature in this work are 850 cc/sec and 800°C, respectively, and h at this air velocity and temperature can be estimated as follows. Specific heat, $C_g$, and thermal conductivity, $k_g$, of air at 800°C and 1 atm are given at $C_g$ = 0.2756 kcal/kg·°C (10) and $k_g$ = 0.06 kcal/m·hr·°C (11), respectively. Thus the Graetz number, Gz, becomes

$$Gz = \frac{V \rho_g C_g}{k_g L} = 14.2$$

In the calculation of Gz, the length of tube, L, was chosen at 1.28 m which is the length of fluidization tube used in this work. The diameter of the tube,

$D_t$, is 61 mm and the Reynolds number ($Re = D_t u \rho_g / \mu$) is calculated at 534. Under this Reynolds number, gas velocity profile in the cross-section of tube can be assumed to be parabolic. On this assumption, Nusselt number ($Nu = hD_t/k_g$) corresponding to $Gz = 14.2$ is equal to 4.2 (12). From this value of Nu, h can be estimated at 4.3 kcal/$m^2 \cdot hr \cdot {}^oC$. This value of h is about one fifth of the heat transfer coefficient between fluidized particles and gas, $h_p$, obtained by Kettenring, Manderfield and Smith (1) and by Walton, Olson and Levenspiel (9). The thickness of gas film on the wall of the fluidization tube is thought to be thinner than the film thickness on the wall of an empty tube, because of rapid movement of particles along the wall. Consequently, it is thought that $h_g$ in Eq. (3.6) is larger than h estimated above, and yet $h_g$ is not widely different from $h_p$ in the first term of this equation.

Besides, the surface area of the tube wall, $F_g$, which contributes to the heat transfer to the fluidizing gas is about $3.0 \times 10^{-2}$ $m^2$. On the other hand, the surface area, $\int_0^{L_f} A_p dL$, of fluidized quartz and fused alumina particles whose amount is 500 and 800 g, respectively, is dependent on the particle size and it is 1.5 and 5.8 $m^2$ in both particles of 16-28 and 60-100

mesh, respectively. Thus, $\int_0^{L_f} A_p dL$ in Eq. (3.6) is about 100 times larger than $F_g$ in the same equation.

From the above study on the heat transfer coefficient and on the heat transfer surface area, it is reasonable to presume that the second term on the left-hand side of Eq. (3.6) can be omitted by comparing it with the first term. And the following equation is obtained instead of Eq. (3.6).

$$h_p \int_0^{L_f} A_p (t_p - t_g) dL - \int_{t_{go}}^{t_f} V \rho_g C_g dt = 0 \qquad (3.7)$$

From Eqs.(3.5) and (3.7), we have,

$$h_w F_w (t_w - t_p) + h_r F_r (t_w - t_p) = \int_{t_{go}}^{t_f} V \rho_g C_g dt \qquad (3.8)$$

$F_w$ and $F_r$ in Eq. (3.8) represent the inner surface area of the fluidization tube through which heat is transferred from the wall to the fluidized bed by conduction and radiation, respectively, and they are represented by,

$$F_w = F_r = \pi D_t L_f \quad (= F_c) \qquad (3.9)$$

The overall heat transfer coefficient, $h_c$, is defined as,

$$h_c = h_w + h_r \tag{3.10}$$

And, by using $F_c$ and $h_c$, Eq. (3.8) can be rewritten as,

$$h_c = \frac{\int_{t_{go}}^{t_f} V \rho_g C_g \, dt}{F_c (t_w - t_f)} \tag{3.11}$$

On the other hand, the heat transfer rate from the tube wall to the fluidized bed by radiation is estimated by the Stefan-Boltzmann's law:

$$Q_r = \sigma F_r \phi (T_w^4 - T_p^4) \tag{3.12}$$

From the facts that the particle concentration in the vicinity of tube wall is rather high and that the size of fluidized particles is sufficiently larger than the wave length of infrared ray, the heat transfer by radiation from the tube wall to the fluidized bed can be regarded as the heat transfer between two concentric tubes (13). On this assumption, $\phi$ in Eq. (3.12) is given by

$$\frac{1}{\phi} = \frac{1}{\varepsilon_w} + \frac{1}{\varepsilon_p} - 1 \tag{3.13}$$

Eq. (3.12) is equal to the second term in the left-hand side of Eq. (3.8), and we have

$$\sigma F_r \phi (T_w^4 - T_p^4) = h_r F_r (t_w - t_p) \qquad (3.14)$$

This equation yields the following expression of $h_r$,

$$h_r = \frac{\sigma \phi (T_w^4 - T_p^4)}{t_w - t_p}$$

$$= \sigma \phi (T_w^2 + T_p^2)(T_w + T_p) \qquad (3.15)$$

The temperature of particles which adjoin to the tube wall and are supplied with heat from the tube wall by radiation is thought to be somewhat higher than that of the particles in the bulk of the fluidized bed. However, since it is difficult to evaluate the temperature of the particles which are adjoining to the tube wall, $T_p$ in Eq. (3.15) is assumed to be equal to the temperature of particles in the bulk of the bed. On this assumption $T_p = T_f$, radiative coefficient of heat transfer can be rewritten as,

$$h_r = \sigma \phi (T_w^2 + T_f^2)(T_w + T_f) \qquad (3.16)$$

The film coefficient of heat transfer between the tube wall and the fluidized bed can be obtained by subtracting Eq. (3.16) from Eq. (3.11) as,

$$h_w = h_c - h_r \qquad (3.17)$$

## 3.3 Experimental

### 3.3.1 Apparatus

Fig. 3.2 demonstrates a schematic illustration of the fluidization apparatus. Fluidization tube is made of 61 mm I.D. and 1280 mm long 18-8 stainless steel tube which provides two fluidized beds, the upper and the lower beds. The upper or main fluidized bed is used for the measurement of heat transfer coefficient and the lower bed is to realize uniform air flow which is sent to the main fluidized bed. It also serves for measuring the gas temperature, $t_{go}$, which can be regarded as the temperature of air blown into the main fluidized bed.

The distributor of the main fluidized bed consists of 300-mesh stainless steel screen sandwiched in between two 1.0 mm thick 18-8 stainless steel plates perforated with 3.5 mm D. holes spaced on a 7.0 mm triangular pitch. The distributor of the lower fluidized bed has a similar construction except for the 2.0 mm diameter of holes perforated through the stainless steel plates.

The flow rate of air is metered with a rotameter or with orifice meters. The fluidization tube is

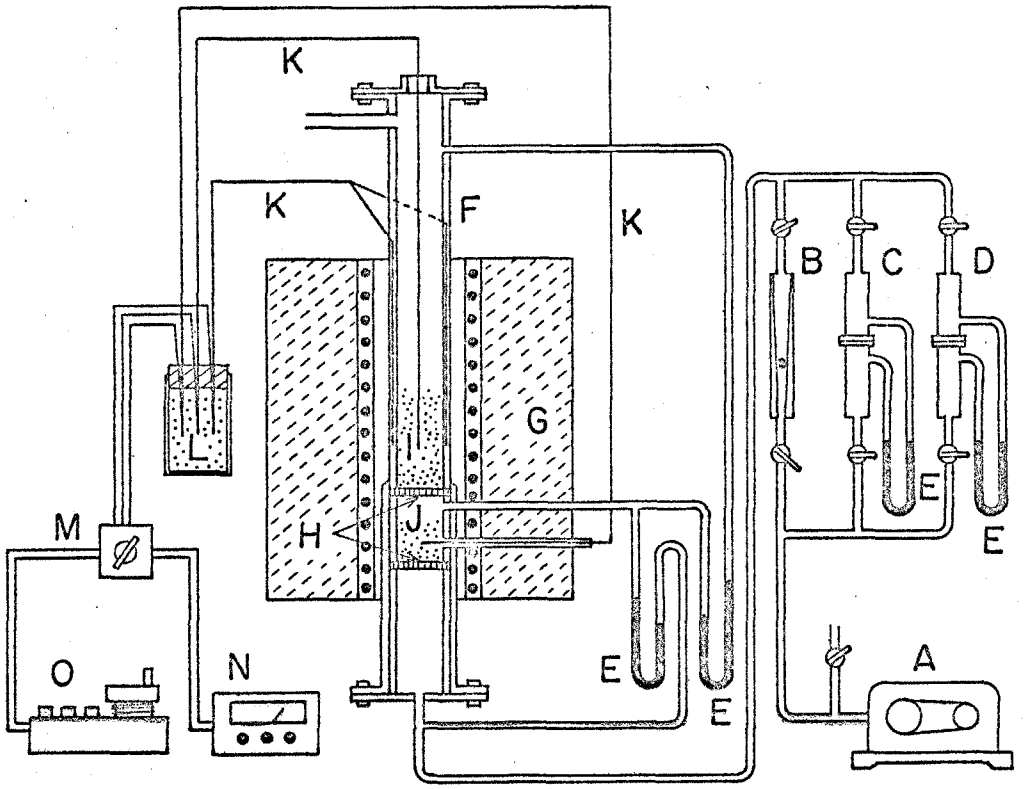


A Blower
B Rotameter(30-150 cc/sec)
C Orifice meter
(150-900 cc/sec)
D Orifice meter
(800-2600 cc/sec)
E Manometer
F Fluidization tube
G Furnace
H Distributor
I Main fluidized bed
J Lower fluidized bed
K Aeropak thermocouple
L Cold junction
M Rotary switch
N Microvoltmeter
O Potentiometer

Fig. 3.2 Apparatus

installed within a furnace whose lower, middle and upper parts are energized and controlled separately in order to realize the desired temperature profile along the tube.

The temperature of tube wall, $t_w$, and of the upper and the lower fluidized beds, $t_f$ and $t_{go}$, respectively, is measured by the 1.6 mm O.D. Aeropak chromel-alumel thermocouples. Four thermocouples for measuring $t_w$ are inserted into 4.0 mm wide and 2.5 mm deep grooves which are spaced on the outer surface of the fluidization tube at a right angle with each other. These grooves are covered with a 1.0 mm thick 18-8 stainless steel plate in order to intercept the radiation from the furnace to the thermocouples. The inlet gas temperature, $t_{go}$, was measured with a thermocouple inserted into the lower fluidized bed through a side tube welded to the fluidization tube. Another thermocouple is inserted from the top of the tube into the main fluidized bed to measure the bed temperature, $t_f$, and its e.m.f. is measured with a potentiometer. The thermocouples measuring $t_w$ and $t_{go}$ are differentially connected to the thermocouple of $t_f$ and their differential e.m.f. were measured by using a microvoltmeter.

### 3.3.2 Material

For the study on the heat transfer rate in a fluidized bed, it is desirable that the fluidized particles of known thermal properties be used and that the particles be stable both chemically and physically at elevated temperatures. And thus, quartz was firstly chosen as the fluidized material in this work.

It is said that the high heat transfer rate to and from a fluidized bed is caused by vigorous agitation of particles in the vicinity of the tube wall (5). And it is supposed that the specific heat and thermal conductivity of particles may affect the heat transfer rate. In order to see whether these effects are significant or not, fused alumina particles were also chosen as the fluidized particles whose heat content per one particle is about 1.5 times larger than that of quartz particles of the same size. Physical properties of quartz and fused alumina are summarized in Table 3.1. These particles were fluidized by air flow in the main fluidized bed.

The minimum fluidization velocity, $u_{mf}$, of the particles at 20°C was determined experimentally and the results were listed in Table 3.2.

Since it is difficult to determine $u_{mf}$ at elevated

Table 3.1 Physical properties of fluidized particles

| temperature | | 500°C | 650°C | 800°C |
|---|---|---|---|---|
| specific heat $C_p$ ($kcal/m^3.°k$) | quartz (18) | 773.1 | 705.3 | 741.4 |
| | fused alumina (18) | 1097.5 | 1160.2 | 1218.8 |
| ratio of specific heat (-) | $\frac{C_p(\text{alumina})}{C_p(\text{quartz})}$ | 1.42 | 1.64 | 1.64 |
| emissivity (-) | quartz (19) | 0.831 | 0.764 | 0.698 |
| | fused alumina (20) | 0.419 | 0.346 | 0.273 |

specific gravity (21):

quartz: 2.64 ($g/cm^3$), fused alumina: 3.99 ($g/cm^3$)

Table 3.2 Minimum fluidization velocity

| particles | size (mesh) | $u_{mf}$ at 20°C (cm/sec) | $u_{mf}$ (cm/sec) | | |
|---|---|---|---|---|---|
| | | | 500°C | 650°C | 800°C |
| quartz | 16-28 | 26.5 | 5.02 | 3.78 | 2.89 |
| | 35-42 | 21.2 | 4.02 | 3.02 | 2.32 |
| | 60-100 | 4.6 | 0.87 | 0.66 | 0.50 |
| fused alumina | 35.42 | 36.0 | 6.82 | 5.14 | 3.93 |
| | 60-100 | 12.0 | 2.27 | 1.71 | 1.31 |

temperatures experimentally, they were estimated as follows. Among evaluation of $u_{mf}$ proposed by many workers (15-17), the following equation is frequently used when the particle size is rather small (14).

$$u_{mf} = \frac{(D_p \phi_p)^2}{150} \frac{\rho_p - \rho_g}{\mu} g \frac{\varepsilon_{mf}^3}{1 - \varepsilon_{mf}} \qquad (3.18)$$

In this equation, the density of gas, $\rho_g$, is so small in comparison with that of particles, $\rho_p$, that it can be omitted. The change of density of particles with temperature is negligible. Consequently, $u_{mf}$ is to be proportional to the reciprocal of gas viscosity, $1/\mu$, and $u_{mf}$ at the bed temperature, $u_{mf(t_f)}$, can be estimated as,

$$u_{mf(t_f)} = u_{mf(20)} \frac{\mu_{(20)}}{\mu_{(t_f)}}$$

where $u_{mf(20)}$ is the minimum fluidization velocity determined at 20°C. Air velocity at 20°C corresponding to $u_{mf(t_f)}$ in the above equation is calculated by the following equation:

$$u_{mf} = \frac{293}{T_f} \frac{\mu_{(20)}}{\mu_{(t_f)}} u_{mf(20)} \qquad (3.19)$$

$u_{mf}$ at 500°, 650° and 800°C estimated with Eq. (3.19) are also summarized in Table 3.2.

Activated alumina and fused alumina particles are used as the fluidized particles in the lower fluidized bed when quartz and fused alumina particles are fluidized in the main bed, respectively. The size of particles fed into the lower fluidized bed are shown in Table 3.3. The minimum fluidization velocities of these particles are slightly lower than or equal to that of particles in the main fluidized bed.

Table 3.3 Size of fluidized particles

| main fluidized bed | | lower fluidized bed | |
|---|---|---|---|
| particles | size (mesh) | particles | size (mesh) |
| quartz | 16- 28 | activated alumina | 28- 32 |
| | 35- 42 | | 28- 32 |
| | 60-100 | | 42- 48 |
| fused alumina | 35- 42 | fused alumina | 42- 48 |
| | 60-100 | | 60-100 |

### 3.3.3 Experimental conditions

Effects of particle size, bed temperature and flow rate of air on the heat transfer coefficient were

studied. The levels of these variables are listed in Table 3.4. The possible differences in the heat transfer coefficient due to the kind of particles were also studied.

Table 3.4 Experimental conditions

| | |
|---|---|
| Fluidized particles: | 500 g of quartz<br>800 g of fused alumina |
| Particle size: | |
| quartz | : 16-28, 35-42 and 60-100 mesh |
| fused alumina | : 35-42 and 60-100 mesh |
| Bed temperature | : 500°, 650° and 800°C |
| Flow rate of air | : 2.74-27.4 cm/sec (at 20°C) |

### 3.3.4 Experimental procedure

The main fluidized bed is charged with 500 g of quartz particles or with 800 g of fused alumina particles. The electric furnace is engergized and the fluidization tube is heated to the temperature mentioned in Table 3.4. Air is blown into the fluidization tube from the bottom at a fixed flow rate

for about 30 min and the main and the lower fluidized beds are allowed to remain in their steady states.

Temperatures of the main fluidized bed, $t_f$, and of the tube wall, $t_w$, are measured at 1 cm intervals in vertical direction from the bottom of the main fluidized bed. An example of the measured temperature profile is illustrated in Fig. 3.3. The variation of wall temperature, $t_f$, was kept almost unchanged throughout the bed. Mean values of $t_f$ and of $t_w$ were inserted to Eqs. (3.11) and (3.16) and $h_c$ and $h_r$ were calculated. Temperature of the lower fluidized bed, $t_{go}$, was also measured and it was used in the calculation of $h_c$ by Eq. (3.11).

Height of the main fluidized bed, $L_f$, was estimated from the relationship between the height from distributor and the pressure difference. Pressure difference was measured by inserting a 10 mm O.D. quartz tube pressure detector from the top of the fluidization tube into the main fluidized bed. This tube was perforated with a 3.5 mm D. hole at a position of 20 mm apart from the closed top. This hole was covered with a 300 mesh stainless steel screen. The other end of this tube was connected to a manometer. Fig. 3.4 illustrates an example of the pressure difference. It is seen in this figure that the pressure

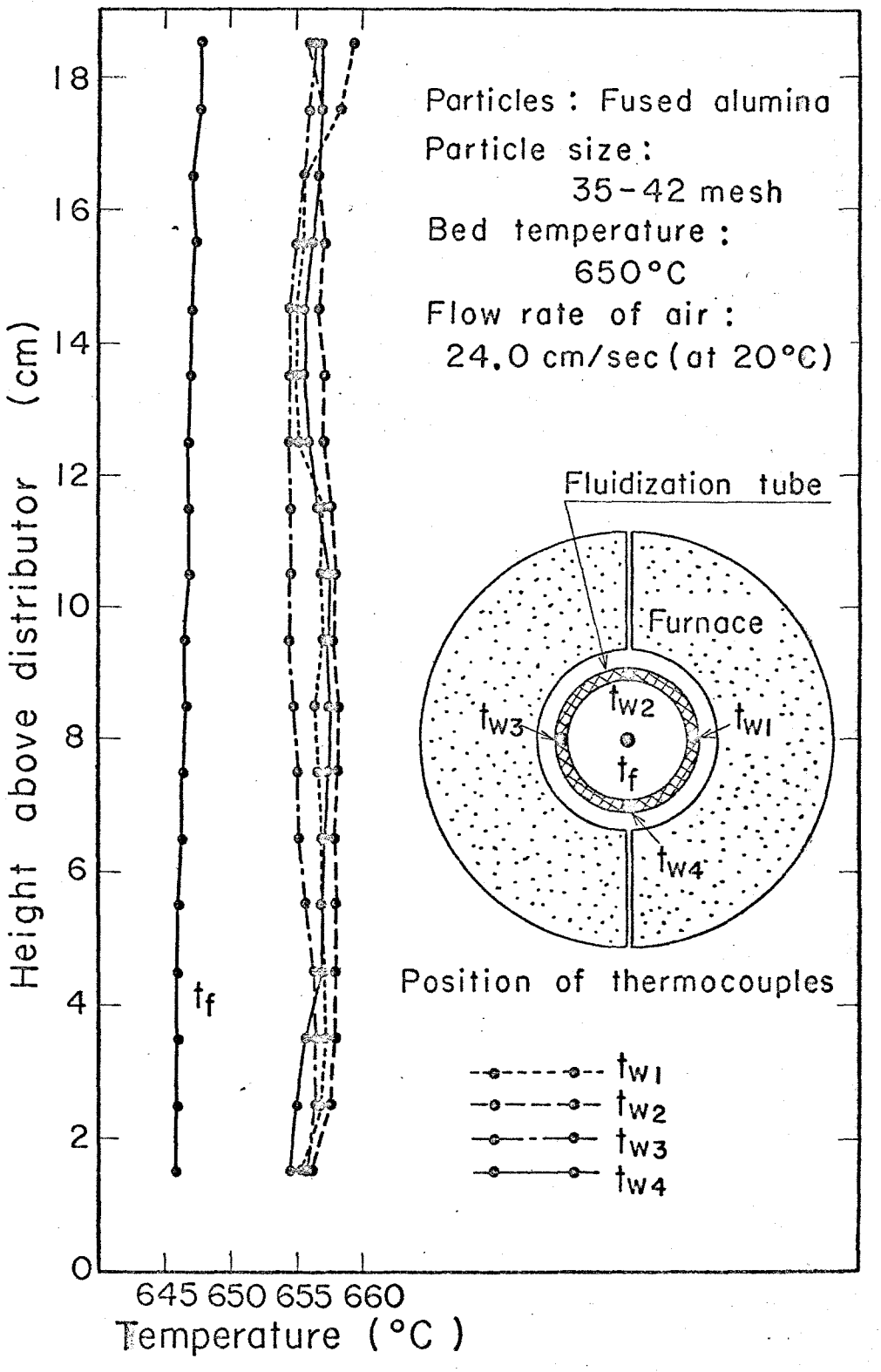


Fig. 3.3 An example of temperature profile along the bed height

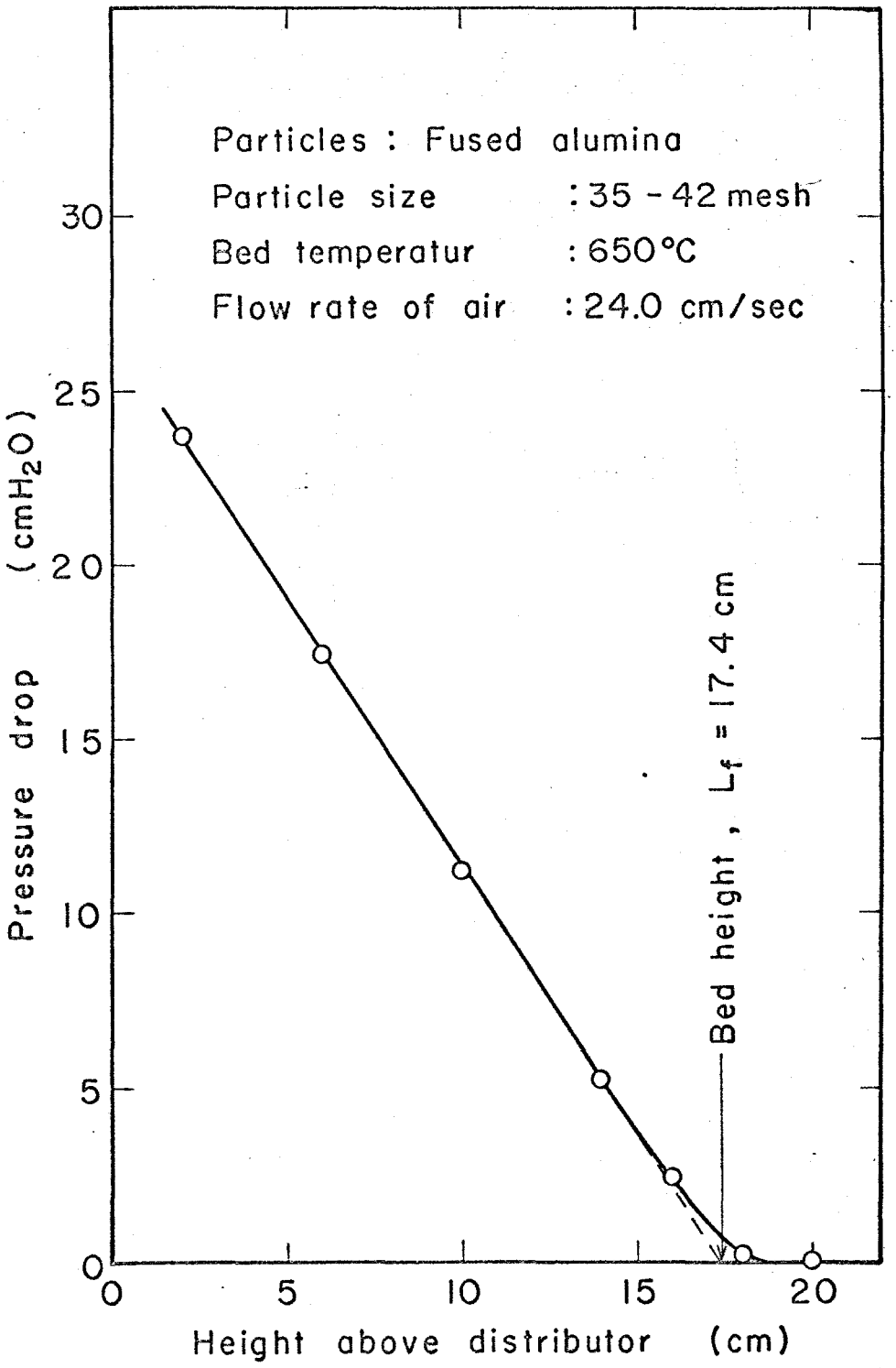


Fig.3.4 An example of estimation of bed height

difference decreases linearly with the height above the distributor and the extrapolated straight line to zero gives the bed height, $L_f$.

## 3.4 Experimental results

Figs. 3.5 and 3.6 represent the film coefficient of heat transfer between the tube wall and the fluidized bed, $h_w$. Fluidized particles were quartz and fused alumina, respectively. It is seen from these figures that the effects of particle size and of bed temperature on $h_w$ are scarcely observed and that $h_w$ increases with the flow rate of air. Baerg, Klassen and Gisher (22) and Bartholomew and Katz (23) mentioned that $h_w$ increases as the air velocity increases and it decreases with further increase in air velocity. This tendency of $h_w$ can not be clarified in the range of air velocity adopted in this work. Any difference in $h_w$ was not found between quartz and fused alumina.

Radiative heat transfer coefficient, $h_r$, was calculated by using Eq. (3.16). Effects of air velocity and of particle size on $h_r$ were scarcely detected, and the bed temperature remarkably affects $h_r$. The values of $h_r$ at each bed temperature were

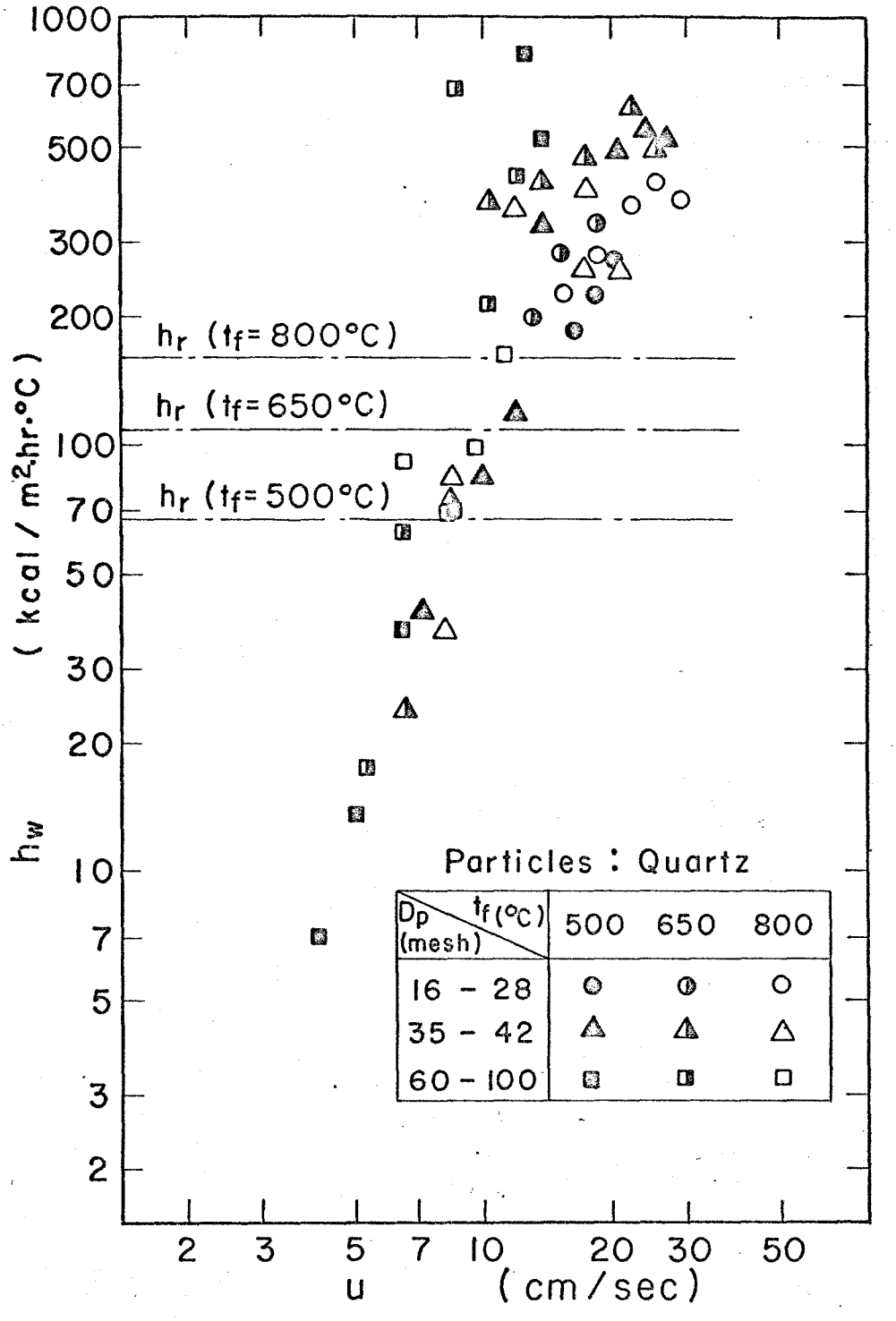


Fig. 3.5 Heat transfer coefficient, $h_w$

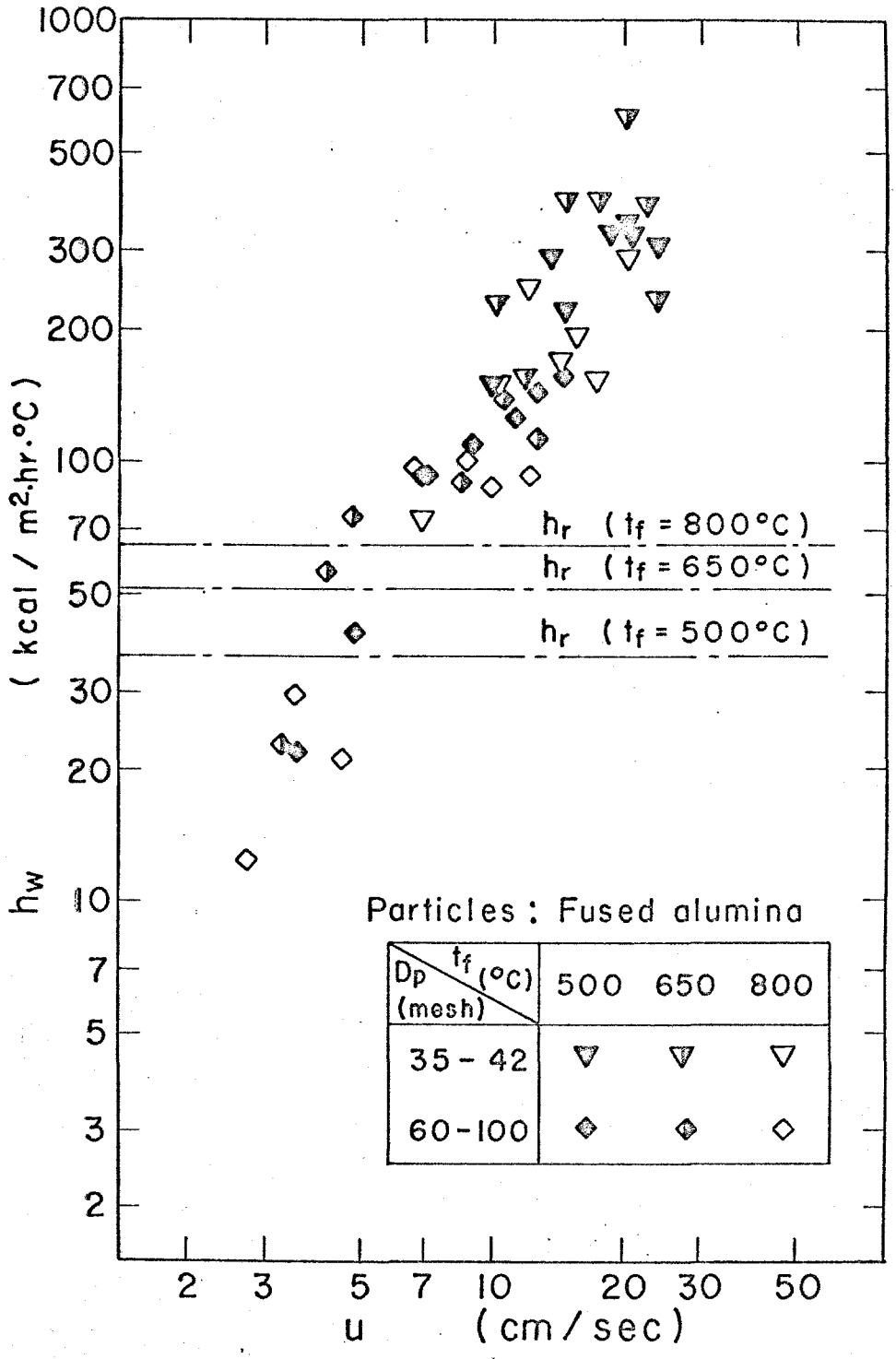


Fig. 3.6 Heat transfer coefficient, $h_w$

within the following range.

Quartz:

| | | |
|---|---|---|
| 500°C | 60- 70 | (kcal/m$^2$·hr·°C) |
| 650°C | 108-110 | ( 〃 ) |
| 800°C | 159-162 | ( 〃 ) |

Fused alumina:

| | | |
|---|---|---|
| 500°C | 35-36 | (kcal/m$^2$·hr·°C) |
| 650°C | 51-52 | ( 〃 ) |
| 800°C | 64-65 | ( 〃 ) |

Their means were also demonstrated in Figs. 3.5 and 3.6, respectively.

It can be said from these figures that $h_w$ is lower than $h_r$ at lower air velocities and that $h_w$ exceeds $h_r$ at higher air velocities. This tendency indicates that the mechanism of heat transfer by radiation becomes very important at elevated temperatures, especially when air velocity is lower. It is said that the film coefficient of heat transfer between tube wall and fluidized bed is usually at about 100 to 600 kcal/m$^2$·hr·°C (30). However, it is seen in Fig. 3.5 that $h_w$ was measured at a value lower than 10 kcal/m$^2$·hr·°C at lower flow rate of air. This lower value of $h_w$ may be caused by the overestimation of $h_r$ which was calculated with Eq. (3.16) on the assumption that $T_p = T_f$.

## 3.5 Discussion

As mentioned in 3.1, most of the previous works (1, 4, 5, 24) on the heat transfer problem in the fluidized bed were carried out at a lower temperature below 200°C, where the radiative heat transfer can be omitted. In this work, on the other hand, film coefficient of heat transfer, $h_w$, was obtained at elevated temperatures of 500° to 800°C by subtracting the radiative heat transfer coefficient, $h_r$, from the overall heat transfer coefficient, $h_c$. It is of basic interest to compare the magnitude of $h_w$ obtained in this work with those obtained by many workers at lower temperature. Since each worker carried out the measurement under different conditions, it may not be a reasonable way to compare the values of $h_w$ itself. Many workers transformed their data into dimensionless numbers and the correlationship was investigated. Among them, the Reynolds number ($Re = D_p G/\mu$) and the Nusselt number ($Nu = h_w D_p/k_g$) were frequently used.

Fig. 3.7 represents the correlationship between Re and Nu calculated from the data obtained in this work. From this figure, the following regression equation can be obtained by the least squares method.

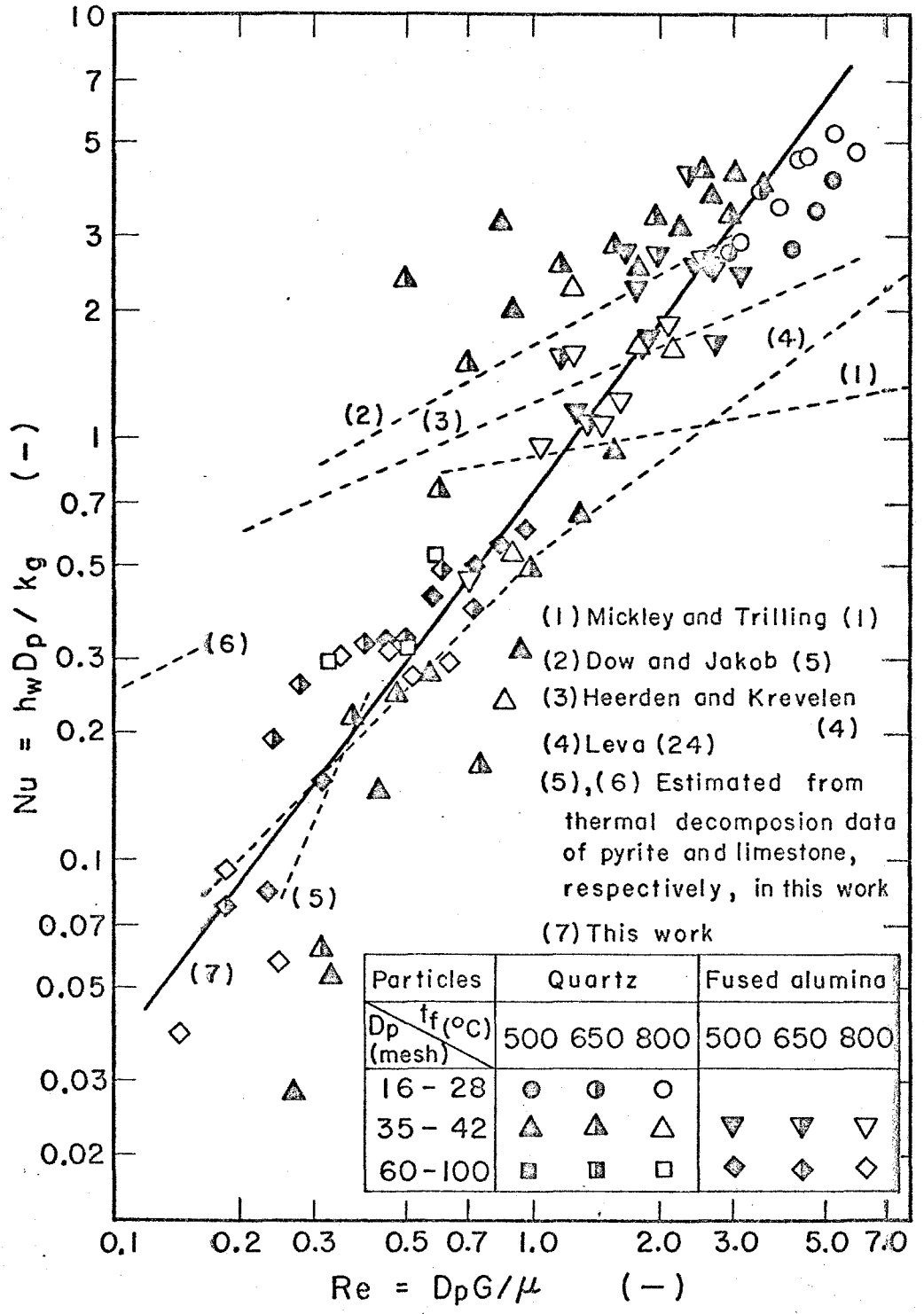


Fig.3.7 Correlationship between Re and Nu

$$Nu = 0.751\, Re^{1.32} \qquad (3.20)$$

The regression lines calculated from the data obtained by Mickley and Trilling (1), Dow and Jakob (5), Heerden and Krevelen (4) and Leva (24) are also illustrated with broken lines in the same figure. Although the coincidence between the regressions of these workers is rather poor, it may be said that the regression obtained in this work coincides fairly well with theirs.

In addition to these results, the correlationship between Re and Nu obtained from the thermal decomposition study of pyrite and limestone particles in a fluidized bed which will be described later are also illustrated in this figure.

It is said that the heat transfer rate between the tube wall and the fluidized bed is affected by the fluidization quality (26). $u/u_{mf}$ and $(u-u_{mf})/u_{mf}$ are often used as the measure of fluidization quality (2, 4). And $h_w$ obtained in this work were plotted against $(u-u_{mf})/u_{mf}$ in Figs. 3.8 and 3.9. These figures indicate a segregation of the data of $h_w$ due to the particle size and $h_w$ for the smaller particle size are lower than those for the larger particle size at a fixed $(u-u_{mf})/u_{mf}$.

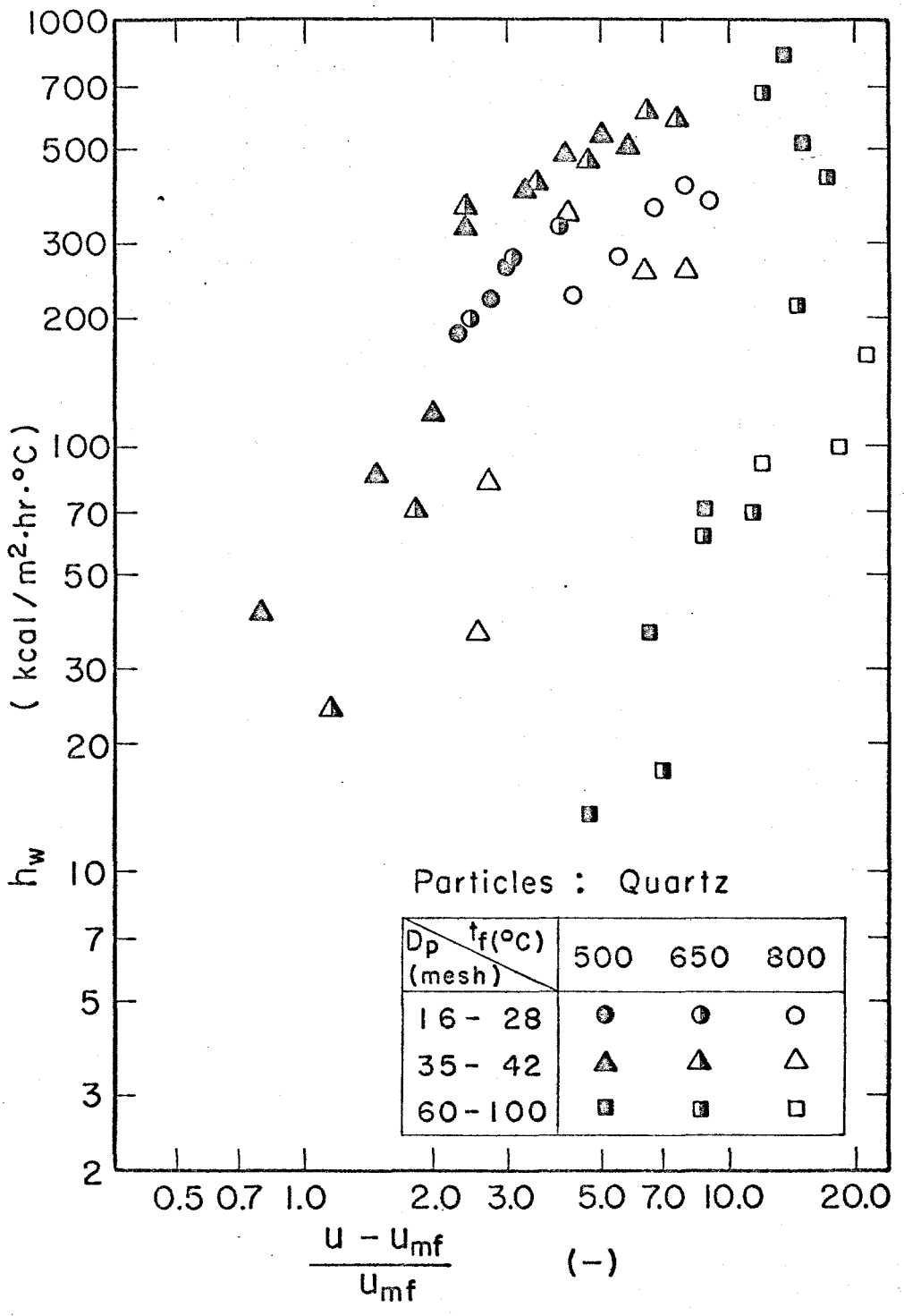


Fig. 3.8 $h_w$ vs. $\frac{u - u_{mf}}{u_{mf}}$

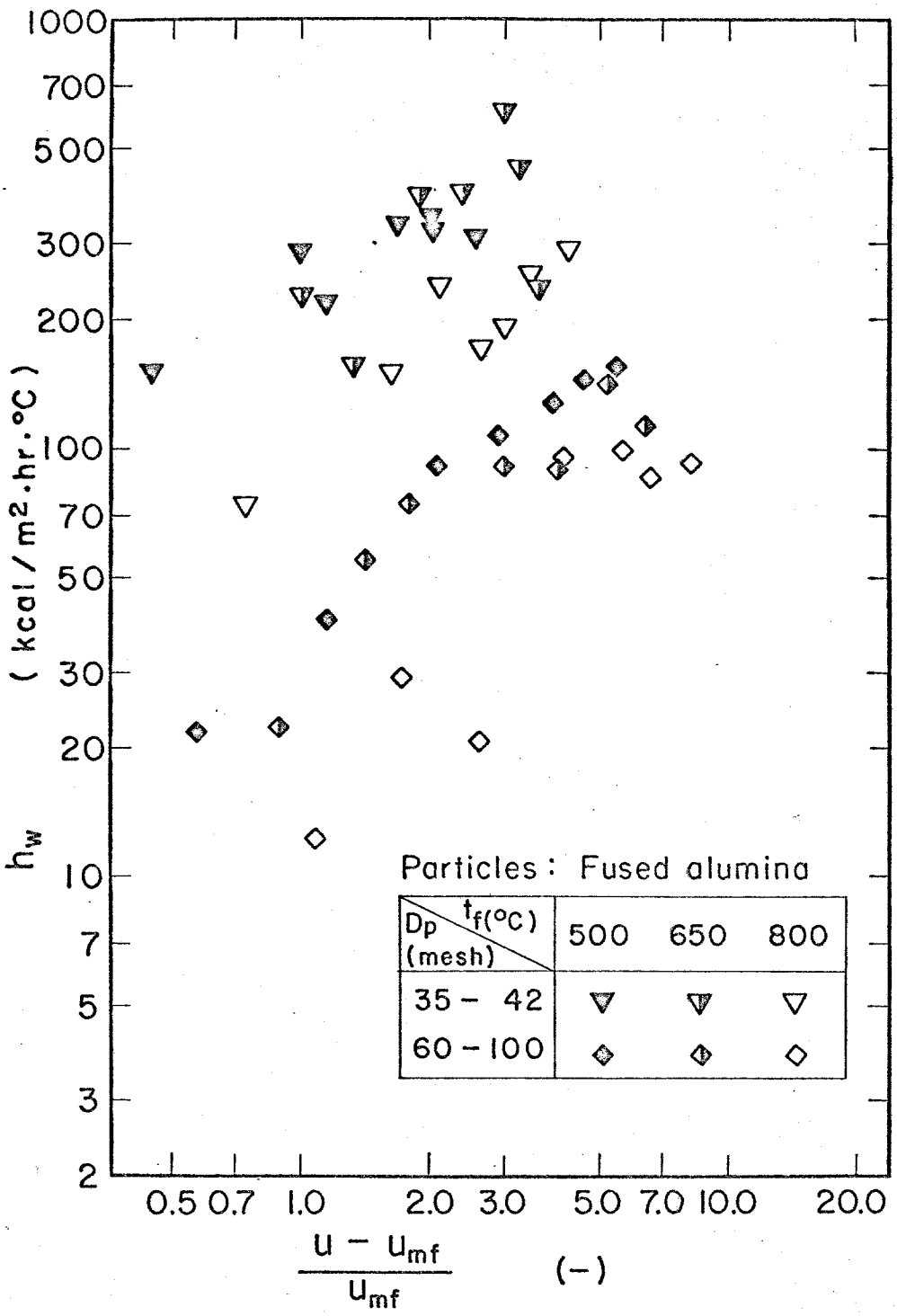


Fig. 3.9 $h_w$ vs. $\frac{u - u_{mf}}{u_{mf}}$

As pointed out by Dow and Jakob (5), the heat transfer between the tube wall and the fluidized bed is accelerated by vigorous circulation of fluidized particles. On the other hand, the excessive air above the minimum fluidization passes through the bed in the form of bubbles and the circulation of particle is mainly caused by these ascending bubbles (27). Keeping these facts in mind, $h_w$ were plotted in Figs. 3.10 and 3.11 against the linear velocity of air above the minimum fluidization at the bed temperature, $(u-u_{mf})T_f/293$. In these figures, segregation of data on $h_w$ is scarcely found, though the variation in $h_w$ seems to be somewhat larger than that in Figs. 3.5 and 3.6.

In Chapter 2, mean, $\mu_c$, and variance, $\sigma_c^2$, of local particle concentration in the fluidized bed were studied in addition to the size and frequency of bubbles, y and f, respectively. It is of interest to pursue the correlationship between heat transfer coefficient and these fluidization characteristics.

Among these characteristics, $\sigma_c^2$ is a measure of nonuniformity in fluidized bed in terms of particle concentration difference between bubble and dense phases. It was mentioned in Chapter 2 that $\sigma_c^2$ increases with the height above the distributor and its

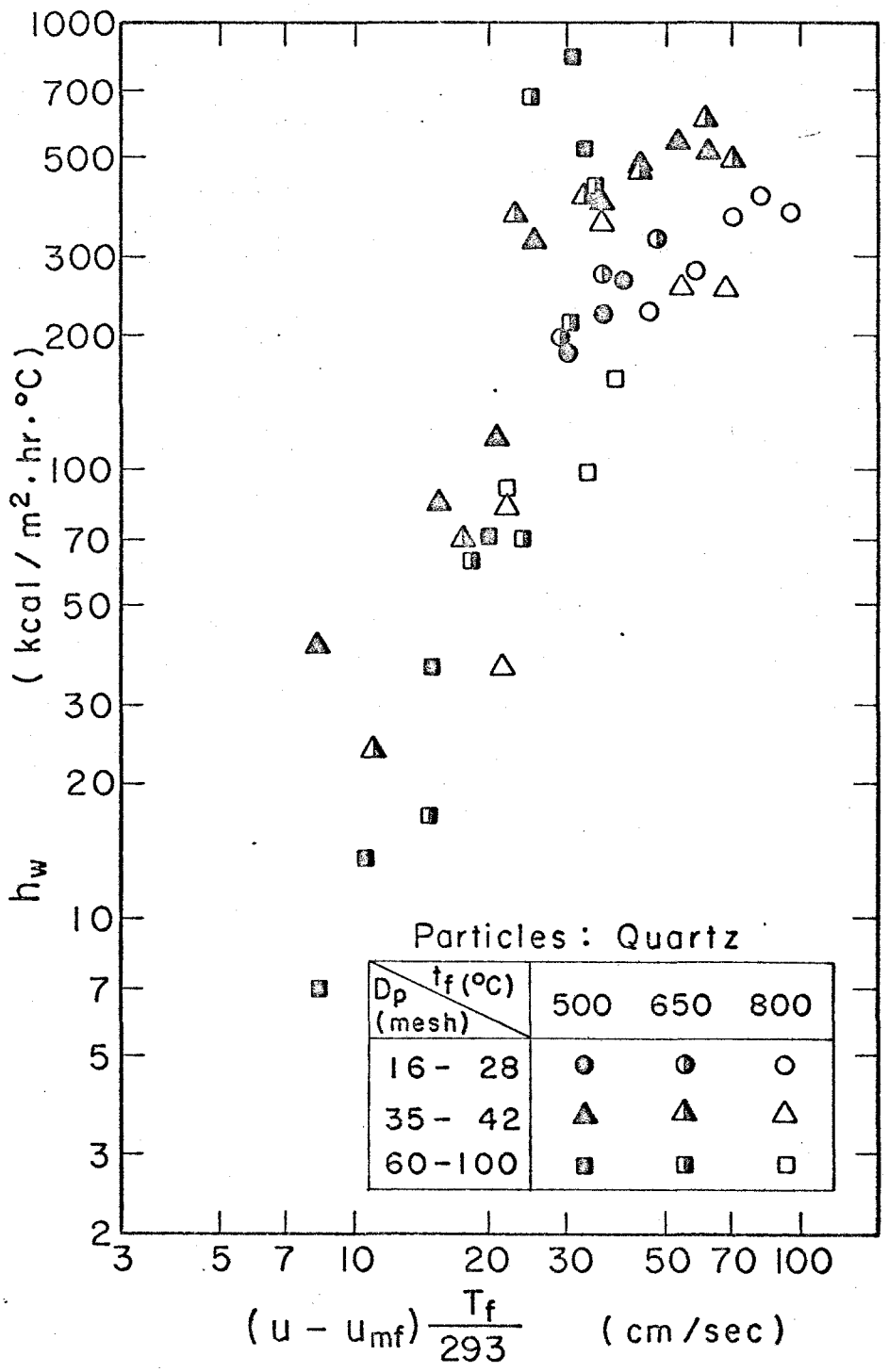


Fig. 3.10 $h_w$ vs. $(u - u_{mf})\frac{T_f}{293}$

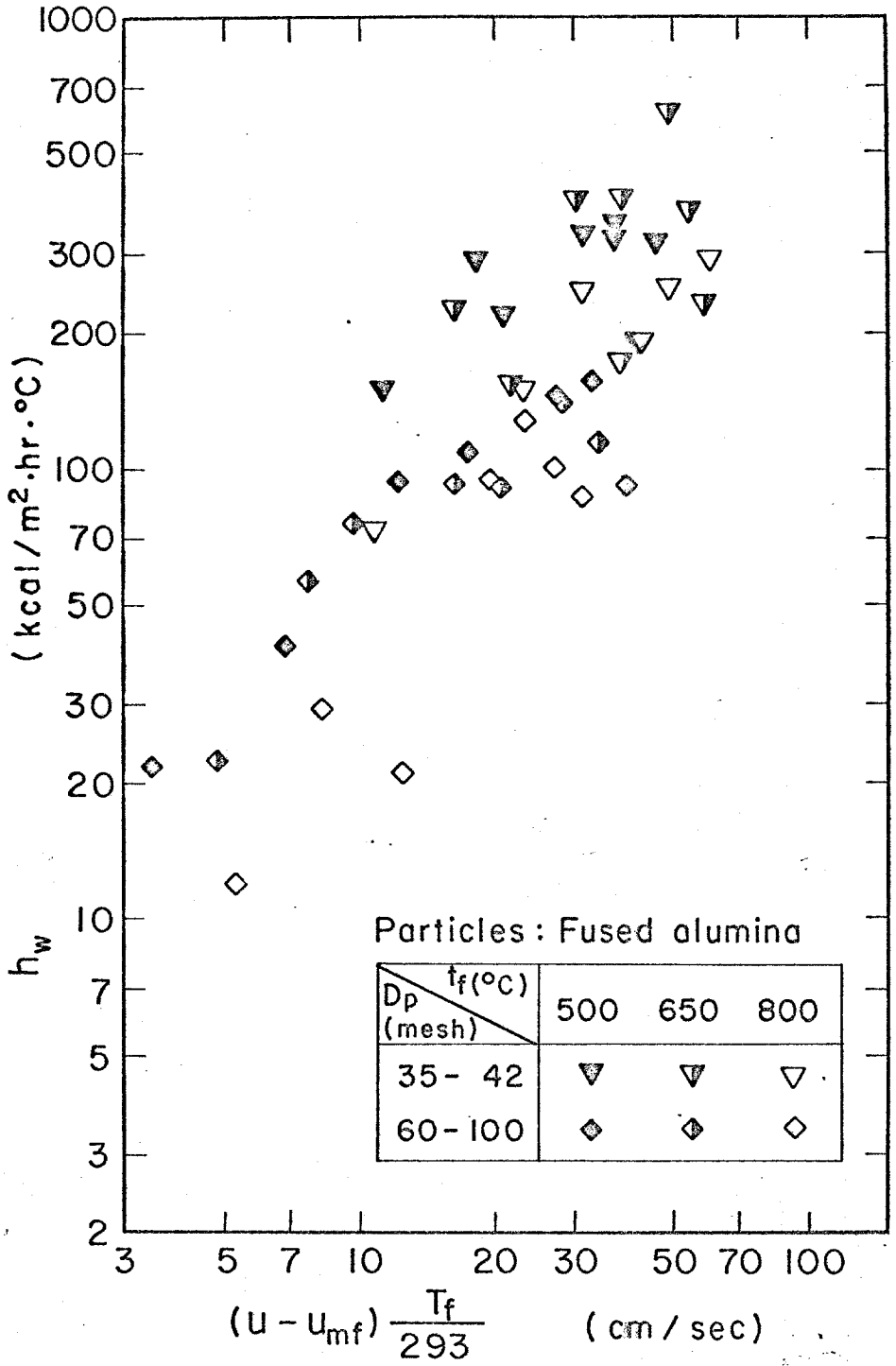


Fig.3.11 $h_w$ vs. $(u - u_{mf}) \frac{T_f}{293}$

variation becomes so slight in the upper part of the bed. This was demonstrated in Fig. 2.8. Mean of $\sigma_c^2$ in the upper part of the fluidized bed was denoted by $\bar{\sigma}_{cm}^2$. $\bar{\sigma}_{cm}^2$ are estimated and correlated with $h_w$ as follows.

In this study, the height of settled bed, $L_c$, and tube diameter, $D_t$, are 10.0 and 6.1 cm, respectively, and thus $L_c/D_t = 1.64$. Fig. 3.12 (a) represents the relationship between $\bar{\sigma}_{cm}^2$ and $L_c/D_t$ at each level of $(u-u_{mf})$. This figure was reproduced from Fig. 2.9 in Chapter 2. $\bar{\sigma}_{cm}^2$ at $L_c/D_t = 1.64$ shown in this figure was plotted against $(u-u_{mf})$ in Fig. 3.12 (b). This is for estimating $\bar{\sigma}_{cm}^2$ from $(u-u_{mf})$ under the experimental conditions. The abscissa of Fig. 3.12 (b) given by $(u-u_{mf})$ at room temperature is to be modified into the linear velocity of air at the bed temperature, $T_f$, which is given by $(u-u_{mf})T_f/293$. Thus, in estimating $\bar{\sigma}_{cm}^2$ from this figure, $\bar{\sigma}_{cm}^2$ corresponding to the value of $(u-u_{mf})T_f/293$, instead of $(u-u_{mf})$, was read. Fig. 3.13 represents the correlation between $h_w$ and $\bar{\sigma}_{cm}^2$ thus estimated. Most of the estimated $\bar{\sigma}_{cm}^2$ is less than 0.12. It is seen in this figure that $h_w$ is widespread at a given value of $\bar{\sigma}_{cm}^2$. This variation of $h_w$ is thought to be caused by the curved form of Fig. 3.12 (b) and it is thought

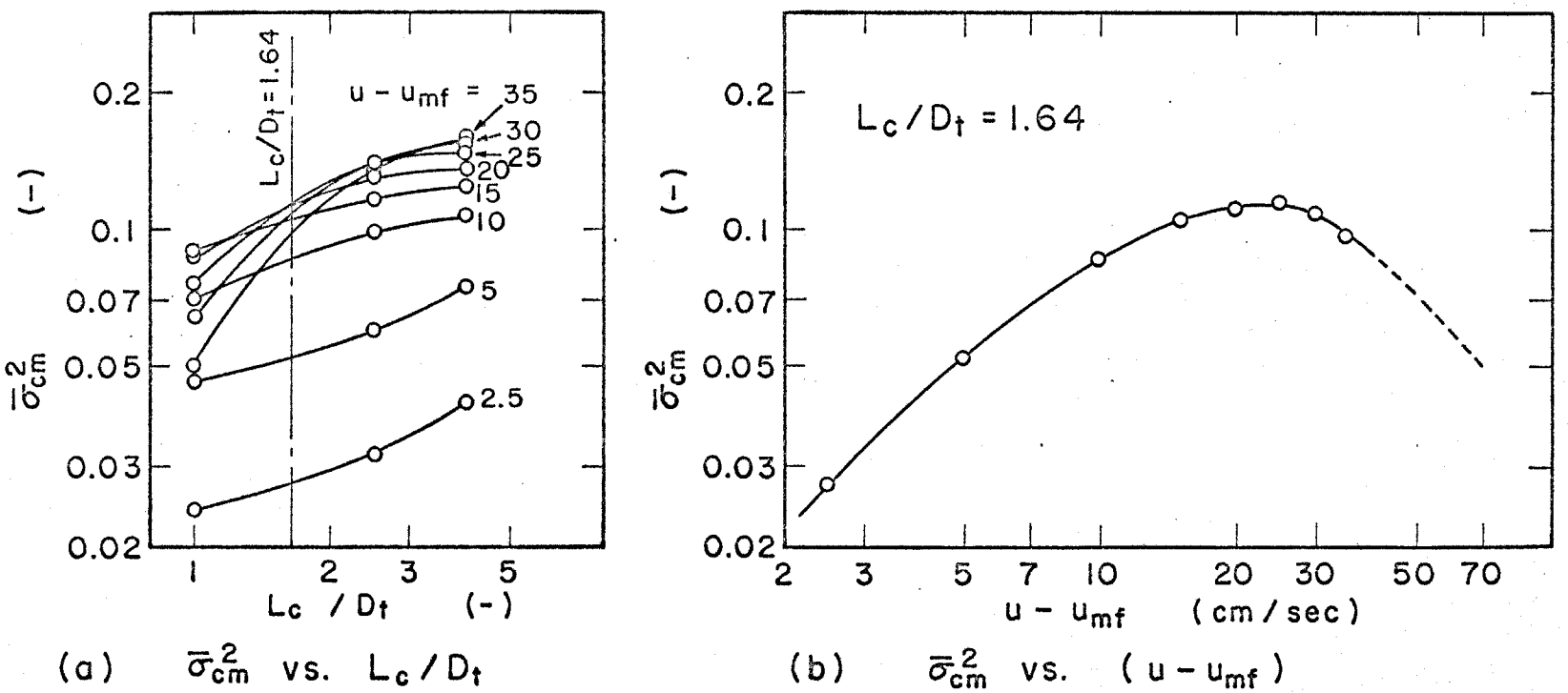


(a) $\bar{\sigma}^2_{cm}$ vs. $L_c / D_t$

(b) $\bar{\sigma}^2_{cm}$ vs. $(u - u_{mf})$

Fig. 3.12 Estimation of $\bar{\sigma}^2_{cm}$ at $L_c / D_t = 1.64$

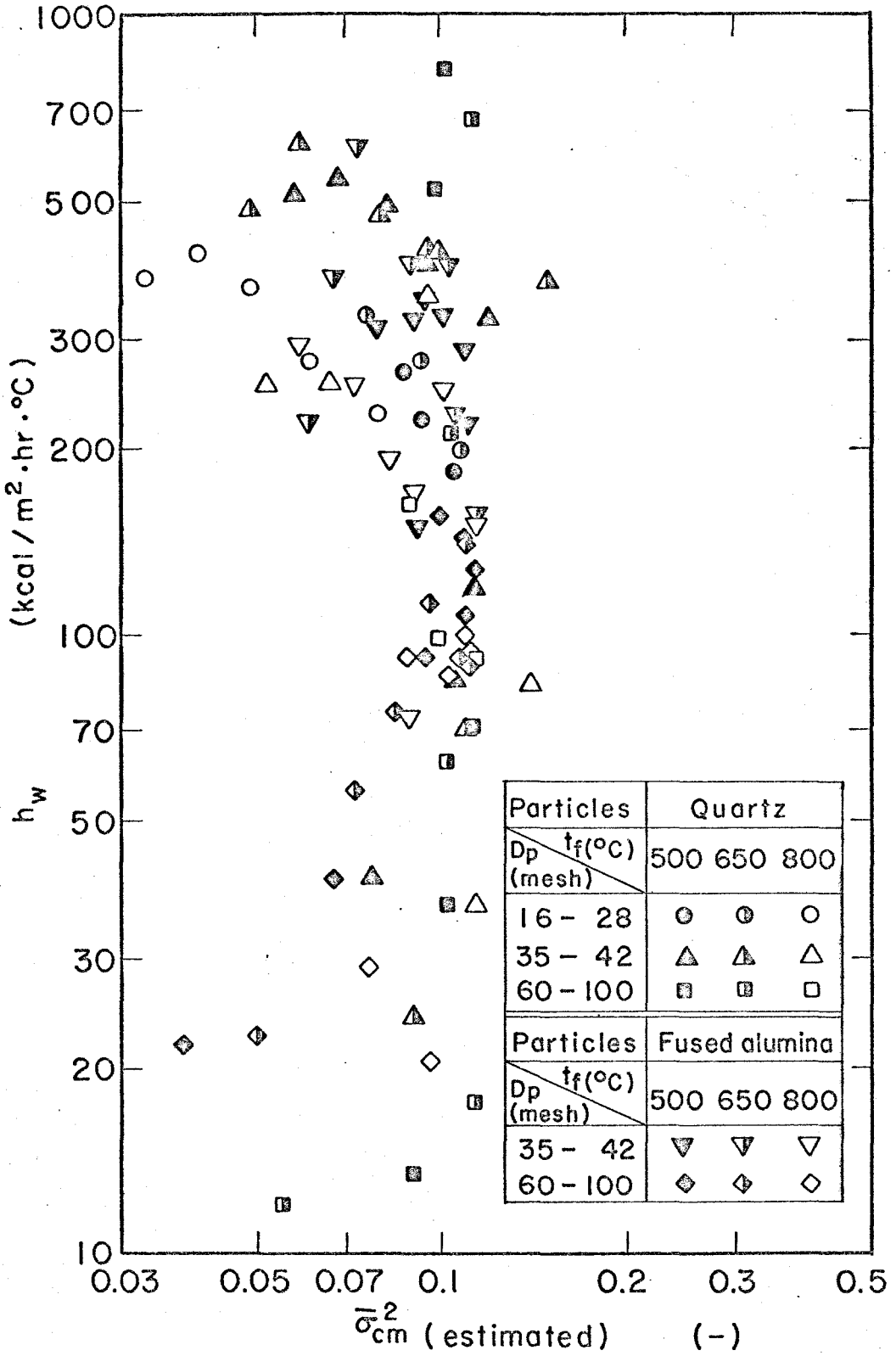


Fig.3.13 Correlationship between $h_w$ and $\bar{\sigma}^2_{cm}$(estimated)

that $\bar{\sigma}_{cm}^2$ may not necessarily be a useful measure of fluidization quality which represents the heat transfer coefficient.

Another measure of fluidization quality is the mean of local particle concentration, $\mu_c$, in the fluidized bed. As shown in Fig. 2.6, $\mu_c$ varies scarcely throughout the bed except in the vicinity of the distributor. $\bar{\mu}_{cm}$, mean of $\mu_c$, decreases linearly with increasing excessive air velocity above the minimum fluidization. This was shown in Fig. 2.7. It is supposed, therefore, that the relationship between $h_w$ and $\bar{\mu}_{cm}$ on logarithmic scales will become a linear one with negative slope because $h_w$ increases linearly with $(u-u_{mf})T_f/293$ on logarithmic scale as shown in Figs. 3.10 and 3.11.

Mickley and Trilling (1) and Wender and Cooper (28) mentioned that the heat transfer coefficient increases with air velocity when it is lower but the coefficient decreases with further increase in air velocity. They suggested that the decrease in heat transfer coefficient at higher air velocities is caused by the lowered particle concentration. Thus, the lowered $\bar{\mu}_{cm}$ may cause the decrease of $h_w$, according to them. However, $h_w$ increases with decreasing $\bar{\mu}_{cm}$ in the range of air velocities studied in this work which

corresponds to the lower air velocity region of the above-mentioned workers. In this region of air velocity, it is thought that the increase of air velocity causes intensified circulation of particles rather than the decrease in effective surface area for heat transfer.

To verify this further, the circulation rate of particles in the fluidized bed is discussed. Movement of particles in the fluidized bed is caused by the ascending bubbles (27). It is suggested by Woolard and Potter (29) that the amount of particles associated with an ascending bubble increases with the bubble size. And thus the size and frequency of bubbles become important factors in the circulation rate of particles. Among them, the bubble frequency is scarcely affected by air velocity as shown in Fig. 2.10. And consequently, it is of interest to investigate the correlationship of $h_w$ with the bubble size.

Correlation between the vertical thickness of bubbles, y, and the height above distributor, z, was shown in Fig. 2.11. y at z = 15 cm which is the height of fluidized bed in this work was estimated from Fig. 2.11 and they are plotted against $(u-u_{mf})$ in Fig. 3.14. It seems that y increases linearly with

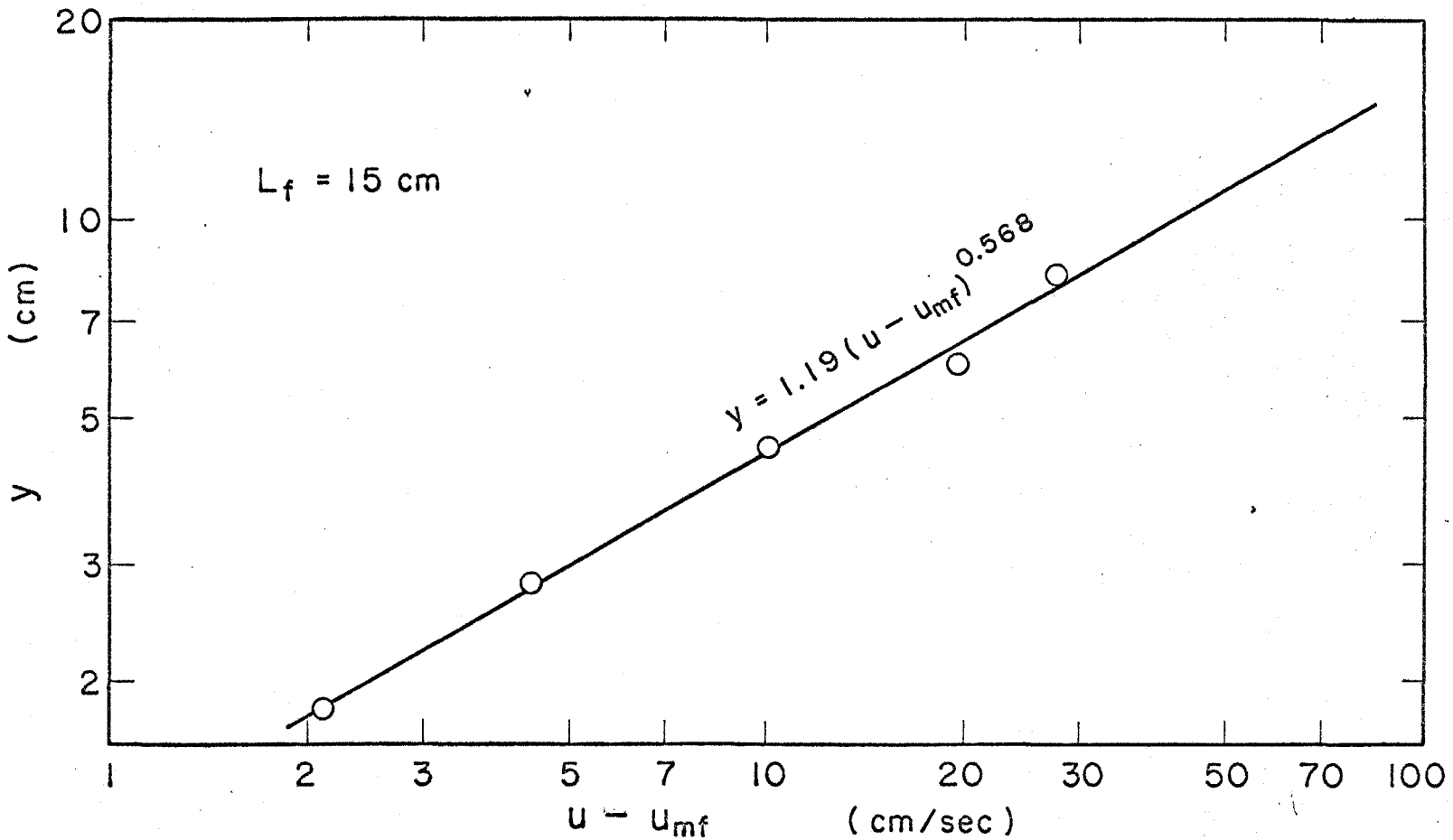


Fig. 3.14 Estimation of vertical thickness of bubble

excess air velocity on logarithmic scales, and the following regression was obtained.

$$y = 1.19\,(u - u_{mf})^{0.568} \tag{3.21}$$

Excessive air velocity at the bed temperature is expressed by $(u-u_{mf})T_f/293$ and, instead of Eq. (3.21), the following expression is to be used for estimating y in the upper part of the fluidized bed.

$$y = 1.19\left\{(u - u_{mf})\frac{T_f}{293}\right\}^{0.568} \tag{3.22}$$

Fig. 3.15 demonstrates the correlationship between $h_w$ and y thus estimated. It is seen in this figure that the segregation of $h_w$ due to the kind and size of particles and to the bed temperature is scarcely observed and that $h_w$ increases with y. It can be said from this figure that, in the range of air velocity studied, the heat transfer coefficient, $h_w$, increases with air velocity because of intensifying particle circulation which is caused by ascending bubbles through the fluidized bed.

Finally, it is of interest to correlate the data of heat transfer in the form of dimensionless number with dimensionless fluidization characteristics. Fluidizing conditions studied in this work include the

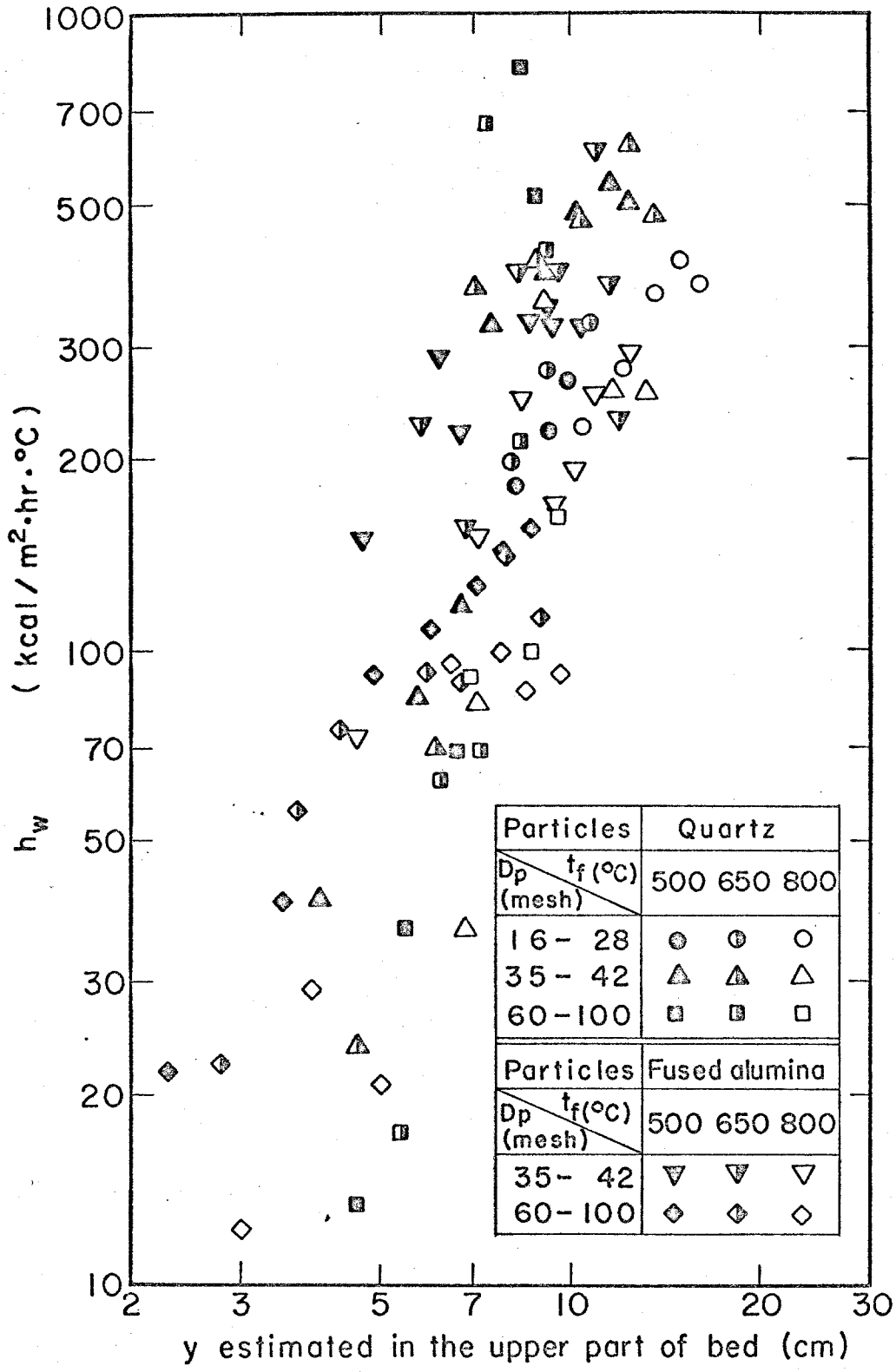


Fig.3.15 Correlationship between $h_w$ and y estimated in the upper part of fluidized bed

size, specific heat and density of the fluidized particle, air velocity, and bed temperature, and the following dimensionless expression is presumed.

$$Nu = a\,Re^{b}\left(\frac{C_p}{C_g}\right)^{c}\left(\frac{\rho_p}{\rho_g}\right)^{d}\left(\frac{D_p}{D_t}\right)^{e} \tag{3.23}$$

The constants, a, b, c, d and e in this equation were estimated by the least squares method by using 88 sets of data for quartz and fused alumina particles and the resulting regression equation is,

$$Nu = 0.00014\,Re^{1.77}\left(\frac{C_p}{C_g}\right)^{-2.85}\left(\frac{\rho_p}{\rho_g}\right)^{0.32}\left(\frac{D_p}{D_t}\right)^{-1.11} \tag{3.24}$$

Statistical significance of this equation and of its individual components were tested. Total sum of squares of logNu and its degrees of freedom are,

$$\left.\begin{aligned} S_T &= \Sigma(\log Nu)^2 - \frac{(\Sigma \log Nu)^2}{88} = 28.96 \\ \phi_T &= 88 - 1 = 87 \end{aligned}\right\} \tag{3.25}$$

Residual sum of squares from Eq. (3.24) and its degees of freedom are,

$$\left.\begin{aligned} S_E &= \Sigma\left\{\log Nu - \log 0.00014\,Re^{1.77}\left(\frac{C_p}{C_g}\right)^{-2.85}\left(\frac{\rho_p}{\rho_g}\right)^{0.32}\left(\frac{D_p}{D_t}\right)^{-1.11}\right\}^2 \\ &= 4.56 \end{aligned}\right\} \tag{3.26}$$

$$\phi_E = 88 - 5 = 83$$

and the sum of squares due to regression and its degrees of freedom are,

$$\left.\begin{aligned} S_R &= S_T - S_E = 24.40 \\ \phi_R &= \phi_T - \phi_E = 4 \end{aligned}\right\} \quad (3.27)$$

F-ratio for testing the statistical significance of Eq. (3.24) was calculated as,

$$F_o = \frac{S_R / \phi_R}{S_E / \phi_E} = 110.9^{**} \quad (3.28)$$

$F_o$ is larger than its critical value of F(4, 83; 0.01) ($< F(4, 60; 0.01) = 3.65$). This means that Eq. (3.24) is significant to express Nu.

Sum of squares due to the individual terms in Eq. (3.24) are,

Re: 9.517

$C_p/C_g$: 0.185

$\rho_p/\rho_g$: 0.085

$D_p/D_t$: 0.934

and the degrees of freedom of each of these terms are 1. Among these four terms, the contribution of $\rho_p/\rho_g$ on Nu is minimum and its significance was tested.

$$F_o = \frac{0.085}{4.56/83} = 1.55 \quad (3.29)$$

$F_o$ is less than its critical value of F(1, 83; 0.05) (>F(1, 120; 0.05) = 3.92). And the term of $\rho_p/\rho_g$ in Eq. (3.24) is not significant and it can be discarded from Eq. (3.23).

Excluding the term of $\rho_p/\rho_g$ from Eq. (3.23) gives

$$Nu = a' Re^{b'} \left(\frac{C_p}{C_g}\right)^{c'} \left(\frac{D_p}{D_t}\right)^{e'} \qquad (3.30)$$

The constants a', b', c' and e' in this equation were estimated by the least squares method and the following regression was obtained.

$$Nu = 0.0029 Re^{1.74} \left(\frac{C_p}{C_g}\right)^{2.09} \left(\frac{D_p}{D_t}\right)^{-1.08} \qquad (3.31)$$

$S_R$ and $S_E$ and their degrees of freedom are,

$$\left.\begin{aligned} S_R &= 24.40 - 0.085 = 24.31 \quad , \quad \phi_R = 3 \\ S_E &= 4.56 + 0.085 = 4.65 \quad , \quad \phi_E = 84 \end{aligned}\right\} \qquad (3.32)$$

F-ratio for testing the significance of Eq. (3.31) is,

$$F_o = \frac{S_R / \phi_R}{S_E / \phi_E} = 146.4^{**} \qquad (3.33)$$

which is larger than its critical value of F(3, 84; 0.01) (<F(3, 60; 0.01) = 4.13). This means that Eq. (3.31) is statistically significant.

Sum of squares due to the individual terms in Eq. (3.31) are,

Re: 9.514

$C_p/C_g$: 0.118

$D_p/D_g$: 0.889

A similar test of significance on the term of $C_p/C_g$ whose contribution to Eq. (3.31) is minimum reveals that $C_p/C_g$ is not significant at a significance level of 5 per cent. Further exclusion of this term from Eq. (3.30) gives

$$Nu = a'' Re^{b''} \left(\frac{D_p}{D_t}\right)^{e''} \tag{3.34}$$

By using the least squares method, the constants a", b", and e" were estimated and the following regression was obtained.

$$Nu = 0.0031\, Re^{1.71} \left(\frac{D_p}{D_t}\right)^{-1.04} \tag{3.35}$$

$S_R$ and $S_E$ and their degrees of freedom on Eq. (3.35) are,

$$\left.\begin{aligned} S_R &= 24.31 - 0.118 = 24.19\ , \quad \phi_R = 2 \\ S_E &= 4.65 + 0.118 = 4.77\ , \quad \phi_E = 85 \end{aligned}\right\} \tag{3.36}$$

By a similar test of significance, Eq. (3.35) was found to be statistically significant. Sum of squares due to the individual terms in Eq. (3.35) are,

Re: 9.512

$D_p/D_t$: 0.837

Contribution of the term of $D_p/D_t$ to Nu is less than that of Re and the F-ratio for testing its significance is calculated as,

$$F_o = \frac{0.837}{4.77/85} = 14.92^{**} \qquad (3.37)$$

$F_o$ is larger than its critical value of F(1, 85: 0.01) (<F(1, 60; 0.01) = 7.08), which means that the term $D_p/D_t$ can not be discarded from Eq. (3.35).

From these statistical investigations, it was concluded that Eq. (3.35) can be adopted as a dimensionless expression of Nu. Fig. 3.16 illustrates the correlationship between the observed Nu and the calculated Nu with Eq. (3.35). It is seen in this figure that any segregation of Nu(obs.) due to the fluidizing conditions are not observed and that the calculated Nu coincides well with the observed values.

## 3.6 Summary

Film coefficient of heat transfer between the wall of fluidization tube and the fluidized bed, $h_w$, was measured at the temperatures of 500°, 650°, and 800°C; the overall heat transfer coefficient, $h_c$, was measured and the radiative heat transfer coefficient, $h_r$, was

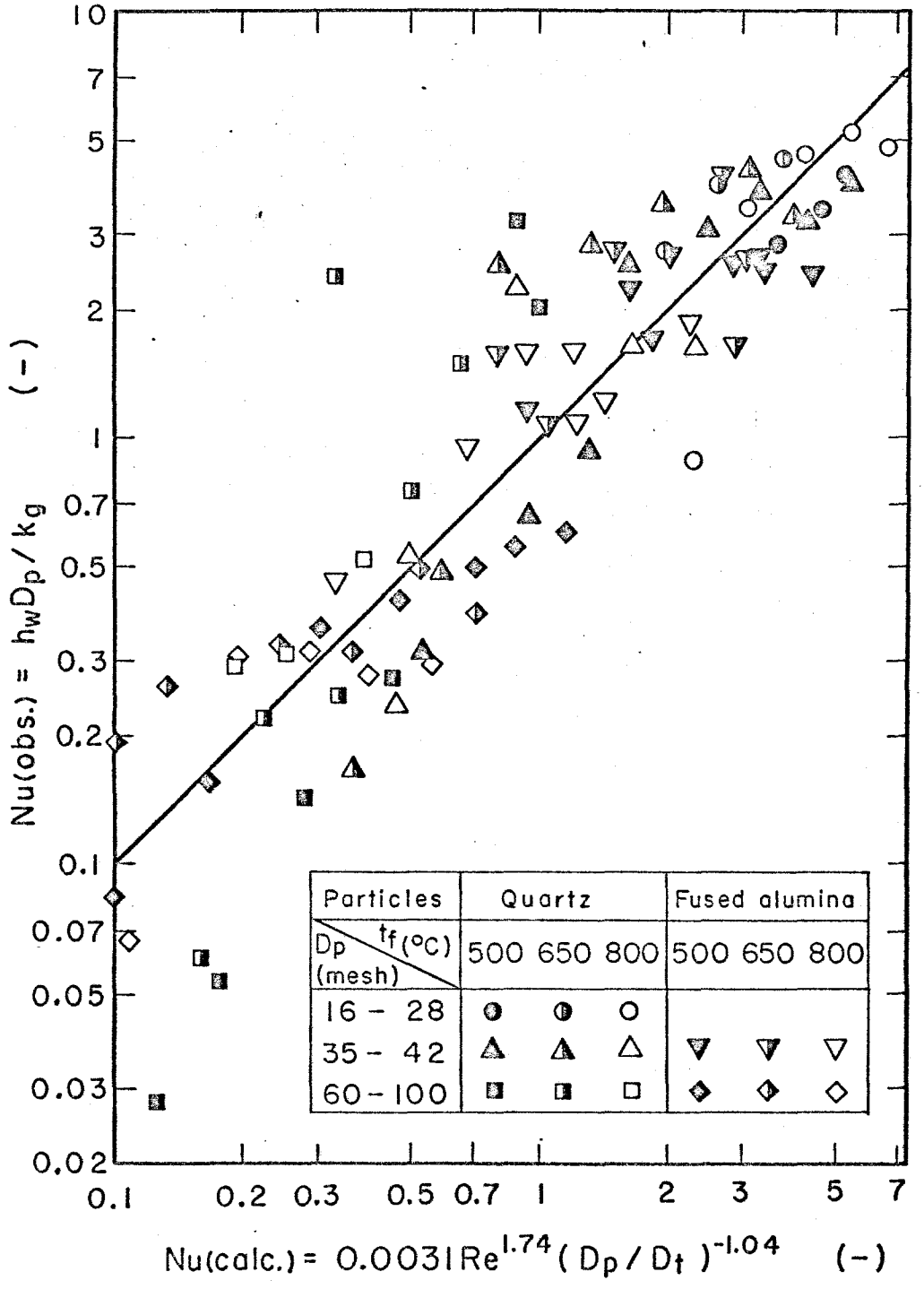


Fig.3.16 Comparison of Nu(calc.) with Nu(obs.)

subtracted. Quartz and fused alumina particles were chosen as the fluidized material. Fluidizing variables studied in this work include the particle size, the bed temperature and the flow rate of air.

Measured $h_w$ was compared with the results obtained by previous workers measured at the temperature below 200°C. The results were summarized in the form of regression of Nusselt number upon Reynolds number. It was found that $h_w$ in this work obtained at elevated temperatures coincides fairly well with those obtained at lower temperatures.

In the range of air velocity studied in this work, $h_w$ increases with the air velocity. $h_w$ for the particles of smaller size is lower than that of larger size at a fixed $(u-u_{mf})/u_{mf}$. Difference of $h_w$ between quartz and fused alumina particles could scarcely be found. Moreover, the effect of bed temperature on $h_w$ was not significant.

Radiative heat transfer coefficient, $h_r$, was calculated by using the Stefan-Boltzmann's equation. Any effects of particle size and flow rate of air on $h_r$ were not detected and the mean values of $h_r$ at each bed temperature was as follows:

| | bed temperature | mean of $h_r$ |
|---|---|---|
| quartz | 500°C | 67.5 (kcal/$m^2$·hr·°C) |
| | 650°C | 109.2 ( " ) |
| | 800°C | 160.8 ( " ) |
| fused alumina | 500°C | 35.9 (kcal/$m^2$·hr·°C) |
| | 650°C | 51.6 ( " ) |
| | 800°C | 64.7 ( " ) |

$h_w$ was found to be correlated with the fluidization characteristic discussed in Chapter 2. Firstly, the correlation between $h_w$ and $\bar{\sigma}_{cm}^2$ was studied. $\bar{\sigma}_{cm}^2$, mean of $\sigma_c^2$ in the upper part of the fluidized bed, is a measure of nonuniformity in the bed in terms of particle concentration difference between dense and bubble phases. It was concluded that $\bar{\sigma}_{cm}^2$ is not necessarily a useful measure of fluidization characteristics to predict the heat transfer coefficient. Secondly, the size of bubbles ascending through the fluidized bed was studied, because it is supposed that the bubble size has important effects on the circulation of particles and that the heat transfer rate is affected by the size of bubbles. The vertical thickness of bubbles, y, was estimated and the correlation between $h_w$ and y was pursued. It is found that $h_w$ increases with y. From these investigations, it was summarized that $h_w$ increases with air velocity because of intensi-

fied particle circulation caused by the ascending bubbles.

In order to express the heat transfer coefficient in a form of dimensionless terms, an expression of

$$Nu = a\,Re^{b}\left(\frac{C_p}{C_g}\right)^{c}\left(\frac{\rho_p}{\rho_g}\right)^{d}\left(\frac{D_p}{D_t}\right)^{e}$$

was presumed and the constants a, b, c, d, and e in the equation were estimated by the least squares method. Statistical significance on the individual terms of this equation was tested by likelihood ratio test and the contributions of the terms of $(C_p/C_g)$ and $(\rho_p/\rho_g)$ to Nu were found not to be significant. The resultant dimensionless equation was,

$$Nu = 0.0031\,Re^{1.71}\left(\frac{D_p}{D_t}\right)^{-1.04}$$

## Notation in Chapter 3

| | | |
|---|---|---|
| g | : acceleration of gravity | $(m/hr^2)$ |
| $h_c$ | : overall heat transfer coefficient | $(kcal/m^2 \cdot hr \cdot {}^{o}C)$ |
| $h_p$ | : heat transfer coefficient between particles and air | $(kcal/m^2 \cdot hr \cdot {}^{o}C)$ |
| $h_r$ | : radiative coefficient of heat transfer | $(kcal/m^2 \cdot hr \cdot {}^{o}C)$ |

$h_w$ : film coefficient of heat transfer between tube wall and particles (kcal/$m^2$·hr·°C)

$k_g$ : thermal conductivity of air (kcal/m·hr·°C)

$t_f$ : bed temperature (°C)

$t_{go}$ : temperature of gas blown into the main fluidized bed (°C)

$t_p$ : temperature of particles (°C)

$t_w$ : wall temperature (°C)

$u$ : air velocity (m/hr)

$u_{mf}$ : minimum fluidization velocity (m/hr)

$y$ : vertical thickness of bubbles (m)

$A_p$ : surface area of fluidized particles per unit bed height ($m^2$/m)

$C_g$ : specific heat of air (kcal/kg·°C)

$C_p$ : specific heat of particles (kcal/kg·°C or kcal/$m^3$·°C)

$D_p$ : particle diameter (m)

$D_t$ : inner diameter of fluidization tube (m)

$F_g$ : area of heat transfer surface between tube wall and air ($m^2$)

$F_r$ : area through which heat flows by radiation ($m^2$)

$F_w$ : area through which heat flows by conduction ($m^2$)

$G$ : mass air velocity (kg/$m^2$·hr)

$Gz$ : Graetz number (-)

$L_c$ : height of settled bed (m)

$L_f$ : height of fluidized bed (m)

$L_{mf}$ : bed height at minimum fluidization (m)

Nu : Nusselt number (-)

Re : Reynolds number (-)

$S_E$ : residual sum of squares (-)

$S_R$ : sum of squares due to regression (-)

$S_T$ : total sum of squares (-)

$T_f$ : absolute temperature of fluidized bed ($^oK$)

$T_p$ : absolute temperature of particles ($^oK$)

$T_w$ : absolute temperature of tube wall ($^oK$)

V : volumetric air velocity ($m^3/hr$)

W : total weight of particles (kg)

$\varepsilon$ : void fraction in fluidized bed (-)

$\varepsilon_{mf}$ : $\varepsilon$ at minimum fluidization (-)

$\varepsilon_p$ : emissivity of particles (-)

$\varepsilon_w$ : emissivity of tube wall (-)

$\theta$ : time (hr)

$\mu$ : viscosity of air (kg/m·hr)

$\mu_c$ : mean of particle concentration (-)

$\bar{\mu}_{cm}$ : mean of $\mu_c$ in the upper part of bed (-)

$\rho_g$ : density of air ($kg/m^3$)

$\rho_p$ : density of particles ($kg/m^3$)

$\sigma$ : Stefan-Boltzmann's constant

($= 4.88 \times 10^{-8} kcal/m^3 \cdot hr \cdot {}^oK^4$)

$\sigma_c^2$ : variation of particle concentration (-)

$\bar{\sigma}_{cm}^2$ : mean of $\sigma_c^2$ in the upper part of bed (-)

$\phi_E$ : degrees of freedom of $S_E$ (-)

$\phi_R$ : degrees of freedom of $S_R$ (-)

$\phi_T$ : degrees of freedom of $S_T$ (-)

## References to Chapter 3


1) Mickley, H. S. and C. A. Trilling: Ind. Eng. Chem., 1949, Vol. 41, No. 6, pp. 1135-1147

2) Wen, C. Y. and M. Leva: A.I.Ch.E. Journal, 1956, Vol. 2, No. 4, pp. 482-488

3) Leva, M., M. Weintraub and M. Grummer: Chem. Eng. Progr., 1949, Vol. 45, No. 9, pp. 563-572
Leva, M. and M. Grummer: Chem. Eng. Progr., 1952, Vol. 48, No. 6, pp. 307-313

4) Heerden, G., P. Nobel and D. W. Van Krevelen: Chem. Eng. Sci., 1951, vol. 1, No. 2, pp. 51-66: Ind. Eng. Chem., 1953, Vol. 45, No. 6, pp. 1237-1242

5) Dow, W. M. and M. Jakob: Chem. Eng. Progr., 1951, Vol. 47, No. 12, pp. 637-648

6) Matsuyama, T.: Kagaku Kogaku (Japanese), 1954, Vol. 18, No. 9, pp. 406-412

7) Frantz, J. F.: Chem. Eng. Progr., 1961, Vol. 57, No. 7, pp. 35-42

8) Heertjes, P. M. and S. W. Mckibbins: Chem. Eng. Sci. 1956, Vol. 5, pp. 161-167

9) Walton, J. S., R. L. Olson and O. Levenspiel: Ind. Eng. Chem., 1952, Vol. 44, No. 6, pp. 1474-1480

10) Hougen, O. A. and K. M. Watson: "Chemical Process Principles", 1943, p. 214, McGraw-Hill Book Co., Inc., New York

11) Perry, J. H.: "Chemical Engineer's Handbook", 3rd Ed., 1950, p. 461, McGraw-Hill Book Co., Inc., New York

12) McAdams, W. H.: "Heat Transmission", 3rd Ed., 1954, p. 231, McGraw-Hill Book Co., Inc., New York

13) Fujishige, H.: Report of the Resources Research Institute (Japan), 1965, No. 62, p. 88

14) Kunii, D. and O. Levenspiel: "Fluidization Engineering", 1968, p. 73, John Wiley and Sons, Inc., New York

15) Leva, M.: "Fluidization", 1959, p. 62, McGraw-Hill Book Co., Inc., New York

16) Wen, C. Y. and Y. H. Yu: A.I.Ch.E. Journal, 1966, Vol. 12, No. 3, pp. 610-612

17) Franz, J. F.: Chem. Eng. Progr., 1966, Vol. 62, Symposium Series No. 62, pp. 21-31

18) Perry, J. H.: "Chemical Engineers' Handbook", 3rd Ed., 1950, pp. 219-223, McGraw-Hill Book Co., Inc.,

New York

19) Soc. Chem. Eng. (Japan): Kagaku Kogaku Binran (Japanese), 3rd Ed., 1958, p. 203, Maruzen Co., Inc., Tokyo

20) McAdams, W. H.: "Heat Transmission", 3rd Ed., 1954, p. 472, McGraw-Hill Book Co., New York

21) Rikagaku Jiten (Japanese), 1958, p. 54 and 732, Iwanami Book Co., Inc., Tokyo

22) Baerg, A., J. Klassen and P. E. Gisher: Can. Journal of Research, 1950, Vol. 28, pp. 287-307

23) Bartholomew, R. N. and D. L. Katz: Chem. Eng. Progr., 1952, vol. 48, Symposium Series No. 4, pp. 3-10

24) Leva, M.: Proceedings of the General Discussion on Heat Transfer, London, I.M.E., A.S.M.E., 1951, pp. 421-425

25) Kettenring, K. N., E. L. Manderfield and J. M. Smith: Chem. Eng. Progr., 1950, Vol. 46, No. 3, pp. 139-145

26) Kunii, D. and O. Levenspiel: "Fluidization Engineering", 1960, p. 266, John Wiley and Sons, Inc., New York

27) Rowe, P. N. and B. A. Partridge: Symposium on the Interaction between Fluids and Particles, London, Instn Chem. Engrs, 1962, pp. 135-140

28) Wender, L. and G. T. Cooper: A.I.Ch.E. Journal,

1958, Vol. 4, No. 1, pp. 15-23

29) Woollard, I.N.M. and O. E. Potter: A.I.Ch.E. Journal, 1968, Vol. 14, No. 3, pp. 388-391

30) Kunii, D.: "Ryudoso" (Japanese), 1962, p. 238, Nikkan Kogyo Shimbun Co., Inc., Tokyo

# CHAPTER 4 THERMAL DECOMPOSITION OF PYRITE

## 4.1 Introduction

Thermal decomposition of solid particles represented by

$$(\text{Solid}) \rightarrow (\text{Solid}) + (\text{Gas})$$

is known to proceed through the following three major sequential steps (5, 6).

1) Heat transfer to the reaction interface within solid particles,
2) Chemical reaction at the interface, and
3) Outward transfer of gas evolved at the interface through the decomposed outer shell of the particle.

It was indicated in many previous works (1-3) on the kinetics of thermal decomposition of solid materials that the progress of reaction at the interface is composed of the processes of nucleation and growth of the decomposed phase, and that the rate of the interfacial reaction increases with temperature. When the temperature is high enough so that the equilibrium partial

pressure of evolved gas is almost 1 atm, the reaction rate at the interface is relatively high and the rates of heat transfer and of gas transfer begin to have important effects on the overall rate of thermal decomposition. Regarding the diffusion rate of gas evolved at the interface, Gafner (4) assumed that the preferred sites where nucleation occurs are randomly disposed throughout the particles, and suggested that appreciable delay between gas evolution and its escape will not occur when the diffusion coefficient is beyond $10^{-9}$ $cm^2/sec$. In the case that the decomposed phase of the particles is porous and that a large amount of heat is consumed by the decomposition, on the other hand, the overall reaction rate is to be determined by the heat transfer rate from the surroundings to the interface (5, 6).

Thermal decomposition of pyrite is represented by Eq. (4.1). The equilibrium pressure of diatomic sulfur gas reaches 1 atm at about 690°C and the enthalpy change in this reaction is about 37 kcal/mole $FeS_2$.

$$FeS_2 = FeS_{1+x} + \frac{1-x}{2} S_2 \qquad (4.1)$$

The thermodynamics (7) and the kinetics (8, 9) of the decomposition and the composition and properties

(9-11) of the decomposed product of pyrite have been studied. Schwab and Philinis (8) measured the thermal decomposition rate of pyrite particles whose size is 0.01 to 0.1 mm in diameter at 600° to 650°C by means of thermogravimetric analysis. This reaction proceeds rapidly in this temperature range and the overall rate of reaction is not affected by the flow rate of carrier gas in the range of gas velocity of 40 to 70 $cm^3$/min $CO_2$. They indicated from these experimental results that the overall reaction rate is not affected by the diffusion rate of sulfur gas through the decomposed shell of pyrite particles. Nishihara and Kondo (9) also studied on the thermal decomposition of pyrite particles of 200 to 250 mesh size. They found that the rate of decomposition satisfies the first order rate equation and that the rate of reaction becomes very rapid at a temperature above 700°C. From the experimental works mentioned above, it is supposed that the decomposed product of pyrite is very porous and the diatomic sulfur gas evloved can easily escape through the layer of decomposed product.

This work will, firstly, pursue the rate of thermal decomposition of pyrite particles of 60 to 100 mesh size in a fluidized bed at the temperature of 650° to 750°C and, secondly, to discuss a few characteristics of the

fluidized bed based upon the experimental results obtained. Under these conditions of fluidization, it is supposed from the results obtained by the previous workers (8, 9) that the overall rate of decomposition occurring at the interface within pyrite particles is so rapid and the resistance to diffusion of diatomic sulfur gas through the decomposed shell can be omitted. And thus the rate of heat transfer from the reactor wall to the interface within pyrite particles is presumed to play an important role in the overall reaction rate. From this point of view, the rate equations assuming the heat transfer controlling model are derived and they are verified by the experimental results.

## 4.2 Rate equation

### 4.2.1 Rate equation in batch process

It is intended in this section to introduce the rate equation for thermal decomposition of pyrite particles in a batch type fluidized bed reactor by assuming that the overall rate is determined by the heat transfer from the surroundings to the fluidized particles.

This model is illustrated in Fig. 4.1.

To obtain the rate equation, the following additional assumptions were also made.

1) Shape of particles is spherical.

2) Decomposition starts at the outer surface of the particle and proceeds toward the center. At any given time during decomposition, undecomposed pyrite remains in the core at a temperature of $t_d$. The decomposed shell is composed of $FeS_{1+x}$ whose outer surface is kept at $t_f$.

3) The temperature of preheated inert gas blown into the fluidized bed is kept equal to the temperature of the fluidized bed, $t_f$. And thus, no heat exchange occurs between the gas and particles in the fluidized bed and only the heat transfer from the reactor wall kept at $t_w$ to the fluidized particles is to be concerned.

4) At any given time during decomposition, the temperature of the fluidized bed, $t_f$, the temperature of reactor wall, $t_w$, and the decomposition temperature, $t_d$, remain at the fixed values, respectively.

5) Diatomic sulfur gas evolving at the interface is heated to $t_f$ during its escape through the outer decomposed shell of pyrite particles.

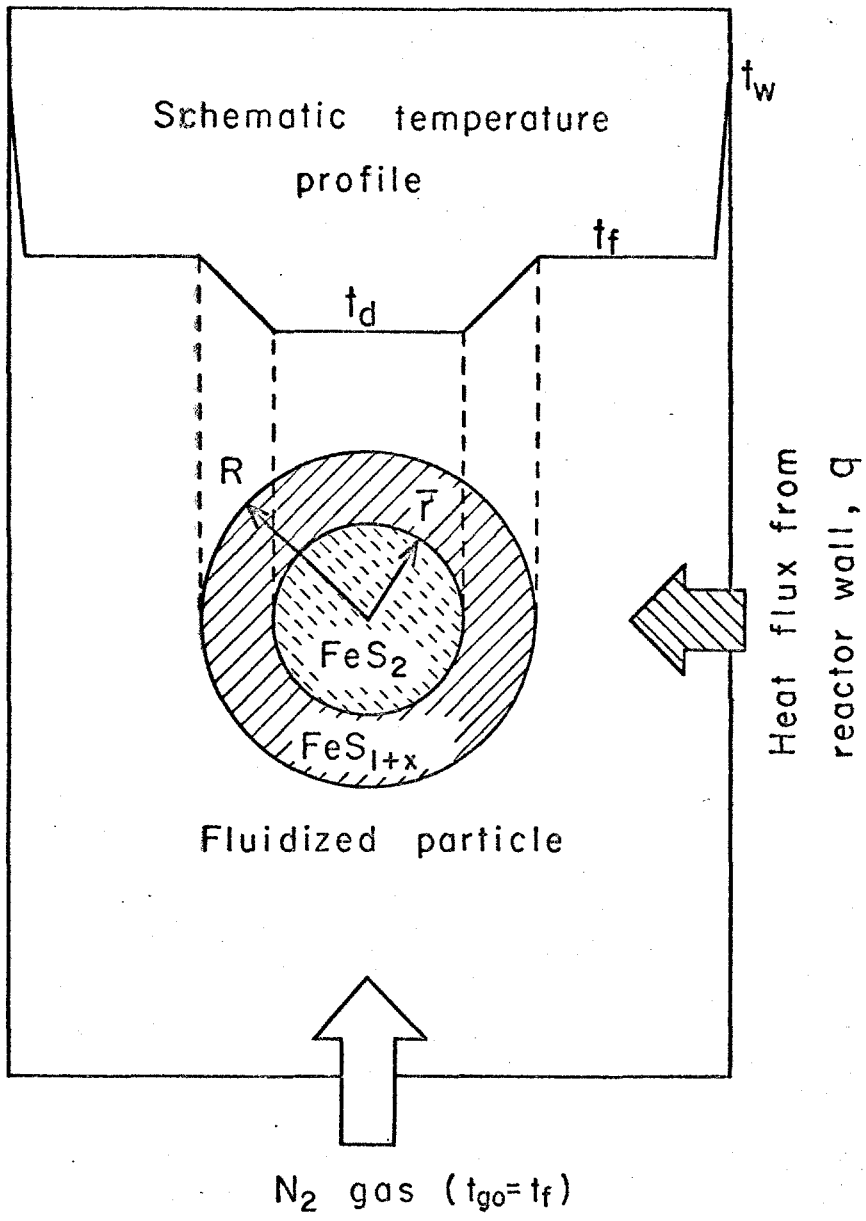


Fig. 4.1 Decomposition scheme for a pyrite particle in batch-type fluidized bed

With the above-mentioned assumptions, we have,

$$q = \Delta H_f \frac{dW}{d\theta} \tag{4.2}$$

Each term of Eq. (4.2) can be written as,

$$q = \pi D_t L_f h_c (t_w - t_f) = 4\pi R \bar{r} N k_e \left( \frac{t_f - t_d}{R - \bar{r}} \right) \tag{4.3}$$

$$\frac{dW}{d\theta} = -4\pi \rho_p \bar{r}^2 N \frac{d\bar{r}}{d\theta}$$

$$= -\frac{3\pi \rho_p \bar{r}^2 D_t^2 L_f (1-\varepsilon)}{4R^3} \frac{d\bar{r}}{d\theta} \tag{4.4}$$

$\Delta H_f$ in Eq. (4.2) is composed of the enthalpy change of thermal decomposition at the temperature of $t_d$ and the heat required to raise the temperature of $FeS_{1+x}$ and $S_2$ from $t_d$ to $t_f$. Thus,

$$\Delta H_f = \Delta H_d + \frac{M_{FeS}}{M_{FeS_2}} \int_{t_d}^{t_f} C_{FeS}\, dt + \frac{M_{S_2}}{2M_{FeS_2}} \int_{t_d}^{t_f} C_{S_2}\, dt \tag{4.5}$$

Since we can relate the fraction decomposed, x, to r by

$$\bar{r} = R(1-x)^{1/3} \tag{4.6}$$

Eq. (4.2) can be rewritten as a function of x by using Eqs. (4.3) to (4.6) :

$$\frac{1}{4} \rho_p D_t (1-\varepsilon) \Delta H_f \frac{dx}{d\theta} = \frac{t_w - t_d}{\frac{1}{h_c} + \frac{4R^2\{1-(1-x)^{1/3}\}}{3D_t (1-x)^{1/3} (1-\varepsilon) k_e}} \tag{4.7}$$

Integration of Eq. (4.7) with the initial condition of $x = 0$ at $\theta = 0$ gives,

$$\frac{1}{4}\rho_p D_t(1-\varepsilon)\Delta H_f\left\{\frac{1}{h_c}-\frac{4R^2}{3D_t(1-\varepsilon)k_e}\right\}x$$

$$+\frac{\rho_p R^2 \Delta H_f}{2k_e}\left\{1-(1-x)^{2/3}\right\}=(t_w-t_d)\theta \qquad (4.8)$$

This is the rate equation for thermal decomposition in a batch type fluidized bed. If the particle size is small and the resistance to heat transfer within particles is neglected, Eq. (4.8) becomes,

$$\frac{1}{4}\rho_p D_t(1-\varepsilon)\Delta H_f x = h_c(t_w-t_d)\theta \qquad (4.9)$$

This rate equation demonstrates a zero-order reaction.

### 4.2.2 Rate equation in continuous process

In order to obtain the rate equation in a fluidized bed continuously operated, the resistance to heat transfer within particles is omitted. This assumption is thought to be valid with smaller particle sizes and it helps to simplify the situation.

Among N particles present in the fluidized bed, n particles are assumed to be partially decomposed at the temperature $t_d$. The remaining (N-n) particles are assumed to be completely decomposed and remain at the temperature of $t_{f\infty}$ which is realized in the batch fluidized bed toward the end of reaction. A sche-

matic temperature profile is illustrated in Fig. 4.2. The temperature of the fluidized bed which was measured, $t_f$, may be considered to be their weighted mean, if the difference of specific heat is neglected,

$$t_f = \frac{1}{N}\left\{(N-n)\,t_{f\infty} + n\,t_d\right\} \tag{4.10}$$

In this model, heat transferred from the reactor wall to the fluidized bed is consumed by decomposing n particles at $t_d$ ; thus the heat transfer equation becomes,

$$q = \pi D_t L_f \frac{n}{N} h_c (t_w - t_d) \tag{4.11}$$

and the heat balance expression per particle under decomposition is,

$$\frac{q}{n} d\theta = -4\pi \rho_p \Delta H_f \bar{r}^2 d\bar{r} \tag{4.12}$$

Integrating Eq. (4.12) with the initial condition of r = R at $\theta = 0$ gives,

$$\frac{q}{n}\theta = -\frac{4}{3}\pi \rho_p \Delta H_f (\bar{r}^3 - R^3) \tag{4.13}$$

Inserting Eq. (4.6) to this equation, we have,

$$\left.\begin{aligned} &x = \frac{3q}{4\pi \rho_p n \Delta H_f R^3}\theta \quad , \quad 0 \leqq \theta \leqq \theta_d \\ \text{and} \qquad &x = x_d \qquad\qquad\quad , \quad \theta \geqq \theta_d \end{aligned}\right\} \tag{4.14}$$

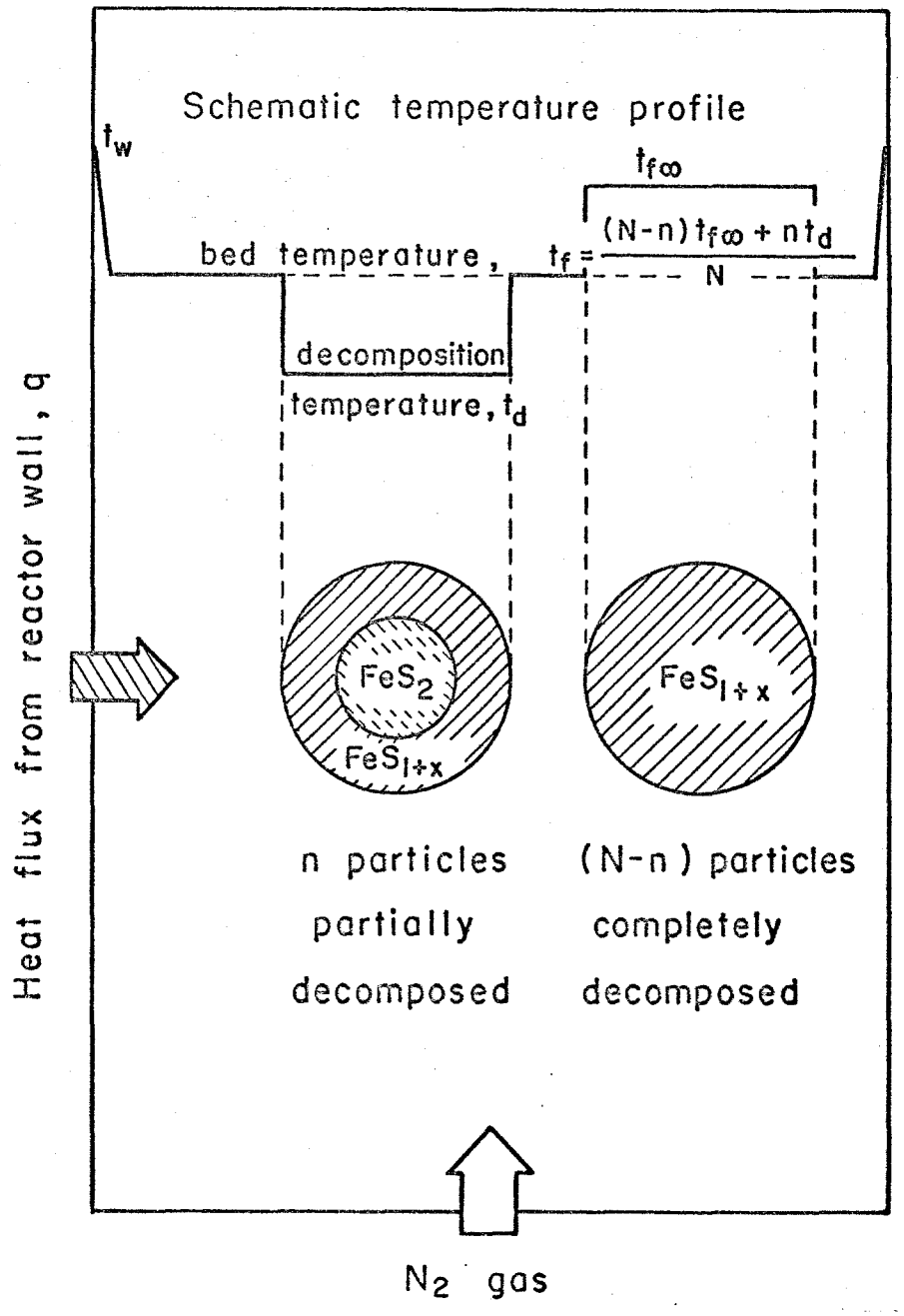


Fig. 4.2 Decomposition scheme for fluidized particles in continuous process : heat transfer resistance within partially decomposed particles is omitted.

Eq. (4.14) demonstrates the relationship between the fraction decomposed of one particle present in the fluidized bed, x, and its residence time, $\theta$, in the bed. It should be noted here that $x_d$ in Eq. (4.14) varies according to the variable composition of decomposed product due to its decomposition temperature (9, 10).

Under the condition of complete mixing in the fluidized bed, the probability density function of the residence time, $f(\theta)$, (12) of particles in the bed is given by,

$$f(\theta) = \frac{F}{W} exp\left(-\frac{F}{W}\theta\right) \qquad (4.15)$$

The mean fraction, X, of decomposed pyrite in the overflow from the bed is obtained by using Eqs. (4.14) and (4.15) as,

$$X = \int_0^{\theta_d} x f(\theta) d\theta + \int_{\theta_d}^{\infty} x_d f(\theta) d\theta$$

$$= \frac{3gW}{4\pi \rho_p n \Delta H_f R^3 F}\left\{1 - exp\left(-\frac{F}{W}\theta_d\right)\right\} \qquad (4.16)$$

Replacing W and n in this equation by,

$$W = \frac{1}{4}\pi D_t^2 L_f (1-\varepsilon)\rho_p \qquad (4.17)$$

and

$$n = N\int_0^{\theta_d} \frac{F}{W} exp\left(-\frac{F}{W}\theta\right) d\theta$$

$$= \frac{3 D_t^2 L_f (1-\varepsilon)}{16 R^3}\left\{1 - exp\left(-\frac{F}{W}\theta_d\right)\right\} \qquad (4.18)$$

Eq. (4.16) becomes,

$$X = \frac{B}{F}\left\{1 - exp\left(-\frac{F}{B}x_d\right)\right\} \qquad (4.19)$$

where

$$B = \frac{\pi D_t L_f h_c (t_w - t_d)}{\Delta H_f} \qquad (4.20)$$

Eq. (4.19) thus derived is the rate equation for thermal decomposition in a continuous fluidized bed in which the complete mixing of particles is assumed.

On the other hand, in the case of upward piston flow of particles assumed in the fluidized bed, instead of complete mixing, the residence time of particles in the bed, $\theta$, is expressed by,

$$\theta = \frac{W}{F} \qquad (4.21)$$

The mean fraction of decomposed pyrite in the overflow, X, is calculated by using Eqs. (4.14) and (4.21) as,

$$\left.\begin{aligned} X &= \frac{B}{F} \quad , \quad 0 \leqq \frac{W}{F} \leqq \theta_d \\ X &= x_d \quad , \quad \frac{W}{F} \geqq \theta_d \end{aligned}\right\} \qquad (4.22)$$

## 4.3 Experimental

### 4.3.1 Apparatus

The apparatus used for the experimental work is shown in Fig. 4.3. The fluidized bed reactor consists of a 45 mm I.D. quartz tube provided with a cone-type distributor with a 5.5 mm diameter steel ball at its bottom. Flow rate of nitrogen gas was metered through a rotameter. Metered nitrogen gas supplied to the fluidized bed was preheated by a nichrome heater. Off gas entraining diatomic sulfur gas was passed through a gas washer where elemental sulfur was removed.

The temperature of fluidized bed, $t_f$, was measured by using an Aeropak alumel-chromel thermocouple of 1.6 mm in diameter which was inserted into the bed from the top of the reactor tube. This thermocouple was covered with a 2.0 mm I.D. quartz tube. The temperatures of the reactor wall, $t_w$, and of nitrogen gas sent into the bed, $t_{go}$, were also measured.

A rotating disc feeder was used for feeding the pyrite particles into the fluidized bed in the continuous process experiments. Its feeding rate was

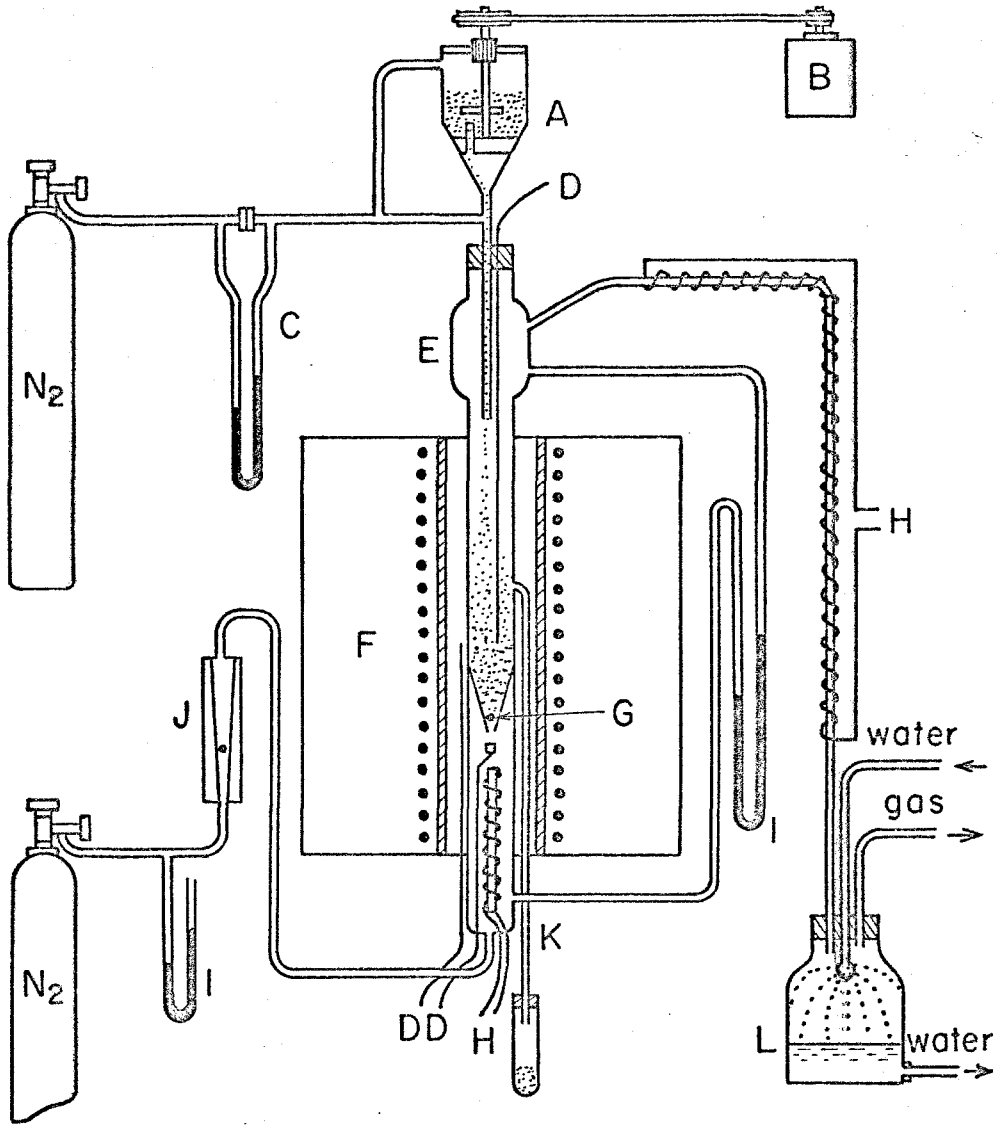


A Feeder
B Synchronous moter
C Orifice meter
D Thermocouple
E Quartz reactor
F Furnace
G Steel ball
H Nichrome heater
I Manometer
J Rotameter
K Overflow tube
L Gas washer

Fig. 4.3 Schematic representation of experimental apparatus

adjusted by changing the opening of the feeding port on the disc.

### 4.3.2 Material

Pyrite lump mined at Yanahara Mine of Dowa Mining Co. Inc., Okayama Prefecture, was used. It was ground to 60 to 100 mesh size. The content of its component minerals was calculated from the chemical analysis and it is shown in Table 4.1.

Table 4.1 Mineralogical analysis of pyrite

| $FeS_2$ | FeS | $Cu_2S$ | Balance | |
|---|---|---|---|---|
| 97.9 | 0.1 | 0.2 | 1.8 | (%) |

### 4.3.3 Experimental conditions

The effects of the bed temperature and of the flow rate of nitrogen gas on the reaction rate of pyrite particles were studied in the batch process experiment. The adopted levels of these variables are listed in Table 4.2.

In the continuous process experiment, the flow

rate of nitrogen gas was kept at 5.66 cm/sec and the effects of the feeding rate of pyrite particles and of the bed temperature on the reaction rate were studied. Their levels adopted are also summarized in Table 4.2.

Table 4.2 Experimental conditions

| | |
|---|---|
| **Batch process experiment** | |
| Bed temperature | 650°, 700° and 750° C |
| Flow rate of $N_2$ | 4.40, 5.66 and 6.92 cm/sec (at 20°C) |
| **Continuous process experiment** | |
| Flow rate of $N_2$ | 5.66 cm/sec (at 20°C) |
| Bed temperature | 650°, 700° and 750° C |
| Feeding rate of pyrite particles | 0.1 to 1.8 kg/hr |

4.3.4 Experimental procedure

1) Batch process experiment

An amount of 150 g of pyrite particles is fed into the reactor tube maintained at a predetermined temperature and fluidized with nitrogen gas flow at a given rate. The bed temperature falls rapidly

owing to the supply of cold particles and recovers to a temperature of $t_f$ and thereafter it remains at this temperature. The bed temperature was observed to reach a temperature which is very near to the original temperature of $t_f$ toward the end of thermal decomposition. This temperature is denoted by $t_{f\infty}$. This change of bed temperature is illustrated in Fig. 4.4. Sample particles were pipetted out of the bed by inserting a 10 mm I.D. quartz syringe from the top of the reactor tube in the course of decomposition and their sulfur content was analyzed.

2) Continuous process experiment

Before starting to feed pyrite particles into the fluidized bed, 150g of the cinder decomposed at 750°C was fluidized at the predetermined temperature listed in Table 4.2 to form a fluidized bed and it was allowed to remain at the steady state. Thereafter, pyrite was fed from a rotating disc feeder at a constant rate. Fluidization was continued for the time, which is required for replacing 95 % of the cinder in the bed, plus 30 min and thereafter, the overflow particles were sampled and analyzed. After the passage of this time duration, the bed was assumed to be at a

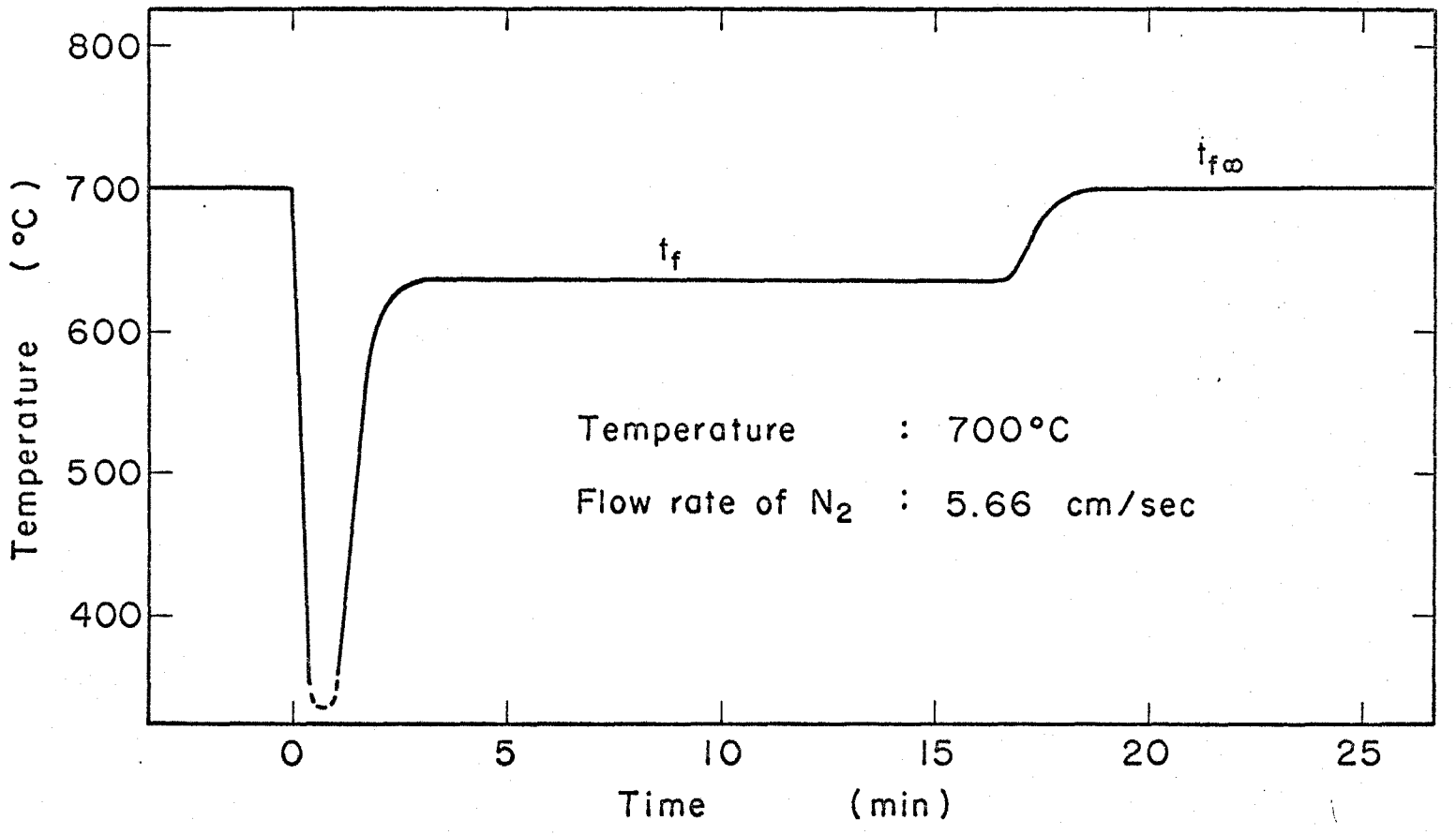


Fig.4.4 An example of change of bed temperature in batch process

steady state of fluidization.

The time required for replacement of 95 % of the cinder was estimated as follows: W kg of the cinder is fluidized in the fluidized bed prior to feeding pyrite particles. At the time $\theta = 0$, the feeding of pyrite is started, whose rate is F kg/hr. The number of pyrite particles fed into the bed per unit time, $N_p$, at the feeding rate of F kg/hr is represented by,

$$N_p = \frac{3F}{4\pi R^3 \rho_p}$$

where R and $\rho_p$ are the radius and the density of pyrite particles, respectively. On the other hand, $N_p$ particles of the mixture of cinder and pyrite overflow out of the bed during the feeding of pyrite particles. Assuming complete mixing of particles in the fluidized bed, the material balance equation concerning the pyrite particles at any given time $\theta$ is given by,

$$F - \eta F = W \frac{\rho_p}{\rho_c} \frac{d\eta}{d\theta} \qquad (4.23)$$

where $\eta$ is the number fraction of pyrite particles in the overflow and $\rho_c$ is the density of the cinder.

Integrating Eq. (4.23) gives,

$$\frac{F\rho_c}{W\rho_p} \int d\theta = \int \frac{d\eta}{1-\eta} + C$$

then

$$\frac{F\rho_c}{W\rho_p}\theta = -\ln(1-\eta) + C \qquad (4.24)$$

Integration constant C in Eq. (4.24) is zero because of the initial condition of $\eta = 0$ at $\theta = 0$, and Eq. (4.24) becomes,

$$\theta = -\frac{W\rho_p}{F\rho_c}\ln(1-\eta) \qquad (4.25)$$

The time required for replacing 95 % of the cinder in the bed is given by putting $\eta = 0.95$ in Eq. (4.25), or

$$\theta = 2.996\,\frac{W\rho_p}{F\rho_c} \qquad (4.26)$$

## 4.4 Experimental results

### 4.4.1 Batch process experiment

Measured fraction of decomposed pyrite, x, is illustrated in Fig. 4.5. It is seen from this figure that x increases linearly with time, $\theta$, in the course of decomposition, except in its final stage. This satisfies the linear Eq. (4.9) whose slope is given by $4h_c(t_w - t_d)/\rho_p D_t(1 - \varepsilon)\Delta H_f$. And this suggests that the rate of thermal decomposition of pyrite is

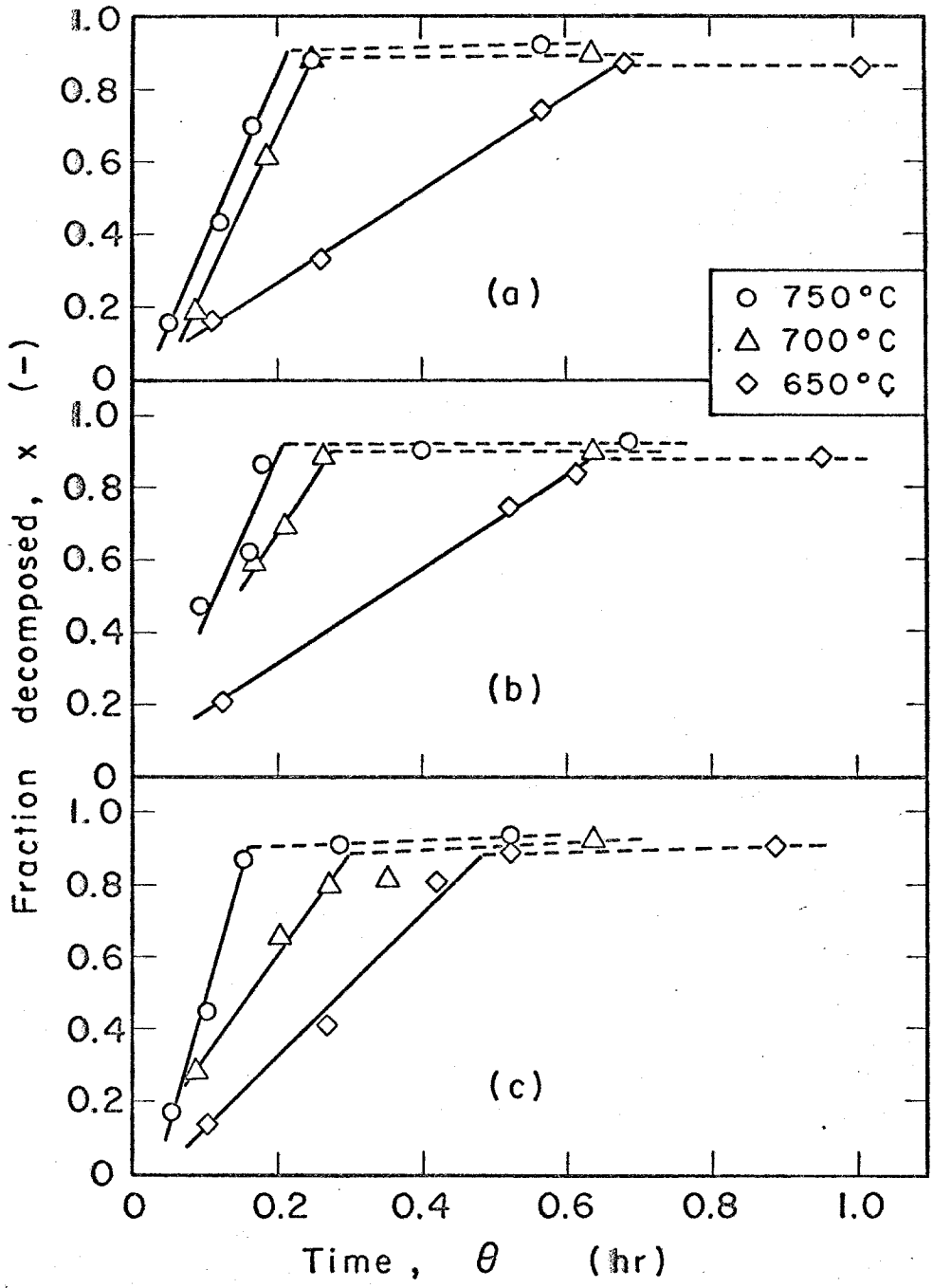


Fig.4.5 Fraction decomposed vs. decomposition time in batch process : (a) flow rate of $N_2$, 4.40 cm/sec ; (b) flow rate of $N_2$, 5.66 cm/sec; (c) flow rate of $N_2$, 6.92 cm/sec.

controlled by the heat transfer rate under the experimental conditions in this work and that the resistance to heat transfer through the decomposed shell within particles of 60 to 100 mesh size can be omitted.

The overall heat transfer coefficient between the reactor wall and the fluidized bed, $h_c$, can be estimated from the slopes of Fig. 4.5 determined by the least squares method. It is shown in Fig. 4.6. In this figure, the linear velocity of nitrogen gas at the bed temperature, $u^*$, is calculated in the form of,

$$u^* = \frac{t_f + 273}{293} \times u$$

Where u is its linear velocity at 20°C. From this figure, the following regression was obtained by the least squares method.

$$h_c = 0.386\, u^{*0.772} \qquad (4.27)$$

## 4.4.2 Continuous process experiment

The mean fraction, X, of decomposed pyrite in the overflow is illustrated in Fig. 4.7 against the reciprocal feeding rate, 1/F. This figure also includes the calculated values of X with Eqs. (4.19) and (4.22) which correspond to the complete mixing and the upward piston flow, respectively. In these calculations,

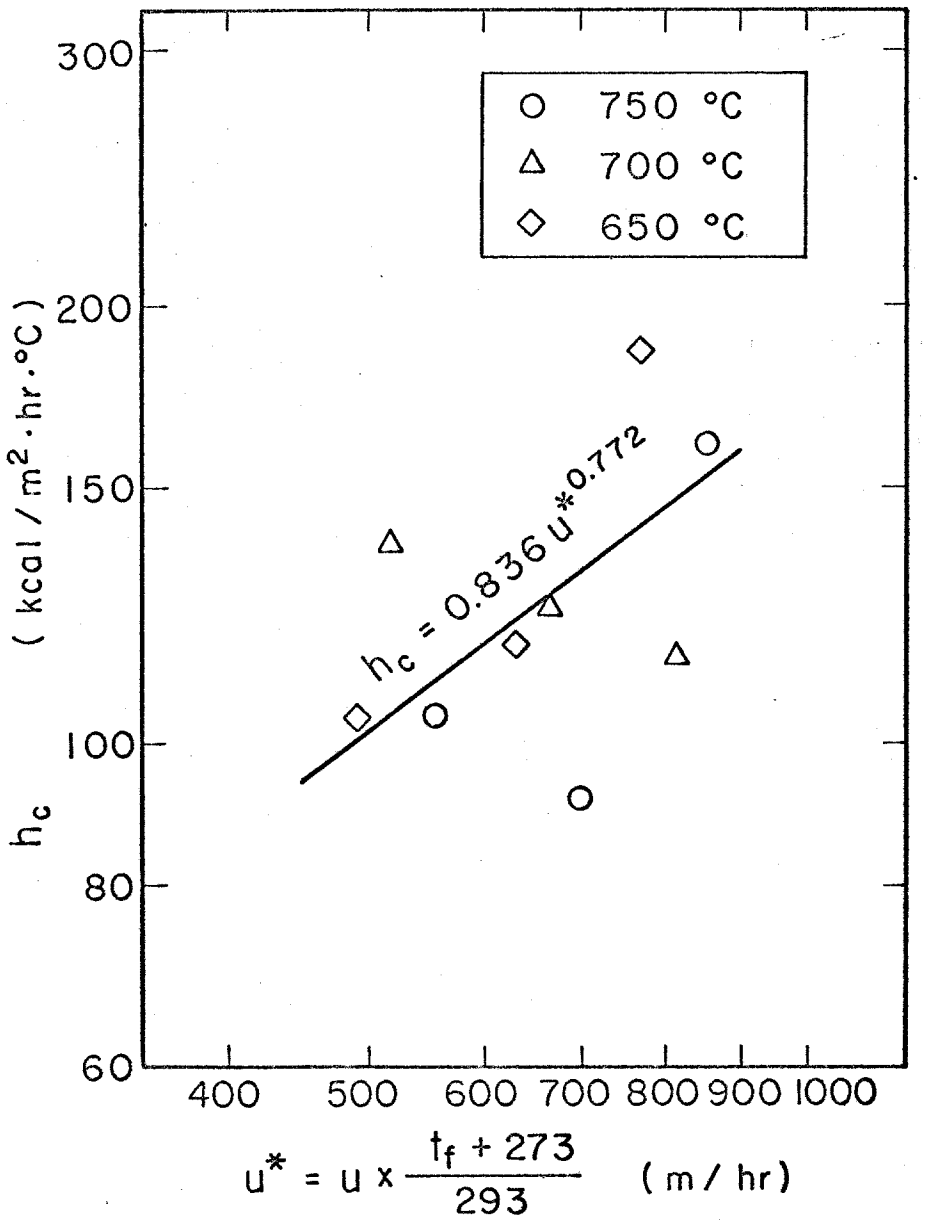


Fig. 4.6 Overall heat transfer coefficient vs. flow rate of nitrogen gas at the fluidized bed temperature

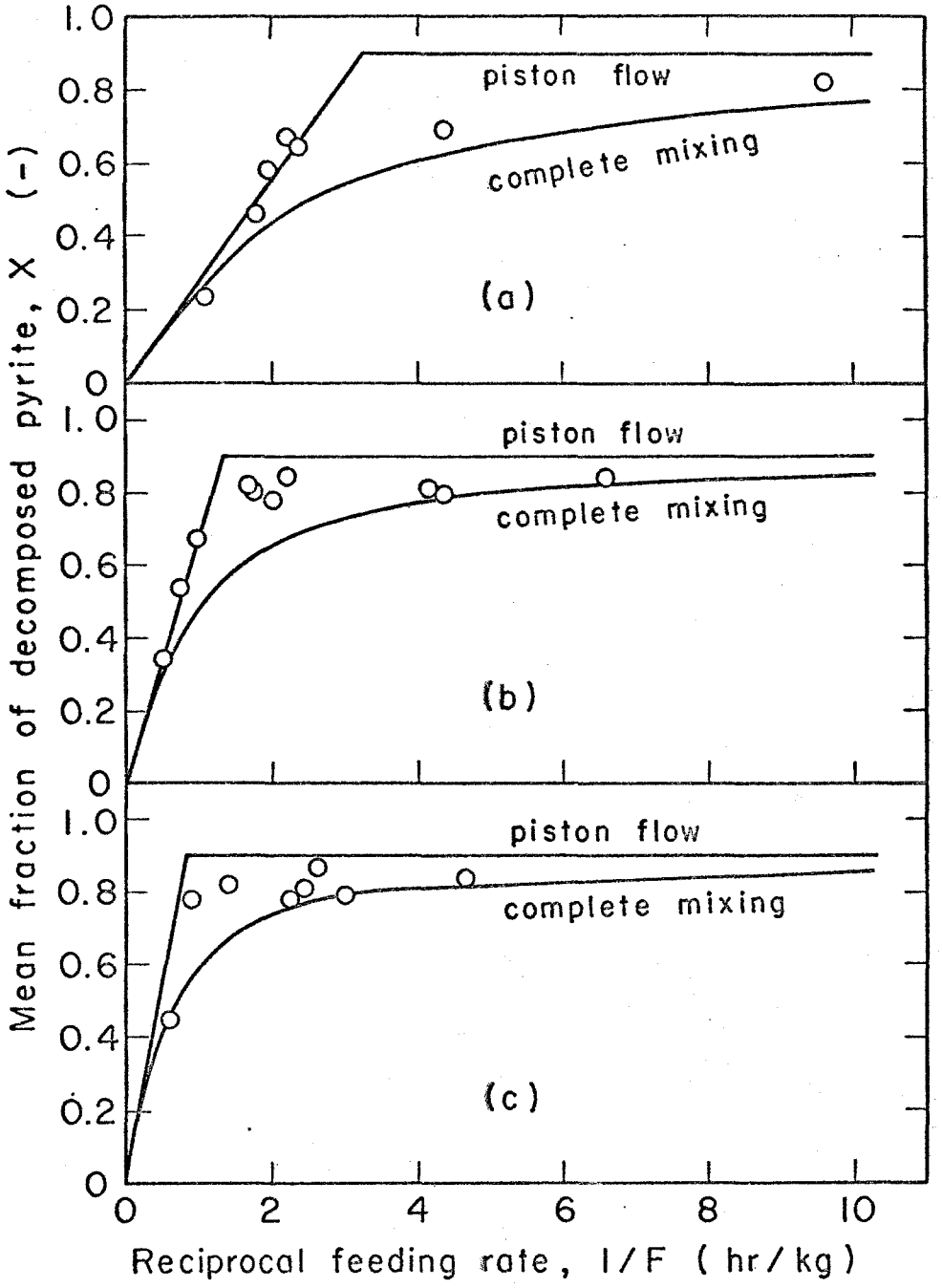


Fig. 4.7 Mean fraction of decomposed pyrite, X, vs. reciprocal feeding rate, 1/F, in continuous process. Flow rate of $N_2$, 5.66 cm/sec; (a) 650°C, (b) 700°C, (c) 750°C

$h_c$ given by Eq. (4.27) and $x_d$ = 0.9 were used and $t_d$ was assumed to be equal to the constant bed temperature, $t_f$, illustrated in Fig. 4.4.

It is seen in Fig. 4.7 that most of X measured at higher feeding rates satisfies Eq. (4.22) which assumes upward piston flow of particles in the fluidized bed and that X tends to deviate from these straight lines for the curves of Eq. (4.19) at lower feeding rates. This may suggest that the pyrite feed and the decomposed product are mixed with each other almost completely at lower feeding rates. This results in a higher mean fraction of decomposed pyrite in the overflow over 0.7. On the other hand, it may be suggested that the fluidized bed tends to segregate into two layers, pyrite-rich layer and decomposed product-rich layer, at higher feeding rates. This correlationship between the feeding rate of pyrite particles and the behavior of particles in the fluidized bed will be further discussed later.

## 4.5 Discussion

From the batch process experiment, it was indicated that the thermal decomposition rate of pyrite particles

is controlled by the heat transfer rate and the overall heat transfer coefficient, $h_c$, was estimated from the experimental results.

It is of interest to compare the film coefficient of heat transfer estimated from the thermal decomposition data of pyrite particles with that obtained in Chapter 3. The amount of heat transferred per unit time from the reactor wall to the fluidized bed is given by,

$$q = h_c F_c (t_w - t_f)$$

$$= h_w F_w (t_w - t_f) + h_r F_r (t_w - t_f) \qquad (4.28)$$

where $F_c = F_w = F_r = \pi D_t L_f$. The first and the second terms on the right-hand side of this equation represent the amount of heat transferred by conduction and radiation, respectively. Radiative heat transfer coefficient, $h_r$, can be estimated in the similar way as mentioned in Chapter 3. The amount of heat transferred by radiation is given by Stefan-Boltzmann's law as,

$$q = \sigma F_r \phi (T_w^4 - T_f^4) \qquad (4.29)$$

Equating this equation with the second term on the right-hand side of Eq. (4.28), we have,

$$h_r = \sigma \phi \frac{T_w^4 - T_f^4}{t_w - t_f}$$

$$= 4.88 \times 10^{-8} \phi (T_w^2 + T_f^2)(T_w + T_f) \qquad (4.30)$$

The heat transfer between the reactor wall and the fluidized bed can be regarded as that between two concentric tubes (13). On this assumption, $\phi$ in Eq. (4.30) is given by,

$$\frac{1}{\phi} = \frac{1}{\varepsilon_w} + \frac{1}{\varepsilon_p} - 1 \qquad (4.31)$$

where $\varepsilon_w$ and $\varepsilon_p$ are the emissivities of the reactor wall and the decomposed shell of pyrite particles, respectively. In the calculation of $h_r$, the value of $\varepsilon_p$ was chosen at 0.85 (14) and that of $\varepsilon_w$ was estimated at 0.58($t_w$ = 650°C), 0.53($t_w$ = 700°C) and 0.49($t_w$ = 750°C) (15). $h_r$ calculated from Eqs. (4.30) and (4.31) are summarized in Table 4.3. The film coefficient of heat transfer, $h_w$, is obtained by subtracting $h_r$ from $h_c$ and they are also listed in Table 4.3.

With the values of $h_w$ thus obtained, the relationship between the Reynolds number and the Nusselt number was obtained. In calculating these dimensionless numbers, the Eucken's equation (16) concerning the thermal conductivity of polyatomic gas and the modified

Table 4.3 Heat transfer coefficient

| Initial bed temperature (°C) | Flow rate of $N_2$ at 20°C (cm/sec) | Heat transfer coefficient (Kcal/m$^2$·hr·°C) | | |
|---|---|---|---|---|
| | | $h_c$ | $h_r$ | $h_w$ |
| 650 | 4.40 | 103.7 | 79.6 | 24.1 |
| | 5.66 | 117.1 | 79.9 | 37.2 |
| | 6.92 | 185.3 | 79.9 | 105.4 |
| 700 | 4.40 | 146.7 | 80.9 | 65.8 |
| | 5.66 | 123.8 | 81.2 | 42.6 |
| | 6.92 | 114.3 | 82.0 | 32.3 |
| 750 | 4.40 | 103.9 | 82.9 | 21.0 |
| | 5.66 | 91.6 | 82.8 | 8.8 |
| | 6.92 | 160.5 | 82.9 | 77.6 |

Hirshfelder's equation (17) on the viscosity of gas were employed. The results are shown in Fig. 4.8. From this figure, the following dimensionless equation was obtained by the least squares method.

$$\frac{h_w D_p}{k_g} = 2.115 \left( \frac{D_p G}{\mu} \right)^{2.334} \qquad (4.32)$$

This equation was also plotted in Fig. 3.7 and it is seen in this figure that Eq. (4.32) coincides closely with Eq. (3.20) which was obtained in the heat transfer experiments in Chapter 3. This also suggests that the heat transfer controlling model represented by Eq. (4.9) is acceptable for the thermal decomposition

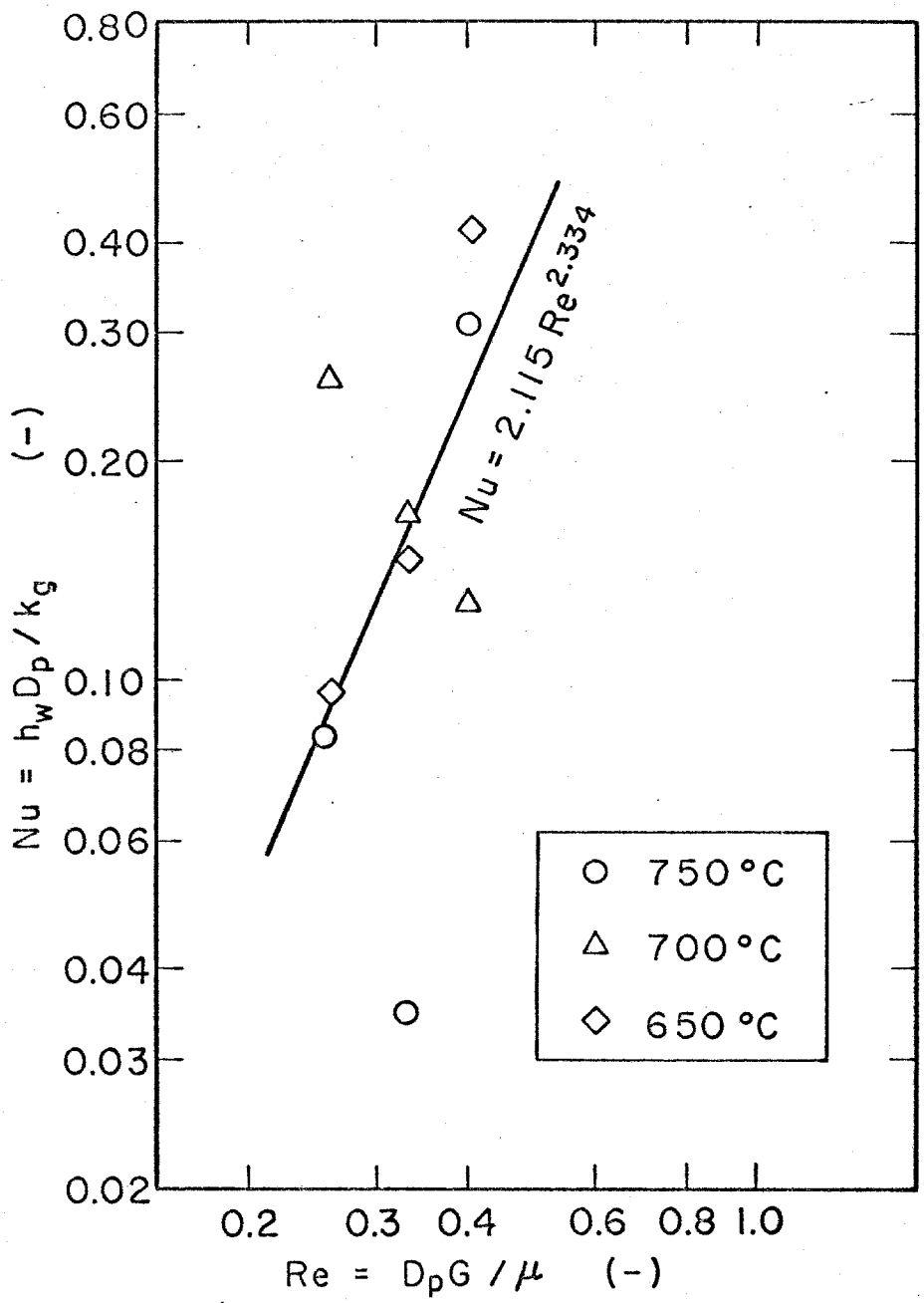


Fig. 4.8 Correlationship between Re and Nu

rate of pyrite particles in a fluidized bed whose particle size is 60 to 100 mesh.

It was mentioned in the continuous fluidization experiment that the mean fraction of decomposed pyrite in the overflow satisfies Eq. (4.22) which assumes the upward piston flow of particles in the fluidized bed at higher feeding rates and that it deviates from Eq. (4.22) and approaches to the curves of Eq. (4.19) on the assumption of the complete mixing of fluidized particles in the bed at lower feeding rates. These behaviors of particles in the fluidized bed are further pursued.

Fluidized bed temperature, $t_f$, given by Eq. (4.10) can be rewritten as,

$$\frac{n}{N} = \frac{t_{f\infty} - t_f}{t_{f\infty} - t_d} \tag{4.33}$$

Under the condition of complete mixing, n/N can be expressed by Eq. (4.18) as,

$$\frac{n}{N} = \int_0^{\theta_d} \frac{F}{W} exp\left(-\frac{F}{W}\theta\right) d\theta$$

$$= 1 - exp\left(-\frac{F}{W}\theta_d\right) \tag{4.34}$$

And Eqs. (4.33) and (4.34) yield,

$$\frac{t_f - t_d}{t_{f\infty} - t_d} = exp\left(-\frac{F}{W}\theta_d\right) = exp\left(-\frac{F}{B}x_d\right) \qquad (4.35)$$

A similar expression of $(t_f - t_d)/(t_f - t_d)$ for the upward piston flow of particles in the fluidized bed is,

$$\left.\begin{aligned} &\frac{t_f - t_d}{t_{f\infty} - t_d} = 1 \qquad \text{for} \quad 0 < \frac{F}{B}x_d < \frac{L_t W x_d}{L_f B \theta_d} \\ &\frac{t_f - t_d}{t_{f\infty} - t_d} = 0 \qquad \text{for} \quad \frac{F}{B}x_d > \frac{L_t W x_d}{L_f B \theta_d} \end{aligned}\right\} \qquad (4.36)$$

Fig. 4.9 illustrates the measured values of $t_f$ in the dimensionless form of $(t_f - t_d)/(t_{f\infty} - t_d)$ and the calculated values with Eqs. (4.35) and (4.36). The plot of $(t_f - t_d)/(t_{f\infty} - t_d)$ in this figure is observed to decrease along the curve of Eq. (4.35) in the lower part of $Fx_d/B$. It leaves off this curve downward at higher $Fx_d/B$. This may also indicate the preferred segregation of particles in the fluidized bed at higher feeding rates. Furthermore, it may be another reason of this downward deviation that the amount of heat which is consumed for heating pyrite particles up to the decomposition temperature can not be omitted at higher feeding rates.

In this connection, the fluidization quality of this fluidized bed is to be inferred. The minimum fluidization velocity of pyrite particles at the bed

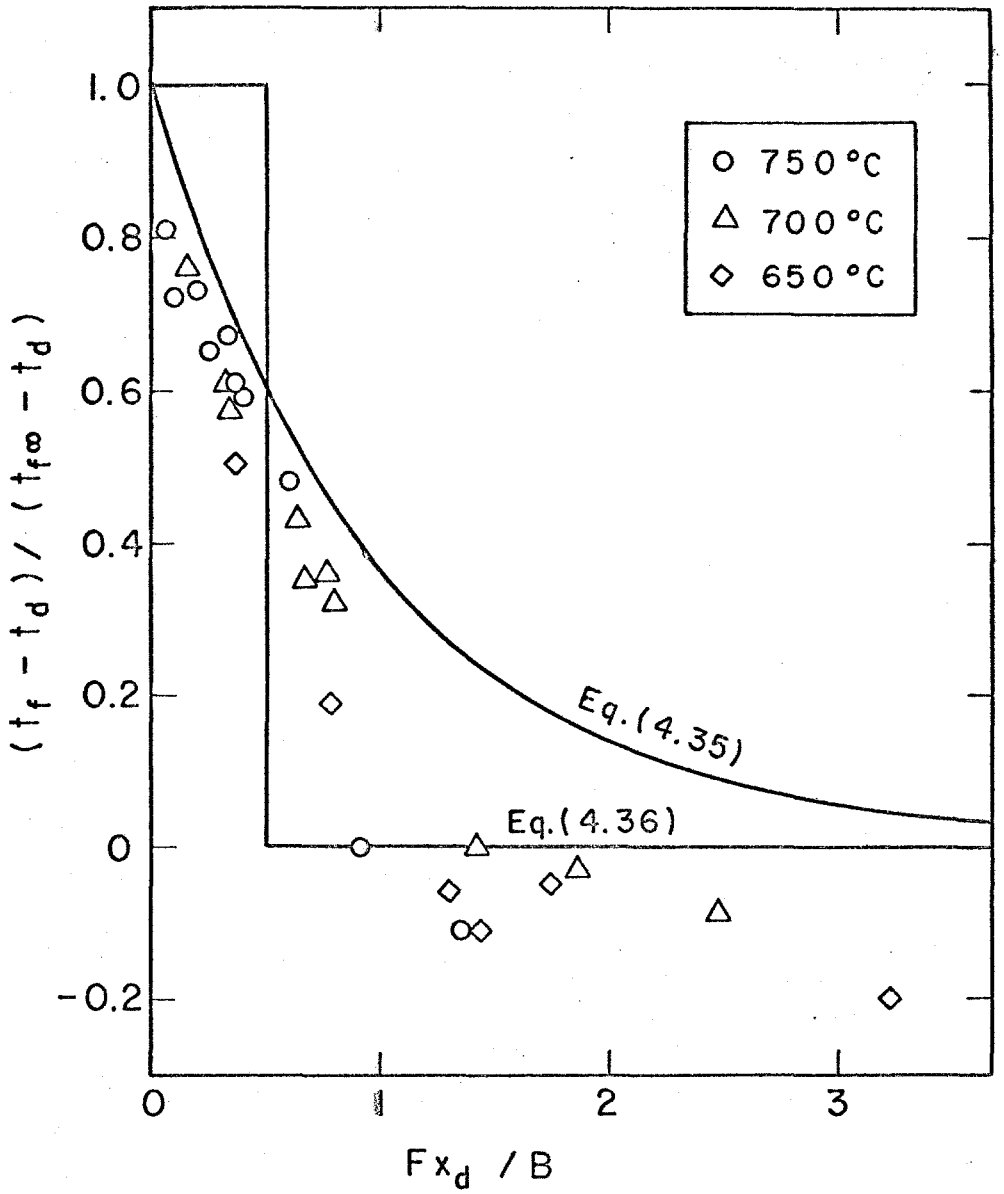


Fig. 4.9 Bed temperature dependence on $Fx_d / B$

temperature of $t_f$ was calculated by the following equation (18).

$$u_{mf} = \frac{(D_p \phi_p)^2}{150} \frac{\rho_p - \rho_g}{\mu} g \frac{\varepsilon_{mf}^3}{1 - \varepsilon_{mf}} \qquad (4.37)$$

In this calculation, the modified Hirshfelder's equation (17) concerning the viscosity of gas was employed and the value of shape factor of particles $\phi_p$ was chosen at 0.75 (19). $u_{mf}$ of pyrite particles calculated with Eq. (4.37) is shown in Table 4.4. The linear velocity of nitrogen gas at 20°C was fixed at 5.66 cm/sec in the continuous process experiment. And the gas velocity at $t_f$ was calculated as follows;

$$u^* = 5.66 \times \frac{t_f + 273}{293}$$

$u^*$ thus calculated is also listed in Table 4.4.

Table 4.4 Flow rate of nitrogen gas

| Initial bed temperature (°C) | $u_{mf}$ (cm/sec) | $u^*$ (cm/sec) | $u^* - u_{mf}$ (cm/sec) | $\frac{u^*}{u_{mf}}$ (-) |
|---|---|---|---|---|
| 650 | 6.76 | 17.83 | 11.07 | 2.64 |
| 700 | 6.71 | 18.80 | 12.09 | 2.80 |
| 750 | 6.68 | 19.76 | 13.08 | 2.96 |

It is seen in Table 4.4 that the excessive gas velocity above the minimum fluidization is in the range of 11

to 13 cm/sec and $u^*$ is about 3 times larger than $u_{mf}$. $u_{mf}$ calculated with Eq. (4.37) decreases with decreasing particle density, $\rho_p$, and $u_{mf}$ of pyrite particles which was shown in Table 4.4 is higher than that of decomposed pyrite because the density of pyrite particles is higher than that of its decomposed product. Therefore $u_{mf}$ of fluidized particles which are composed of pyrite particles and its decomposed product is lower than that of pyrite particles. Thus, it can be said that the excessive gas velocity above minimum fluidization is higher than 11 to 13 cm/sec. Under these fluidizing conditions, it is supposed from Fig. 2.11 that the gas bubbles of relatively large size are formed. $\bar{\sigma}_{cm}^2$, a measure of the nonuniformity of particle concentration in the fluidized bed, is also thought to be of larger values according to Fig. 2.9. It is a reasonable thought, therefore, that the particles are well agitated in the fluidized bed owing to the vigorous bubbling and that the upward piston flow of particles may not be expected to occur in the fluidized bed.

With this thought in mind, the distribution of the fraction of decomposed pyrite particles in the vertical direction of fluidized bed was examined; the mixture composed of pyrite particles and the cinder particles decomposed at 750°C was fluidized at room

temperature. About 0.05 g of the fluidized mixture was sampled at different heights above the bottom of the bed and the composition was measured by magnetic separation. Sample probe used in this experiment is illustrated in Fig. 4.10. 3.5 mm D. holes at an interval of 2 cm were drilled into a stainless steel rod of 7 mm diameter and these holes were covered with stainless steel foil. Two stainless steel wires which are connected to the foils serve to open and to close the holes by pulling these wires up. Sampling of mixture was carried out at 5, 10, 20, 30, 40, 50, and 60 min after the start of fluidization. An example of the measured fraction of decomposed cinder is illustrated in Fig. 4.11. In this figure, $w_d$ and $w_p$ are the weights of the cinder and of the pyrite, respectively. Any significant change in the weight fraction of decomposed cinder, $w_d/(w_p + w_d)$, was not found during the course of fluidization and $w_d/(w_p + w_d)$ in this figure can be regarded as the fraction realized in the steady state of fluidization. It is seen in this figure that $w_d/(w_p + w_d)$ remains almost unchanged in the fluidized bed except in its upper part; it increases rapidly in the upper part of the fluidized bed. This means that the pyrite particles and the decomposed particles are completely mixed with each other in the

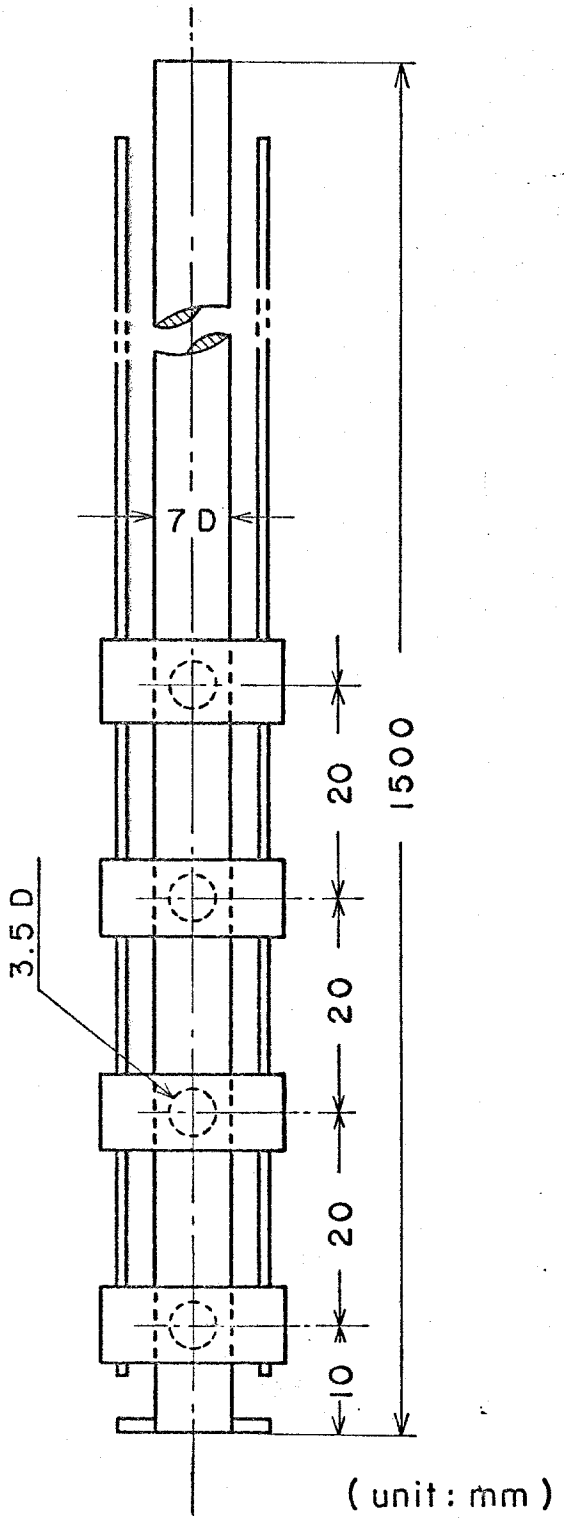


Fig. 4.10 Sample probe

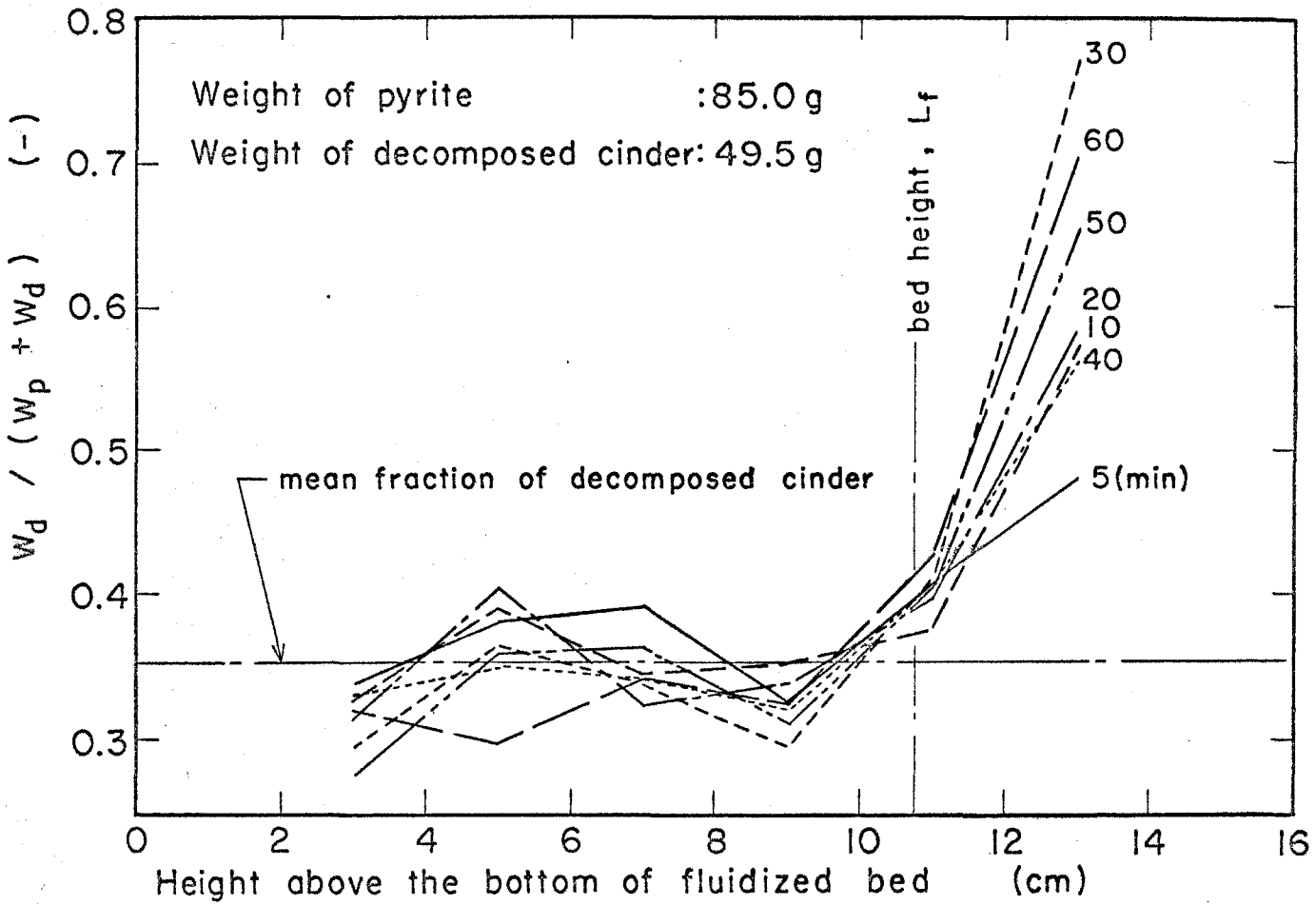


Fig. 4.11 Vertical distribution of the fraction of decomposed cinder

bulk of the fluidized bed, and a preferred segregation of the decomposed cinder occurs at the surface of the bed. The mean values of $w_d/(w_p + w_d)$ thus measured in the fluidized bed for several mixtures of different composition are summarized in Fig. 4.12. It is evident in this figure that the difference between $w_d/(w_p + w_d)$ in the bulk of the fluidized bed and that in its upper portion increases along with the decrease in the fraction of cinder in the mixture.

The density of pyrite particles is 5.00 $g/cm^3$ (17). And the density of the cinder was measured as follows. An amount of pyrite particles was weighed and poured slowly into the graduated cylinder. From the volume occupied by the particles, the void fraction, $\varepsilon$, of the settled bed composed of pyrite particles can be calculated. The volume occupied by an amount of the decomposed cinder was measured in the same way. Assuming that the void fraction of the settled bed composed of the cinder is same as that of pyrite particles, the density of the cinder, $\rho$, was calculated by

$$\rho = \frac{W}{V(1-\varepsilon)}$$

Where W and V are the weight of the particles and the volume occupied. The density of the cinder thus

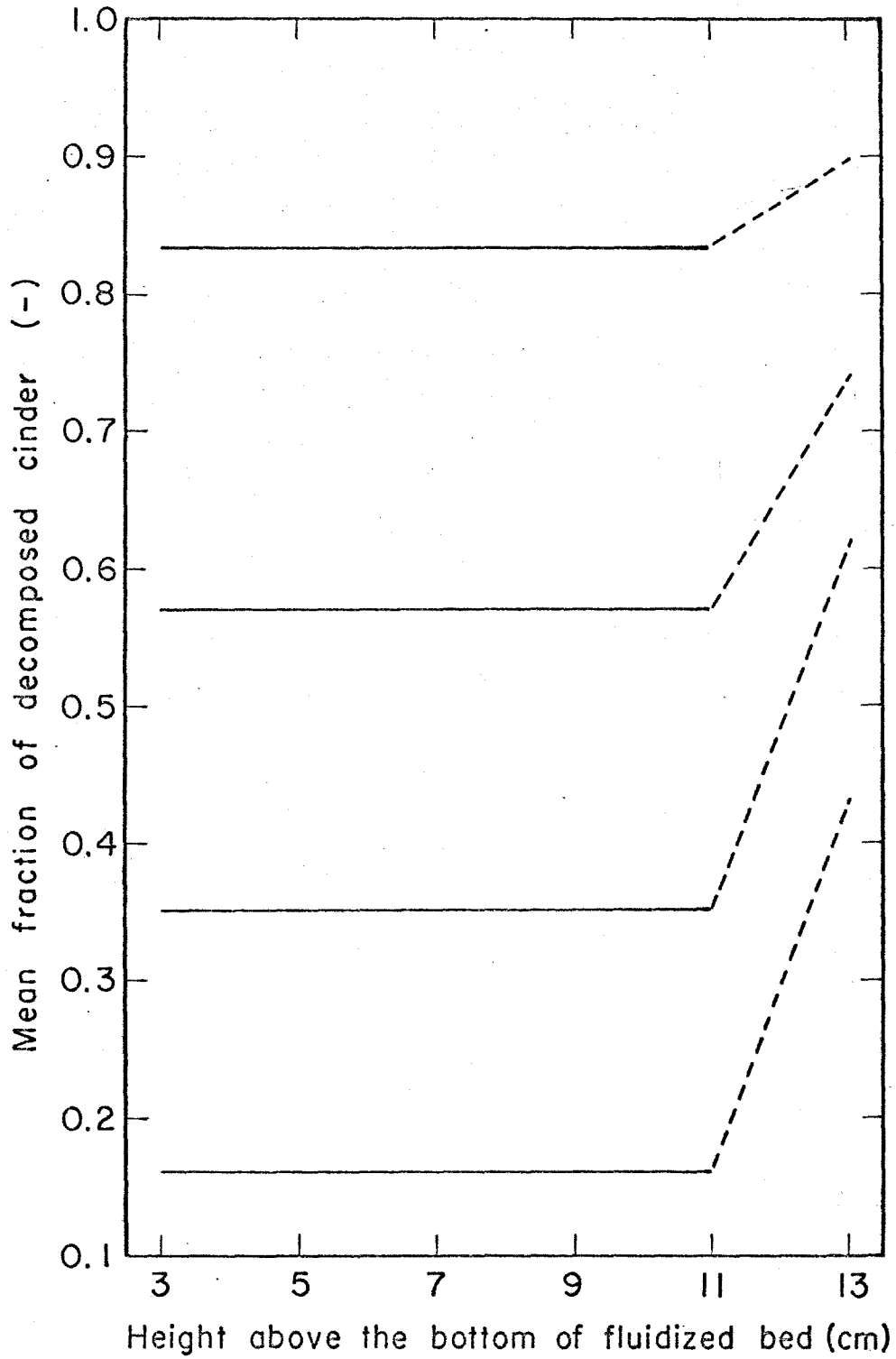


Fig. 4.12 Mean fraction of decomposed cinder vs. height above the bottom of fluidized bed

obtained was 2.97 $g/cm^3$ which is lower than that of pyrite particles. And it is thought that the possible segregation of the cinder in the upper part of the fluidized bed which was observed in Figs. 4.11 and 4.12 is caused partly by this density difference between pyrite particles and the decomposed product. In addition to this density difference, it is thought that the particle size is reduced by the thermal decomposition and the finer cinder particles are easily thrown up by the gas stream above the surface of fluidized bed.

At higher feeding rates of pyrite particles in the continuous process experiment, the fluidized mixtur is composed of a large amount of pyrite particles and a small amount of the cinder particles. And it was mentioned in Fig. 4.7 that the mean fraction of decomposed pyrite in the overflow coincides with the straigh line of Eq. (4.22) which assumes the upward piston flow of particles in the fluidized bed. This may be interpreted as follows. Because of the possible segregation of cinder particles in the upper part of the fluidized bed, the mean fraction of decomposed pyrite in the overflow deviates from Eq. (4.19) which assumes the complete mixing of particles in the fluidized bed and it approaches to Eq. (4.22) which assumes the upward

piston flow of particles within the bed.

The dimensionless temperature of the fluidized bed, $(t_f - t_d)/(t_{f\infty} - t_d)$, at higher feeding rates shown in Fig. 4.9 also revealed itself at a lower value than that calculated by Eq. (4.35) which assumes the complete mixing. This may be understood as follows. The amount of fluidized pyrite particles which are being decomposed in the bulk of the bed is larger than the amount presumed in Eq. (4.35) because of the large difference in the fraction of cinder between the bulk and the upper part of the fluidized bed. Furthermore, as mentioned above, the amount of sensible heat of pyrite which is consumed by heating the particles up to the decomposition temperature can not be omitted at higher feeding rates of pyrite particles.

On the other hand, at lower feeding rates of pyrite particles, both the mean fraction of decomposed pyrite in the overflow shown in Fig. 4.7 and the dimensionless temperature of the fluidized bed $(t_f - t_d)/(t_{f\infty} - t_d)$ in Fig. 4.9 coincide with their values calculated by Eq. (4.19) and Eq. (4.35), respectively, which assume a complete mixing of particles in the fluidized bed. This may be because the difference in the fraction of cinder is not significant between the bulk and the

upper portion of the fluidized bed.

## 4.6 Summary

The thermal decomposition of pyrite particles of 60 to 100 mesh size was carried out in a fluidized bed. Rate equations for batch process and continuous process were proposed on the assumption of heat transfer as the rate-controlling step and they were verified experimentally.

For the batch process, a linear rate equation of Eq. (4.9) was derived which neglected the resistance to heat transfer through the decomposed shell within the particles. It was found that this rate equation satisfies the experimental results. The overall heat transfer coefficient between the reactor wall and the fluidized bed was estimated from the experimental results and the radiative heat transfer coefficient was calculated by using Stefan-Boltzmann's law. The film coefficient of heat transfer was obtained by subtracting the radiative heat transfer coefficient from the overall heat transfer coefficient and it was found that the film coefficient of heat transfer is

in fair agreenent with that obtained in Chapter 3.

Two rate equations of Eqs. (4.19) and (4.22) were derived for the continuous process, assuming the complete mixing and the upward piston flow of particles in the fluidized bed, respectively. The former was found to be satisfactory for the fluidized bed of lower feeding rates and the latter for the bed of higher feeding rates of pyrite particles. The tendency of segregation of particles in the fluidized bed realized at higher feeding rates was also suggested from the bed temperature measurements.

In order to examine the suggested segregation of particles in the fluidized bed, the mixture composed of pyrite particles and the cinder particles decomposed at 750°C was fluidized at room temperature. Sample particles were taken from various heights of the fluidized bed and the composition was measured by magnetic separation. The results of this experiment indicated that the fraction of the cinder remains almost unchanged in the bulk of the fluidized bed and that a preferred segregation of cinder was found at the surface of the bed. The degree of this segregation increases along with the decreasing fraction of cinder in the fluidized mixture. It was suggested from these experimental

results that this preferred segregation at the surface of the fluidized bed is the reason why the rate equation assuming upward piston flow of particles holds for the fluidized bed containing a lower fraction of decomposed cinder particles which is realized at higher feeding rates.

## Notation in Chapter 4

$h_c$ : overall heat transfer coefficient (kcal/$m^2$·hr·°C)

$h_r$ : radiative heat transfer coefficient (kcal/$m^2$·hr·°C)

$h_w$ : film coefficient of heat transfer (kcal/$m^2$·hr·°C)

$k_e$ : effective thermal conductivity of decomposed layer within particle (kcal/m·hr·°C)

$k_g$ : thermal conductivity of gas (kcal/m·hr·°C)

n : number of decomposing particles in fluidized bed (-)

q : rate of heat transfer from reactor wall to fluidized bed (kcal/hr)

r : radius of reaction interface within particles (m)

t : temperature (°C)

| | | |
|---|---|---|
| $t_d$ | : decomposition temperature | ($^oC$) |
| $t_f$ | : temperature of fluidized bed | ($^oC$) |
| $t_{f\infty}$ | : temperature of fluidized bed composed of decomposed particles | ($^oC$) |
| $t_{go}$ | : temperature of gas blown into fluidized bed | ($^oC$) |
| $t_w$ | : temperature of reactor wall | ($^oC$) |
| $u$ | : linear velocity of gas at 20$^oC$ | (m/hr) |
| $u^*$ | : linear velocity of gas at $t_f$ | (m/hr) |
| $u_{mf}$ | : minimum fluidization velocity | (m/hr) |
| $w_d$ | : weight of decomposed particles | (kg) |
| $w_p$ | : weight of pyrite particles | (kg) |
| $x$ | : fraction of decomposed pyrite | (-) |
| $x_d$ | : fraction of decomposed pyrite at the final stage in batch process experiment | (-) |
| $C_{FeS}$ | : specific heat of FeS | (kcal/kg·$^oC$) |
| $C_{FeS_2}$ | : specific heat of $FeS_2$ | (kcal/kg·$^oC$) |
| $C_{S_2}$ | : specific heat of $S_2$ | (kcal/kg·$^oC$) |
| $D_p$ | : particle diameter | (m) |
| $D_t$ | : diameter of fluidization tube | (m) |
| $F$ | : feeding rate of pyrite | (kg/hr) |
| $F_c$ | : heat transfer area | ($m^2$) |
| $F_r$ | : surface area through which heat is transferred by radiation | ($m^2$) |

| | | | |
|---|---|---|---|
| $F_w$ | : | surface area through which heat is transferred by conduction | ($m^2$ |
| G | : | mass velocity of nitrogen gas | ($kg/m^2 \cdot hr$ |
| $\Delta H_d$ | : | enthalpy change of decomposition at $t_d$ | (kcal/kg |
| $L_f$ | : | height of fluidized bed | (m |
| $L_t$ | : | height of thermocouple above the bottom of fluidized bed | (m |
| $M_{FeS}$ | : | molecular weight of FeS | (- |
| $M_{FeS_2}$ | : | molecular weight of $FeS_2$ | (- |
| $M_{S_2}$ | : | molecular weight of $S_2$ | (- |
| N | : | number of particles in fluidized bed | (- |
| Nu | : | Nusselt number | (- |
| R | : | radius of particle | (m |
| Re | : | Reynolds number | (- |
| $T_f$ | : | absolute temperature of fluidized bed | ($^\circ K$ |
| $T_w$ | : | absolute temperature of reactor wall | ($^\circ K$ |
| W | : | total weight of particles present in fluidized bed | (kg |
| X | : | mean fraction of decomposed pyrite in overflow | (-) |
| $\varepsilon$ | : | void fraction of fluidized bed | (-) |
| $\varepsilon_{mf}$ | : | void fraction at minimum fluidization | (-) |
| $\varepsilon_p$ | : | emissivity of particle | (-) |
| $\varepsilon_w$ | : | emissivity of reactor wall | (-) |

$\eta$ : number fraction of pyrite particles in overflow (-)

$\theta$ : time (hr)

$\theta_d$ : decomposition time (hr)

$\mu$ : viscosity of nitrogen gas (kg/m·hr)

$\rho_c$ : density of decomposed pyrite ($kg/m^3$)

$\rho_P$ : density of pyrite ($kg/m^3$)

$\phi_P$ : shape factor of pyrite particle (-)

## References to Chapter 4


1) Tompkins, F. C. : Ind. Eng. Chem., 1952, Vol. 44, No. 6, pp. 1336-1338

2) Hill, R. A. : Trans. Farad. Soc., 1958, Vol. 54, pp. 685-690

3) Hashimoto, E. : Nippon Kagaku Zasshi (Japanese), 1961, Vol. 82, No. 11, pp. 1456-1461

4) Gafner, G. : Trans. Farad. Soc., 1959, Vol. 55, pp. 981-984

5) Narsimhan, G. : Chem. Eng. Sci., 1961, Vol. 16, pp. 7-20

6) Satterfield, C. N. and F. Feaks : A.I.Ch.E. Journal 1959, Vol. 5, No. 1, pp. 115-121

7) Wunderlich, G. : Z. Elektrochem., 1952, Vol. 56, pp. 218-223

8) Schwab, G. M. and J. Philinis : J. Am. Chem. Soc., 1947, Vol. 69, pp. 2588-2596

9) Nishihara, K. and Y. Kondo : Mem. Fac. Eng., Kyoto Univ., 1958, Vol. 20, pp. 285-306

10) Juza, R. and W. Biltz : Z. Anorg. Allgem. Chem., 1932, Vol. 205, pp. 273-286

11) Haraldsen, H. : Z. Anorg. Allgem. Chem., 1937, Vol. 231, pp. 78-96 ; 1941, Vol. 246, pp. 169-194, 195-226

12) Aris, R. : "The Optimal Design of Chemical Reactor 1961, p. 37, Academic Press, New York

13) Fujishige, H. : Report of the Resources Research Institute (Japan), 1965, No. 62, p. 88

14) Fujishige, H. : ibid., 1965, No. 62, p. 98

15) Mori, Y. and F. Yoshida : "Shoron Kagaku Kogaku", 1962, p. 652, Asakura Book Co., Inc., Tokyo

16) Bird, R. B., W. E. Stewart and E. N. Lightfoot : "Transport Phenomena", 1962, p. 257, John Wiley and Sons, Inc., New York

17) Bird, R. B., W. E. Stewart and E. N. Lightfoot : ibid., p. 23

18) Kunii, D. and O. Levenspiel : "Fluidization Engineering", 1969, p. 72, John Wiley & Sons,

Inc., New York

19) Takagi, Y., D. Komiyama, I. Kajihara, A. Kuriyama and K. Tarumi : Kagaku Kikai (Japanese), 1952, Vol. 16, No. 5, pp. 141-145

# CHAPTER 5 THERMAL DECOMPOSITION OF LIMESTONE

## 5.1 Introduction

Thermal decomposition of limestone is represented by

$$CaCO_3 = CaO + CO_2$$

The equilibrium pressure of $CO_2$ reaches 1 atm at about 900°C and the enthalpy change of this reaction is about 43 kcal/mole $CaCO_3$. Thermal decomposition of limestone is of general importance in the extraction metallurgy and in the chemical industries and the fluidization technique is being applied to this reaction (23).

Many workers (1-9) endeavored to clarify the mechanism of this reaction partly because of practical importance of this material in the industries and partly because of theoretical interest based on its well-known physical properties.

Furnas (1) studied the thermal decomposition of limestone particles of 2 to 8 cm diameter at the

temperature of 800° to 1100°C. He demonstrated that this reaction takes place in a very narrow zone within the particle, or, at the phase boundary between calcium carbonate and calcium oxide and that this zone advances from the outside to the interior of the particle at a constant rate determined by the reaction temperature. Britton, Gregg and Winsor (2) found that the decomposition rate is proportional to the area of reaction interface at the temperature between 720° and 790°C. As pointed out by Hashimoto (3), the formation of the interface observed by these workers is due to the sufficiently high rate of nucleation and growth of the decomposed phase.

Hashimoto (3, 5) and Ingraham and Marier (4) studied the effect of the partial pressure of carbon dioxide on the decomposition rate of limestone over a wide range of $CO_2$ pressure of 50 to 600 mmHg at the temperature of 790° to 900°C. Hashimoto (3) obtained the following empirical rate equation from the decomposition data,

$$k = A \frac{P^{\circ}_{CO_2} - P_{CO_2}}{P^{\circ}_{CO_2}} \exp\left(b \frac{P^{\circ}_{CO_2} - P_{CO_2}}{P^{\circ}_{CO_2}}\right)$$

where k is the decomposition rate per unit interface area, $P^{\circ}_{CO_2}$ is the equilibrium pressure of $CO_2$ and both

A and b are the empirical constants. Ingraham (4) also found that the decomposition rate is proportional to $(P^{o}_{CO_2} - P_{CO_2})/P^{o}_{CO_2}$. Hyatt, Cutler and Wadsworth (6) presented the following rate equation assuming that the overall reaction rate is determined by the rate of the interfacial reaction.

$$v = \frac{1 - (P^{o}_{CO_2} - P_{CO_2})}{BP_{CO_2} + (1/v_o)}$$

where v is the decomposition rate in terms of the rate of weight loss per unit area of the interface, $v_o$ is v at $P_{CO_2} = 0$, and B is a constant determined by the reaction temperature. It was indicated in this equation that the reaction rate is proportional to the area of reaction interface under the condition that both temperature and pressure of carbon dioxide are fixed at the constant values, respectively. Most of the works mentioned above were carried out below 900°C and their conclusion may be summarized as follows: the decomposition rate of limestone is determined by the reaction rate at the interface and this rate is influenced by the temperature and the pressure of carbon dioxide.

It is said, on the other hand, that heat or mass transfer rate begins to play an important role at

higher temperatures above 900°C, because the rate of the interfacial reaction becomes sufficiently high. Satterfield and Feakes (7) prepared a cylinder of calcium carbonate of 2 cm diameter and 7 cm long and a sphere of 2 cm diameter by agglomerating the precipitated calcium carbonate of 0.2 $\mu$ average diameter. They measured the temperature at the center of the cylinder and the sphere during thermal decomposition above 1000°C and found that the central temperature remains at the equilibrium decomposition temperature most of the time during the reaction. This reveals that the overall decomposition rate is determined solely by the rate of heat transfer. Furthermore, they studied the thermal decomposition of the agglomerate composed of powdered calcium carbonate of 10 to 15 $\mu$. In this case, the central temperature was found to be higher than the equilibrium decomposition temperature. Based on this result, they indicated that some nucleation or chemical activation process partially plays a role in the overall decomposition rate of calcium carbonate of this particle size. They also measured the permeability of carbon dioxide through the calcium oxide layer and suggested that the resistance offered to the passage of carbon dioxide through this layer has only a minor effect on the

overall reaction rate.

Narsimhan (8) derived a rate equation by assuming that the rate of heat transfer from the furnace through the outer decomposed shell of a limestone particle into the decomposing interface within the particle determines the overall rate. He compared this rate equation with the data obtained by Satterfield and Feakes (7) and found that the rate of thermal decomposition of limestone pellet of 2 cm in diameter at 1000°C satisfied his rate equation. Sugiyama et al. (9) also tried to derive a rate equation on the presumption that the temperature at the surface of a limestone particle changes with the time elapsed and that the rate of heat transfer from the surface to the interface within the particle controls the overall reaction rate. They also found that the overall decomposition rate of limestone particle of 1.0 to 2.7 cm diameter satisfies their rate equation at 1000°C.

As mentioned above, many works were published on the thermal decomposition of calcium carbonate. However, the decomposition data of limestone particles in a fluidized bed are scarcely found (10). It is of interest to clarify the decomposition rate of limestone particles in a fluidized bed, since the rate of heat transfer in a fluidized bed is much higher than

that in a fixed bed (11) and this is advantageous for the endothermic reactions with large enthalpy change such as the decomposition of limestone. Furthermore, since an amount of information is available on the thermal decomposition rate of limestone as mentioned above, it is of basic interest to compare the rate of thermal decomposition of limestone particles in a fluidized bed with the results obtained by these workers.

It is intended in this work to study the thermal decomposition rate of limestone particles of 60 to 100 mesh size in a fluidized bed. Bed temperature was chosen at 825° to 875°C. At this temperature, it may be supposed from the previous works (3-6) that the reaction rate at the interface may play an important role. On the other hand, since heat required for the reaction is supplied through the reactor wall to the fluidized bed, the rate of this heat transfer is also thought to be indispensable in the overall reaction rate.

In Chapter 4, a rate equation of pyrite particles in the fluidized bed was derived for the batch process experiment by assuming that the overall reaction rate is controlled by the rate of heat transfer from the reactor wall to the fluidized bed. Moreover, two

rate equations for continuous process experiment were derived by assuming the complete mixing and the upward piston flow of particles in the fluidized bed, respectively. It is intended in this chapter to verify the adaptability of these rate equations to the thermal decomposition of limestone particles in the fluidized bed. It is also intended to compare the rate of thermal decomposition of limestone particles in the fluidized bed with that obtained by the previous workers mentioned above. In addition, the rate equations applied to the thermal decomposition of pyrite and limestone particles in the fluidized bed are compared and examined.

## 5.2 Experimental

### 5.2.1 Experimental apparatus and the procedure

The fluidization apparatus used in this study is the same as that used for the thermal decomposition of pyrite. It was shown in Fig. 4.3. In this experiment, air is used as the fluidizing gas in place of nitrogen: it is supplied from a two-impeller type rotary blower.

The experimental work was composed of batch process experiment and continuous process experiment. These experiments were conducted substantially in the same way as mentioned in 4.3.4.

In the batch process experiment, an amount of 150 g of limestone particles of 60 to 100 mesh size was fed into the reactor maintained at a predetermined temperature to which the air flow was supplied at a given rate. The fluidized bed temperature remained unvaried for the major part of the reaction time, and an example is illustrated in Fig. 5.1. Sample particles were pipetted out of the fluidized bed in the course of decomposition and the composition was analysed by measuring the weight loss after heating it at 1200°C.

In the continuous process experiment, an amount of 150 g cinder was fluidized to form a steady state fluidized bed at a predetermined temperature and flow rate of air. And thereafter, limestone particles were fed at a constant rate from a rotary disc feeder. Fluidization was continued for the time duration required for the replacement of 95 % of the cinder in the fluidized bed plus 30 min and then the overflow particles were sampled and analysed.

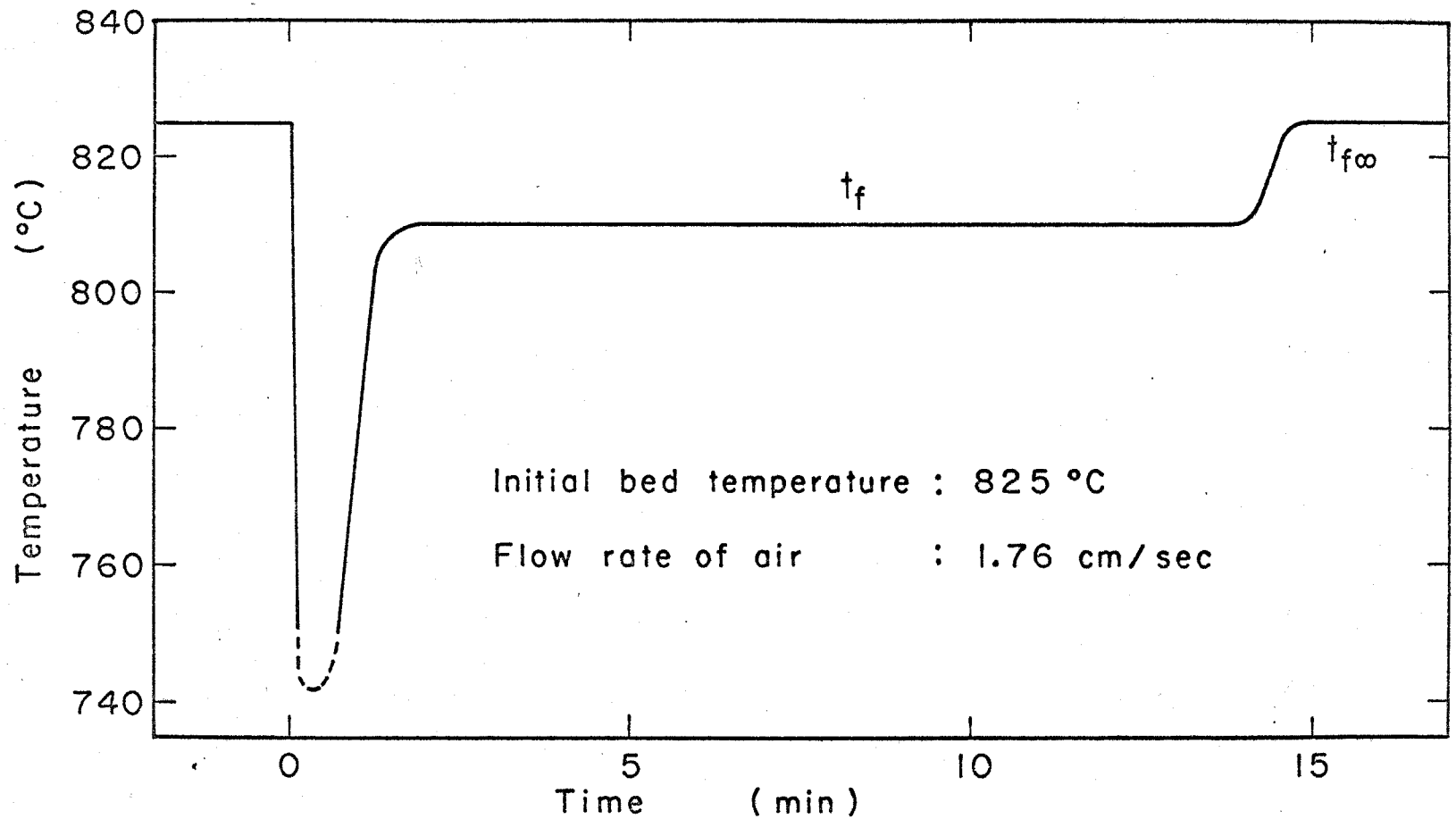


Fig. 5.1 An example of change of fluidized bed temperature in batch process

### 5.2.2 Material

Limestone lump offered through the courtesy of Ube Industrial Company Inc. was ground and sized into 60 to 100 mesh size. It was identified by the weight loss after ignition and by X-ray to be practically pure calcium carbonate.

### 5.2.3 Experimental conditions

In the batch process experiment, the bed temperature and the flow rate of air were chosen as the independent variables and their levels are listed in Table 5.1.

Table 5.1 Experimental conditions

| | |
|---|---|
| Batch process experiment | |
| Bed temperature | 825°, 850°, 875°C |
| Flow rate of air | 1.19, 1.76, 2.89 cm/sec (at 20°C) |
| Continuous process experiment | |
| Flow rate of air | 2.89 cm/sec (at 20°C) |
| Bed temperature | 825°, 850°, 875°C |
| Feeding rate of limestone | 0.1 to 1.4 kg/hr |

In the continuous process experiment, the flow rate of air was fixed at 2.89 cm/sec and the effects of bed temperature and the feeding rate of limestone particles were studied. The adopted levels are also summarized in Table 5.1.

## 5.3 Experimental results

### 5.3.1 Batch process experiment

Measured fraction decomposed, x, is illustrated in Fig. 5.2 against the fluidization time . It is seen in this figure that x increases linearly with the time $\theta$ and that the slope of the straight lines obtained by the least squares method changes according to the bed temperature and the flow rate of air.

In Chapter 4, a zero order rate equation was derived on the presumptions that the overall decomposition rate is determined by the heat transfer rate and that the resistance to heat transfer through the outer decomposed shell of the particles is omitted. This rate equation was shown in Eq. (4.9). From the facts that the temperature of the fluidized bed remains constant during the course of thermal decompo-

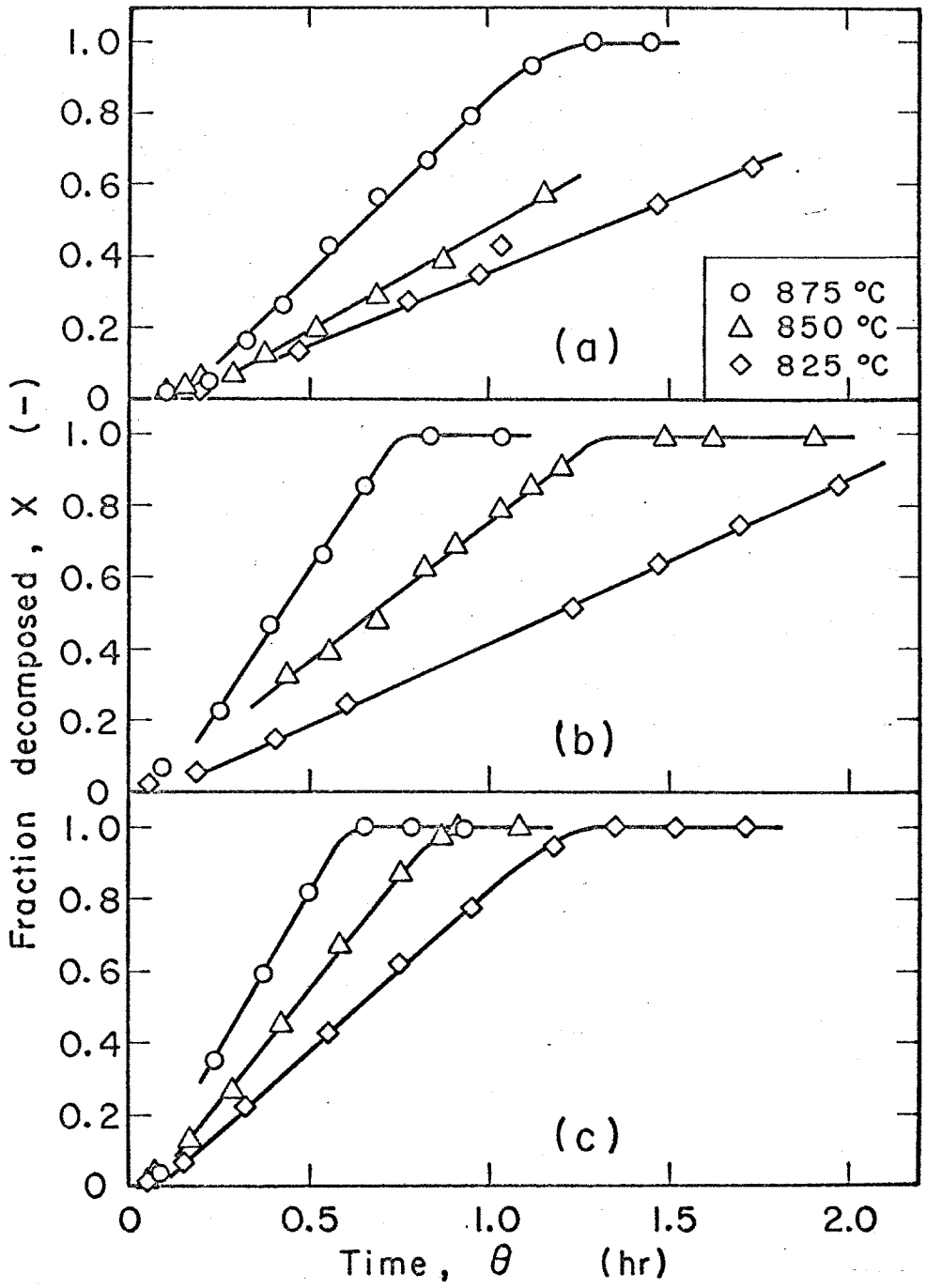


Fig.5.2 Fraction decomposed vs. decomposition time in batch process; flow rate of air : (a) 1.19 cm/sec, (b) 1.76 cm/sec, (c) 2.89 cm/sec

sition as shown in Fig. 5.1 and that the fraction decomposed increases linearly with the reaction time, it is reasonable to presume under the experimental conditions in this work that the overall decomposition rate is determined by the rate of heat transfer from the reactor wall to the fluidized bed. And thus the experimental results satisfied Eq. (4.9) and the slope of straight lines in Fig. 5.2,(b), can be represented by,

$$\theta = \frac{4 h_c (t_w - t_d)}{\rho_p D_t (1-\varepsilon) \Delta H_f} \qquad (5.1)$$

The overall heat transfer coefficient between the reactor wall and the fluidized bed, $h_c$, can be estimated from Eq. (5.1). It is shown in Fig. 5.3. In this figure, the linear velocity of air at the temperature of the fluidized bed, u*, was calculated by,

$$u^* = u \times \frac{t_f + 273}{293}$$

where u is the linear velocity at 20°C. The following regression was obtained from Fig. 5.3 by using the least squares method.

$$h_c = 24.3\, u^{*0.304} \qquad (5.2)$$

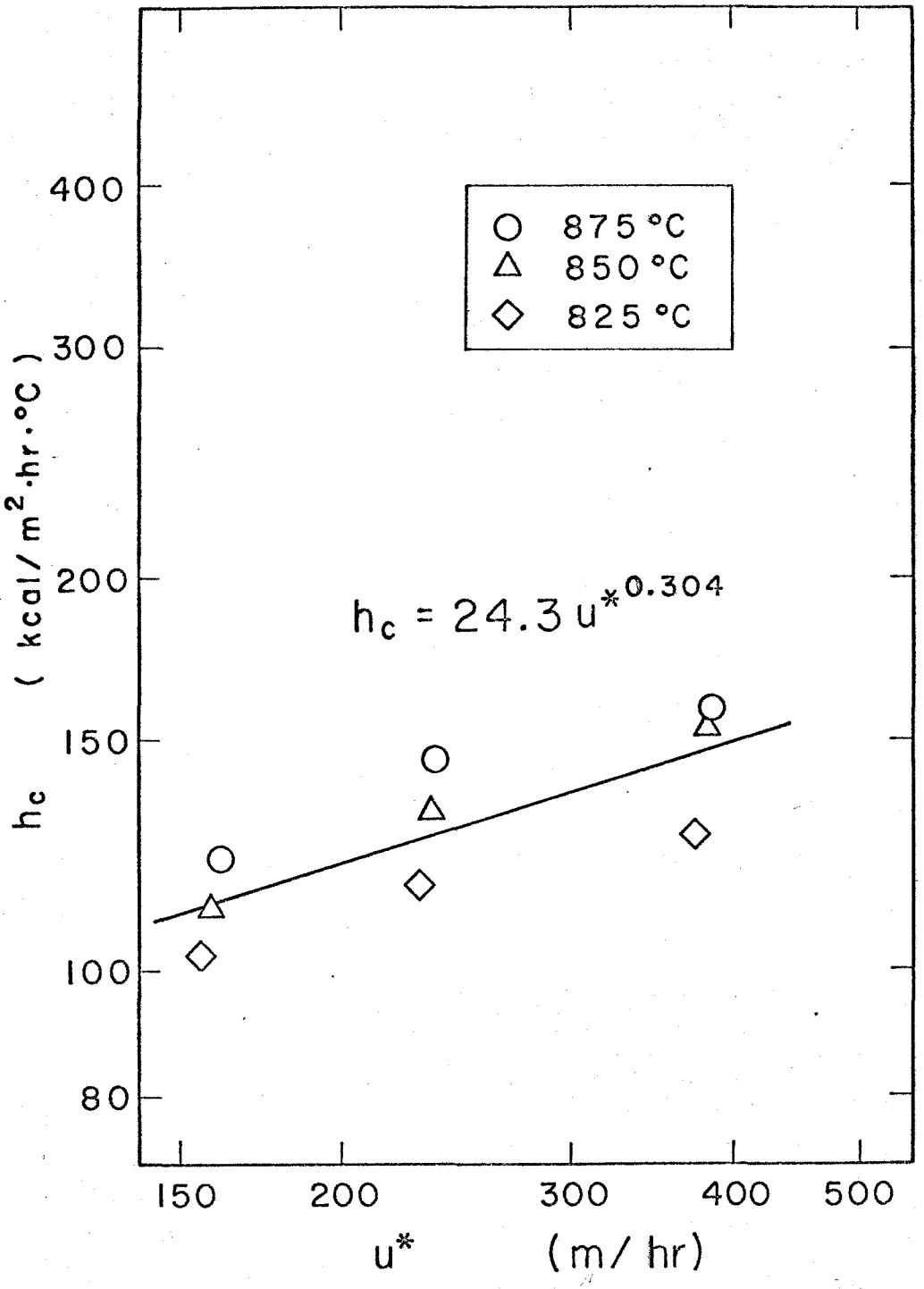


Fig.5.3 Overall heat transfer coefficient

### 5.3.2 Continuous process experiment

The mean fraction, X, of decomposed limestone in the overflow is illustrated in Fig. 5.4 against the reciprocal feeding rate, 1/F. The calculated values of the mean fraction, X, with Eq. (4.19) for complete mixing and with Eq. (4.22) for upward piston flow of particles are also plotted in this figure. In the calculation of these values, $h_c$ given by Eq. (5.2) and $x_d = 1.0$ were used and $t_d$ was assumed to be equal to the constant temperature of the fluidized bed, $t_f$, given in Fig. 5.1.

When the fluidized bed temperature is kept at 825° and 850°C, it is seen from Fig. 5.4 that most values of the measured X satisfy Eq. (4.22) which assumes upward piston flow of particles in the fluidized bed. In the experiment where the bed temperature is kept at 875°C, on the other hand, it is seen from the same figure that X measured at higher feeding rates coincides with the curves of Eq. (4.19) which assumes complete mixing of the particles in the fluidized bed and X tends to deviate from this equation to the straight line of Eq. (4.22). These correlationships between X and the reciprocal feeding rate is thought to be rather different from those observed

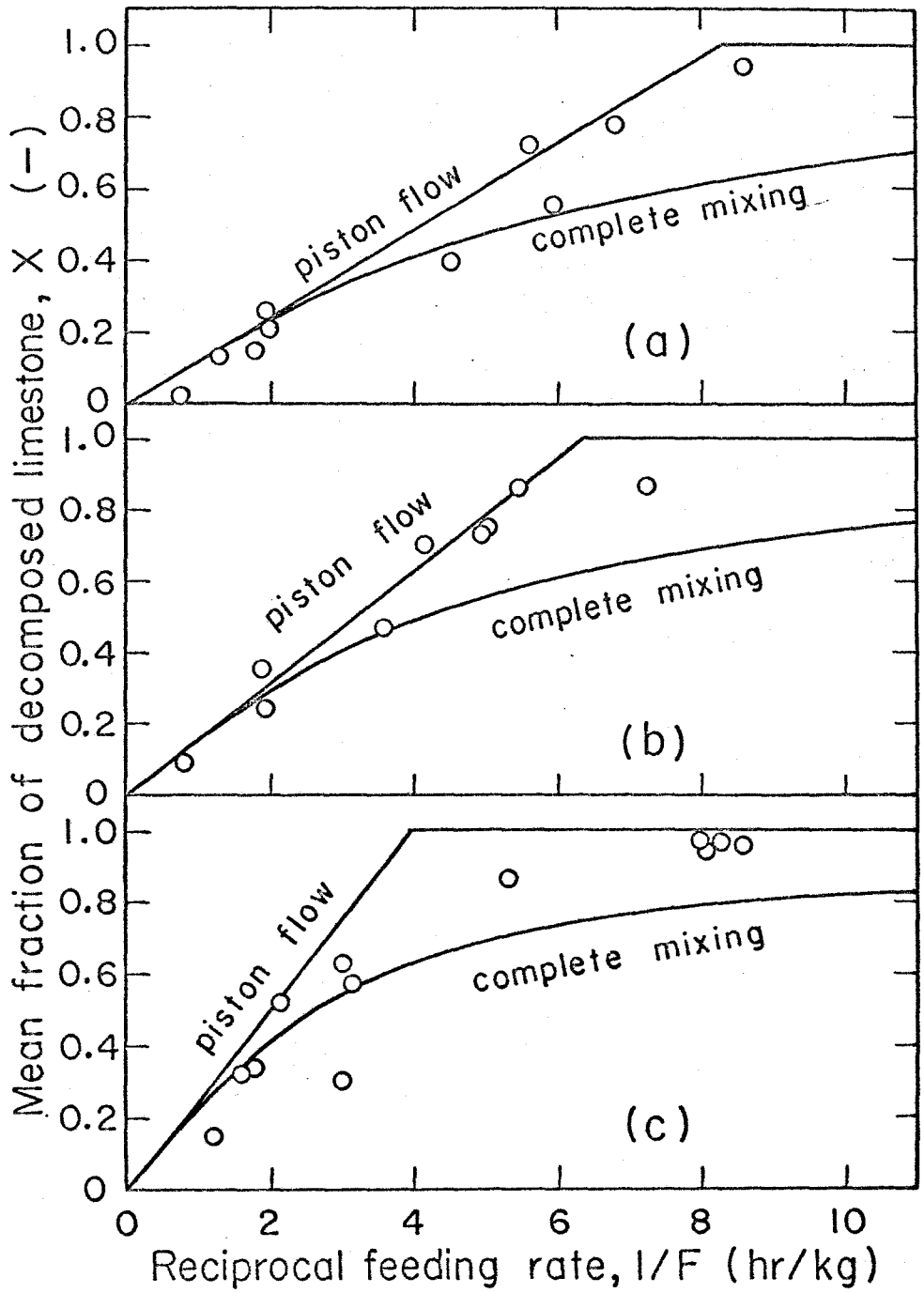


Fig.5.4 Mean fraction of decomposed limestone, X, vs. reciprocal feeding rate, 1/F, in continuous process. Initial bed temperature : (a)825°C, (b)850°C, (c)875°C

in the thermal decomposition of pyrite. This tendency will be discussed later.

## 5.4 Discussion

Concerning the batch process experiment, it was mentioned in 5.3.1 that the fraction decomposed, x, increases linearly with the reaction time as shown in Fig. 5.2 and that this satisfies the linear rate equation of Eq. (4.9). The overall heat transfer coefficient between the reactor wall and the fluidized bed, $h_c$, was estimated from Eq. (5.1) and was illustrated in Fig. 5.3. The film coefficient of heat transfer between the reactor wall and the fluidized bed, $h_w$, can be estimated from $h_c$ thus obtained. And it is of basic interest to compare $h_w$ with that obtained in Chapter 3, because it may also offer an indication in determining the rate controlling step in the thermal decomposition of limestone particles in a fluidized bed.

The amount of heat transferred from the reactor wall to the fluidized bed is given by,

$$q = h_c F_c (t_w - t_f)$$
$$= h_w F_w (t_w - t_f) + h_r F_r (t_w - t_f) \qquad (5.3)$$

where $F_w$ and $F_r$ are the area through which heat is transferred by conduction and by radiation, respectively, and they can be represented by,

$$F_w = F_r = \pi D_t L_f \quad (= F_c) \tag{5.4}$$

From Eqs. (5.3) and (5.4), the following expression is obtained.

$$h_w = h_c - h_r \tag{5.5}$$

The amount of heat transferred by radiation is given by Stefan-Boltzmann's law as:

$$q_r = \sigma F_r \phi ( T_w^4 - T_f^4 ) \tag{5.6}$$

Insertion of this equation into the second term on the right-hand side of Eq. (5.3) yields,

$$h_r = \sigma \phi \frac{T_w^4 - T_f^4}{t_w - t_f}$$

$$= 4.88 \times 10^{-8} \phi ( T_w^2 + T_f^2 )( T_w + T_f ) \tag{5.7}$$

Moreover, the radiative heat transfer between the reactor wall and the fluidized bed is regarded as the heat transfer between two concentric tubes (12) and $\phi$ in Eq. (5.7) is given by,

$$\frac{1}{\phi} = \frac{1}{\varepsilon_w} + \frac{1}{\varepsilon_p} - 1 \qquad (5.8)$$

where $\varepsilon_w$ and $\varepsilon_p$ are the emissivities of the reactor wall and of the decomposed shell of limestone particles, respectively. $\varepsilon_p$ is assumed at 0.27 (13) and $\varepsilon_w$ is at 0.42 ($t_w$ = 825°C), 0.40 ($t_w$ = 850°C) and 0.38 ($t_w$ = 875°C) (14), respectively. The results of calculation are summarized in Table 5.2.

In addition, the correlationship between the Reynolds number ($D_p G/\mu$) and the Nusselt number ($h_w D_p/k_g$) is to be discussed by using $h_w$ listed in Table 5.2. In the calculation of these dimensionless numbers, thermal conductivity and viscosity of air, $k_g$ and $\mu$, were presumed at $6.16 \times 10^{-2}$ kcal/m·hr·°C (15) and $4.60 \times 10^{-4}$ poise (16), respectively. The results are illustrated in Fig. 5.5 and the following regression equation was obtained by the least squares method.

$$\frac{h_w D_p}{k_g} = 0.826 \left( \frac{D_p G}{\mu} \right)^{0.516} \qquad (5.9)$$

This equation was also plotted in Fig. 3.7. It may be seen in this figure that Eq. (5.9) lies somewhat higher than the straight line of Eq. (3.20), though the difference between these two regression lines is not

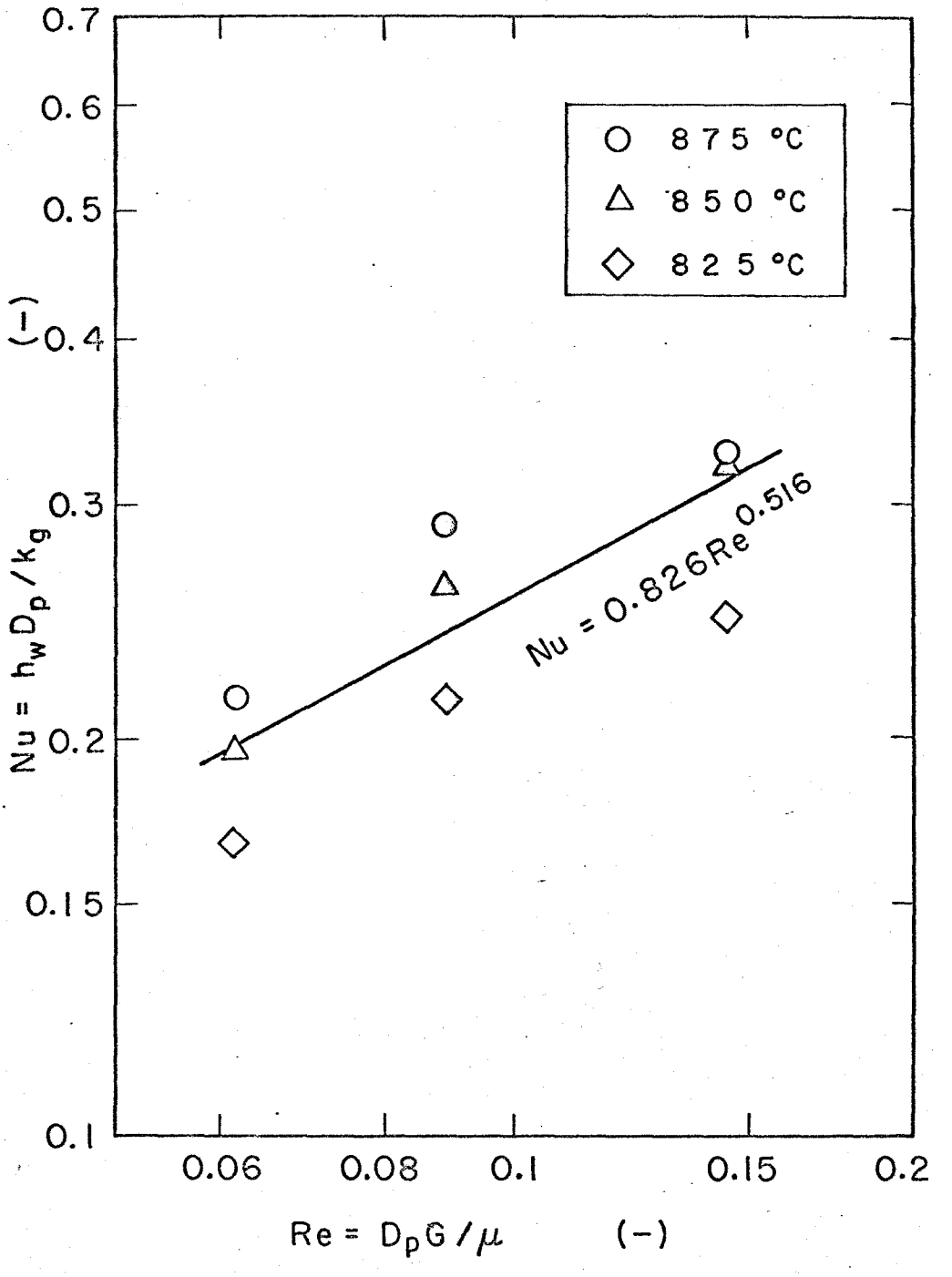


Fig.5.5 Correlationship between Re and Nu

Table 5.2 Heat transfer coefficient

| Initial bed temperature (°C) | Flow rate of air at 20°C (cm/sec) | Heat transfer coefficient (kcal/m$^2$·hr·°C) | | |
|---|---|---|---|---|
| | | $h_c$ | $h_r$ | $h_w$ |
| 825 | 1.19 | 102.4 | 49.8 | 52.6 |
| | 1.76 | 117.2 | 49.7 | 67.5 |
| | 2.89 | 127.1 | 49.3 | 77.8 |
| 850 | 1.19 | 111.9 | 51.5 | 60.4 |
| | 1.76 | 132.3 | 51.8 | 80.5 |
| | 2.89 | 153.9 | 51.4 | 102.5 |
| 875 | 1.19 | 121.4 | 53.6 | 67.8 |
| | 1.76 | 145.0 | 53.0 | 92.0 |
| | 2.89 | 159.3 | 52.9 | 106.4 |

significant when both of them are compared with the regressions obtained by the other workers. It may be thought that the deviation of Eq. (5.9) from Eq. (3.20) is mainly caused by the error in estimating $\varepsilon_p$ in Eq. (5.8). It may also be thought that this deviation occurs when the heat transfer controlling model presumed in this work is not completely applied to the thermal decomposition of limestone particles in the fluidized bed. However, it is expected that Eq. (5.9)

lies below Eq. (3.20) when the elementary reaction steps other than the heat transfer affect the overall rate, because the overall rate of thermal decomposition of limestone particles is reduced when the resistance to the reaction steps other than the heat transfer, such as the interfacial reaction and the mass transfer of $CO_2$ through the decomposed shell, can not be omitted. Therefore, from the facts observed in this work that the fluidized bed temperature remains unchanged during the major part of the reaction time as shown in Fig. 5.1, that the fraction decomposed increases linearly with time as shown in Fig. 5.2 and that the deviation of Eq. (5.9) from Eq. (3.20) is not significant as compared with the regression lines obtained by the other workers, it may be reasonable to presume that the overall rate of thermal decomposition of limestone particles in the fluidized bed is determined by the rate of heat transfer from the reactor wall to the fluidized bed.

It was mentioned in 5.1 that the rate of interfacial reaction occurring within particles plays an important role in the overall reaction rate when the temperature is below 900°C (3-6) and that the overall reaction rate is mainly determined by the heat transfer rate at higher temperatures above 1000°C (7-9).

The temperature of the fluidized bed was chosen in this work at 825° to 875°C and, nevertheless, it was suggested above that the overall decomposition rate is determined by the rate of heat transfer from the reactor wall to the fluidized bed. This conclusion is somewhat different from the results obtained by Ingraham (4) and by Hyatt, Cutler and Wadsworth (6).

In order to clarify the situation, the experimental conditions adopted in this work are compared with the other works. Ingraham (4) studied the thermal decomposition rate of precipitated calcium carbonate of about 0.5 g at 780° to 850°C by thermogravimetric analysis. Hyatt, Cutler and Wadsworth (6) used a plate crystal of calcium carbonate of about 0.1 cm thick and 1.0 to 1.5 cm wide and long whose weight was about 0.6 g. This crystal was placed in a platinum screen basket and decomposed at 800° to 950°C. Under these experimental conditions where a small amount of calcium carbonate is decomposed, a large amount of heat can easily be supplied from the surroundings to the decomposing specimen. And thus the conditions of heat transfer from the surroundings to the surface of calcium carbonate particles is more favorable and is thought to be somewhat different from the conditions adopted in this work.

The rate of heat transfer from the reactor wall to the fluidized bed is represented by,

$$q = \pi D_t L_f (h_w + h_r)(t_w - t_f) \qquad (5.10)$$

On the other hand, the surface area of limestone particles is,

$$A = N \pi D_p^2 \qquad (5.11)$$

where N is the number of particles present in the fluidized bed and is expressed by,

$$N = \frac{6W}{\pi D_p^3 \rho_p} \qquad (5.12)$$

Inserting Eq. (5.12) into Eq. (5.11), we have,

$$A = \frac{6W}{D_p \rho_p} \qquad (5.13)$$

Consequently, the heat transfer rate per unit surface area of limestone particles is given by the following equation.

$$\frac{q}{A} = \frac{\pi D_t L_f D_p \rho_p (h_w + h_r)}{6W} (t_w - t_f) \qquad (5.14)$$

Under the fluidizing conditions that the flow rate of air is 1.76 cm/sec and the bed temperature is 850°C, $(h_w + h_r)$ is obtained at 132.2 kcal/$m^2$·hr·°C from Table 5.2.

Inserting this value into Eq. (5.14), q/A becomes

$$\frac{q}{A} = 1.31\,(t_w - t_f) \qquad \left(\frac{kcal}{m^2 \cdot hr}\right) \qquad (5.15)$$

This equation demonstrates that an amount of heat of 1.31 kcal can be supplied from the surroundings to the unit surface of limestone particles per unit time when the temperature difference between the reactor wall and the fluidized bed is $1^{\circ}C$.

On the other hand, Hyatt, Cutler and Wadsworth (6) measured the rate of thermal decomposition of a crystal of calcium carbonate which was kept at $850^{\circ}C$ in a tube furnace of 1 in inner diameter. The flow rate of nitrogen gas was maintained at 90 $cm^3$ per minute. Under these experimental conditions, the rate of heat transfer from the surroundings to the surface of the calcium carbonate crystal is represented by,

$$q = F_c\,(h_r + h)(t_F - t_S) \qquad (5.16)$$

where h is the convective heat transfer coefficient between the nitrogen gas and the crystal surface and $t_F$ and $t_S$ are the temperatures of the furnace and of the crystal surface, respectively. The thickness of the plate crystal of calcium carbonate used in their work was 0.1 cm and this value is about 10 times

larger than the diameter of limestone particles of 60 to 100 mesh size. And thus the resistance to heat transfer through the outer decomposed shell of calcium carbonate crystal may not be omitted. The amount of heat transferred through the decomposed shell to the reaction interface is represented by,

$$q = F_c k \frac{t_s - t_I}{z} \tag{5.17}$$

where k is the effective thermal conductivity of the decomposed shell, $t_I$ is the temperature at the interface and z is the thickness of the decomposed shell. Combining Eqs. (5.16) and (5.17), we have,

$$q = \frac{F_c (t_F - t_I)}{\frac{1}{h_r + h} + \frac{z}{k}} \tag{5.18}$$

Thus, the rate of heat transfer per unit interface area within the crystal is,

$$\frac{q}{F_c} = \frac{t_F - t_I}{\frac{1}{h_r + h} + \frac{z}{k}} \tag{5.19}$$

The radiative heat transfer coefficient, $h_r$, in this equation can be estimated as follows. The amount of heat transferred by radiation is expressed by,

$$q_r = F_c h_r (t_F - t_s) \tag{5.20}$$

And it can also be represented by the Stefan-Boltzmann's law as follows.

$$q_r = F_c \phi \sigma ( T_F^4 - T_S^4 ) \qquad (5.21)$$

When the surface area of the crystal, $F_c$, is sufficiently small as compared with the inner surface area of the furnace, $\phi$ in Eq. (5.21) becomes (21)

$$\phi = \varepsilon_c \qquad (5.22)$$

where $\varepsilon_c$ is the emissivity of outer decomposed shell of calcium carbonate crystal. From Eqs. (5.20) to (5.22), we obtain,

$$h_r = 4.88 \times 10^{-8} \varepsilon_c ( T_F^2 + T_S^2 )( T_F + T_S ) \qquad (5.23)$$

The furnace temperature, $T_F$, was not given in their work. Assuming $T_F = T_S$ and equating them to $(850 + 273) = 1123^{\circ}K$, the radiative heat transfer coefficient, $h_r$, is calculated at 74.7 $kcal/m^2 \cdot hr \cdot {}^{\circ}C$, where the value of $\varepsilon_c$ was presumed at 0.27 (13).

The convective heat transfer coefficient, h, in Eq. (5.16), on the other hand, was estimated at 1.3 $kcal/m^2 \cdot hr \cdot {}^{\circ}C$ by using the Pohlhausen's equation (22);

$$\frac{hL}{k_g} = 0.664 \left( \frac{L u \rho_g}{\mu} \right)^{\frac{1}{2}} \left( \frac{C_g \mu}{k_g} \right)^{\frac{1}{3}} \qquad (5.24)$$

where L is the length of crystal of calcium carbonate. The effective thermal conductivity of the decomposed layer, k, was measured at 0.68 kcal/m·hr·°C by Satterfield and Feakes (7).

Since $q/F_c$ shown in Eq. (5.19) decreases with increased thickness of decomposed shell, z, the minimal value of $q/F_c$ at z = 0.05 cm is calculated by using $h_r$, h and k estimated above and we have,

$$\frac{q}{F_c} = 71.9\,(t_F - t_I) \qquad \left(\frac{kcal}{m^2 \cdot hr}\right) \qquad (5.25)$$

This means that an amount of heat more than 71.9 kcal is supplied from the surroundings to the unit surface of the crystal per unit time when the temperature difference between the furnace and the interface within calcium carbonate crystal is 1°C. This value is almost sixty times larger than the value calculated above for the fluidized bed.

These inspections revealed that a large amount of heat can easily be supplied from the surroundings to the interface within the calcium carbonate specimen and that the resistance to heat transfer may be omitted by comparing it with the resistance to the interfacial decomposition within the particle, when a small amount of calcium carbonate is placed in a large space of a furnace. In the fluidized bed, however, a large

amount of limestone particles are fluidized and the heat transfer rate per unit surface area of limestone particles is rather low and the resistance to heat transfer from the reactor wall to the fluidized particles can not be omitted. This is the reason why the overall decomposition rate of limestone particles in a fluidized bed is determined by the heat transfer rate at the temperature of 825° to 875°C.

Further inspection is made on the rate of thermal decomposition of limestone particles. Hyatt, Cutler and Wadsworth (6) found that the overall rate of thermal decomposition of a calcium carbonate crystal is controlled by the rate of chemical reaction occurring at the interface within the crystal and the rate is proportional to the interfacial area within the crystal. The decomposition rate constant, $\alpha$ , was measured at $2.71 \times 10^{-3}$ g/min·cm$^2$ at 850°C.

With this value of decomposition rate, the time required for the thermal decomposition of limestone particles of 60 to 100 mesh size used in this work was estimated. From the assumption that the reaction rate is proportional to the interfacial area within the particles proposed by Hyatt, Cutler and Wadsworth (6), the thermal decomposition rate of a limestone particle is represented by the following equation.

$$-\frac{dw}{d\theta} = 4\pi r^2 \alpha \qquad (5.26)$$

where r is the radius of the decomposing interface. In this equation, $w$ is the weight of undecomposed limestone within the particle at time, $\theta$, and it is expressed by,

$$w = \frac{4}{3}\pi r^3 \rho_p \qquad (5.27)$$

From Eqs. (5.26) and (5.27), we obtain,

$$-dr = \frac{\alpha}{\rho_p} d\theta \qquad (5.28)$$

Integration of Eq. (5.28) with the conditions of r = R at $\theta = 0$ and r = 0 at $\theta = \theta_d$ gives

$$\theta_d = \frac{\rho_p}{\alpha} R \qquad (5.29)$$

Inserting $\rho_p = 2.71$ g/cm$^3$, $\alpha = 2.71 \times 10^{-3}$ g/min·cm$^2$ and R = $9.7 \times 10^{-3}$ cm into this equation, we obtain $\theta_d = 9.8$ min.

Furnas (1), on the other hand, measured the thermal decomposition rate of the crushed limestone particle of 2 to 8 cm diameter. As mentioned in 5.1, he found that the interface proceeds from the surface to the interior of the particle at a constant rate, and the following regression equation was presented.

$$\log \alpha' = 0.003145\, t - 3.3085 \qquad (5.30)$$

where $\alpha'$ is the rate of advance of the interface in cm/hr and t is the temperature in $^{o}$C. Putting t = 850$^{o}$C in Eq. (5.30) yields $\alpha'$ = 0.232 cm/hr. By using this value, the time, $\theta_d$, required for the completion of thermal decomposition of limestone particles of 60 to 100 mesh size is calculated at 2.5 min. Ingraham (4) measured the rate of thermal decomposition of precipitated calcium carbonate in the air stream at 850$^{o}$C. The rate constant, $\alpha$, calculated from his data is 0.01 g/min$\cdot$cm$^2$. By using $\alpha$ = 0.01 g/min$\cdot$cm$^2$ in Eq. (5.29), $\theta_d$ = 2.6 min is obtained. This value of $\theta_d$ is very close to that estimated from the data obtained by Furnas and it is somewhat shorter than that estimated from the results obtained by Hyatt, Cutler and Wadsworth (6) who used a calcium carbonate crystal in their work.

On the other hand, it is seen from Fig. 5.2 that the time, $\theta_d$, required for thermal decomposition of limestone particles in the fluidized bed at 850$^{o}$C is about 80 and 50 min at the flow rate of air at 1.76 and 2.89 cm/sec, respectively. These values of $\theta_d$ in the fluidized bed are much higher than the time values estimated above which presumes that a small

amount of calcium carbonate particles are decomposed. It can be mentioned from these investigations that this difference in the reaction time, $\theta_d$ , in the thermal decomposition of limestone particles is caused by the additional resistance to heat transfer from the surroundings to limestone particles which can not be neglected in a fluidized bed.

In the continuous process experiment, it was mentioned that the mean fraction of decomposed limestone, X, satisfies Eq. (4.19) at 875°C which presumes complete mixing of particles in the fluidized bed, when the feeding rate of limestone particles is higher. On the other hand, X tends to deviate at lower feeding rates from this equation to the straight line of Eq. (4.22) which assumes the upward piston flow of particles; it was supposed that the possible segregation of particles occurs in the fluidized bed. In order to investigate these behaviors of particles further, the vertical distribution of fraction decomposed along the height of continuous fluidized bed was studied.

An amount of 0.01 to 0.1 g of particles was sampled from the fluidized bed at an interval of 2 cm in vertical direction and their composition was analyzed. Sample probe shown in Fig. 4.10 was used. The fluidization conditions in this experiment were:

the feeding rate of limestone particles was 0.2 and 0.5 kg/hr, the air velocity was 2.89 cm/sec and the bed temperature was maintained at 825°, 850° and 875°C. Because of small amounts of samples taken, the variation of data was rather wide. And their mean values at individual heights are illustrated in Figs. 5.6 and 5.7. In these figures, the mean fraction of decomposed limestone, X, in the overflow was also plotted. The overflow pipe is located at a height of 13 cm above the bottom of the fluidized bed. It is seen from Fig. 5.6 that the fraction of decomposed limestone remains almost unchanged within the bulk of the fluidized bed and it increases rapidly at the height of overflow pipe. On the other hand, however, this segregation at the surface of the fluidized bed was not observed in Fig. 5.7 which was obtained at higher feeding rates.

The density of limestone particles is 2.71 $g/cm^3$ (17) and the density of the decomposed product was measured at 2.04 $g/cm^3$. And it is thought that the segregation of particles at the upper part of the fluidized bed which was observed in Fig. 5.6 is partly caused by the density difference between limestone particles and its decomposed product. In addition, the formation of finer particles caused by the thermal

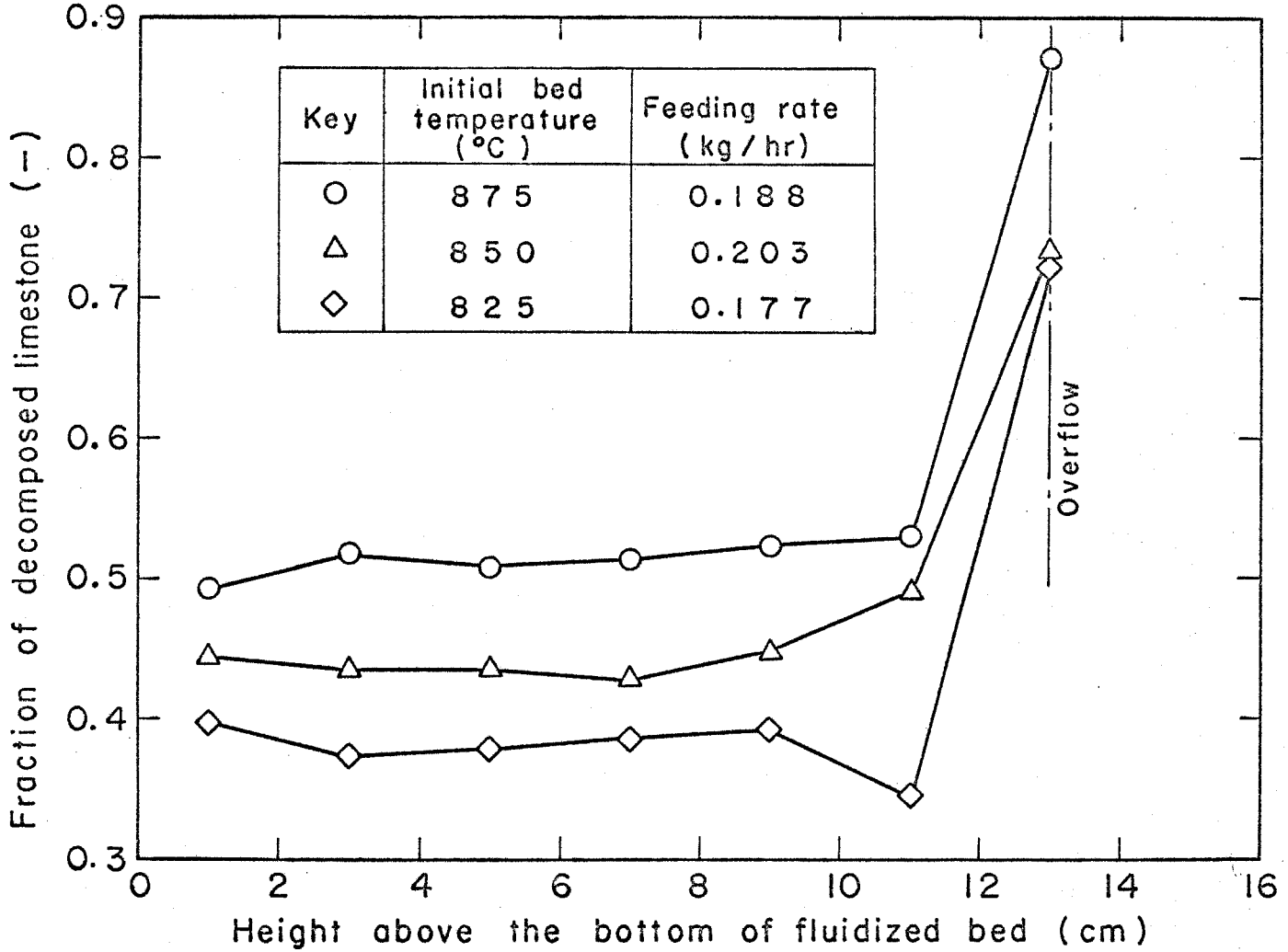


Fig.5.6 Vertical distribution of decomposed limestone

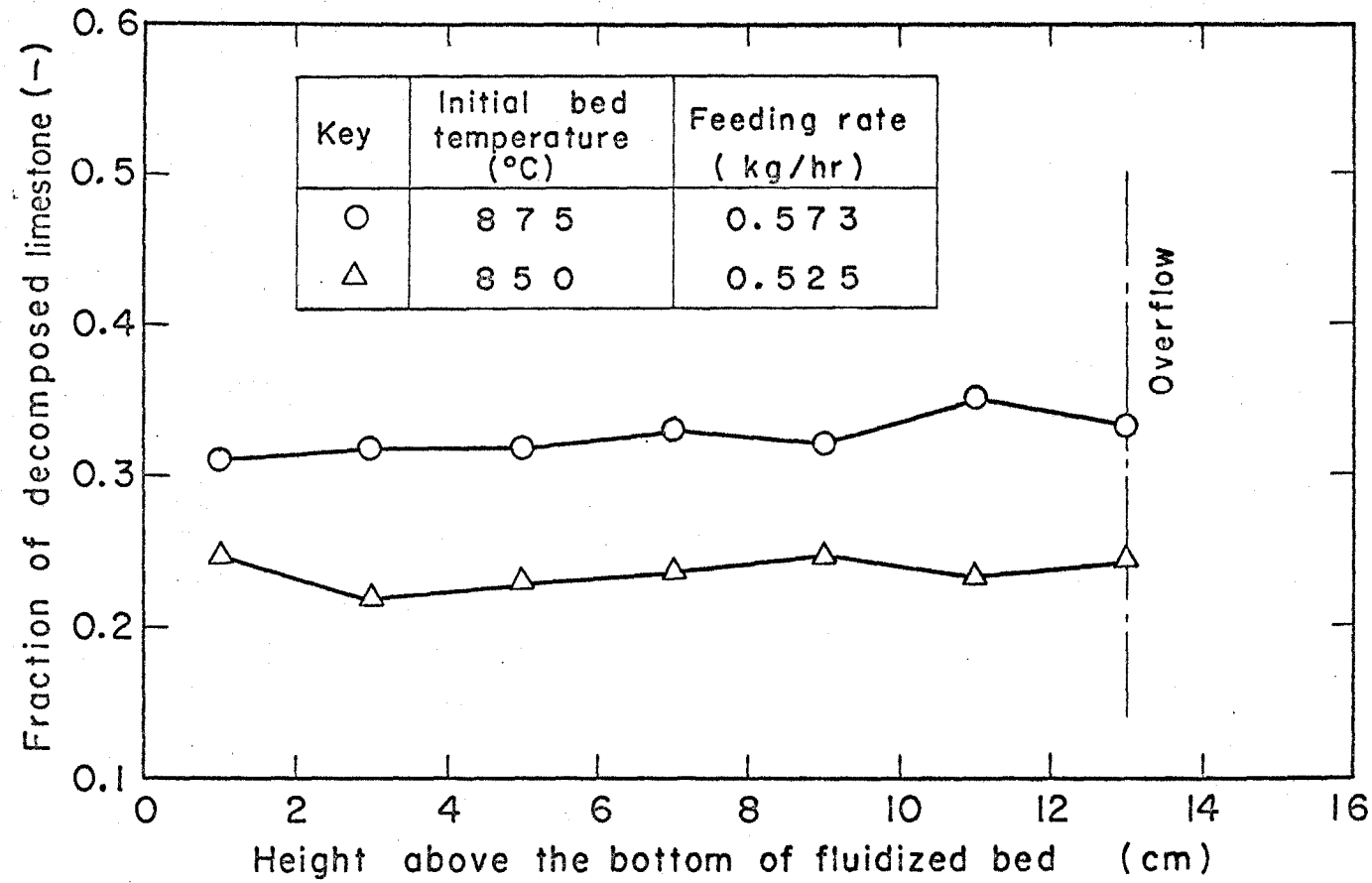


Fig.5.7 Vertical distribution of decomposed limestone

decomposition may also be another reason for the segregation. The reciprocal feeding rate, 1/F, illustrated in Figs. 5.6 and 5.7 are about 5.5 and 2.0 hr/kg, respectively. It is seen in Fig. 5.4 that X at 1/F = 5.5 is near the straight lines of Eq. (4.22) which assumes the upward piston flow of particles in the fluidized bed. From this, it can be said that the mean fraction of decomposed limestone in the overflow deviates at lower feeding rates from Eq. (4.19) which assumes the complete mixing of particles in the fluidized bed, because of the possible segregation of particles in the upper part of the fluidized bed and that it approaches to the straight lines of Eq. (4.22) which assumes the upward piston flow of particles in the fluidized bed. It is seen in Fig. 5.4, on the other hand, that the curve of Eq. (4.19) is so close to the straight line of Eq. (4.22) at 1/F = 2.0 and it is difficult from this figure to judge the behavior of particles in the fluidized bed at higher feeding rates. However, it can be mentioned from Fig. 5.7 that the mean fraction of decomposed limestone in the overflow satisfies Eq. (4.19) which assumes the complete mixing of particles in the fluidized bed at higher feeding rates.

In the thermal decomposition of pyrite particles,

on the other hand, it was mentioned that the mean fraction of decomposed pyrite in the overflow deviates from Eq. (4.19) at higher feeding rates and that this deviation becomes minor at lower feeding rates. And the correlationship between the feeding rate and the behavior of fluidized particles seems to be somewhat different between limestone particles and pyrite particles. Further inspection is made, therefore, on the segregation of particles in the upper part of fluidized bed.

Urabe et al. (19) measured the particles size distribution of fluidized particles in vertical direction in the fluidized bed. They found that the particles are completely mixed within the bulk of bed and that the segregation due to the difference in particle size was observed at the bed surface where the particle concentration is lower. This experimental result was explained as follows. Particles are thrown up by the ascending bubbles above the surface of fluidized bed and the size distribution of these particles is supposed to be same as that in the bulk of fluidized bed. The particle concentration at this level is fairly dilute and individual particles can move more freely; the particles of larger size fall again into the bulk of fluidized bed and the

particles of smaller size are hung in the air stream. And thus the segregation of particles due to the size difference occurs at the surface of fluidized bed.

On the other hand, Fukuda (24) fluidized the mixture of glass beads and alumina particles whose density are 2.5 and 4.0 $g/cm^3$ respectively and measured the vertical distribution of the fraction of alumina particles. It was found that both of these particles are completely mixed with each other in the bulk of the fluidized bed and that the fraction of alumina particles decreases above the surface of the fluidized bed. Kuramasu (25) also carried out a similar experiment with glass beads and nickel beads whose densities are 2.5 and 8.8 $g/cm^3$, respectively. Although the segregation of glass beads was observed at the surface of the fluidized bed, any significant segregation of particles was not observed in the bulk of the fluidized bed even with this large density difference except when the gas velocity was below twice that of the minimum fluidization. It can be said from these experimental results that segregation of particles occurs at the surface of the fluidized bed owing to the difference of particle size and to the difference of density, although the bulk of the fluidized bed is regarded as uniform.

It was mentioned in Figs. 4.11 and 4.12 which concerns the thermal decomposition of pyrite particles that the fraction decomposed remains almost unchanged in the bulk of the fluidized bed and it increases abruptly at the level of the overflow pipe. These results coincide with the fact mentioned above. In the thermal decomposition of limestone particles, it is shown in Fig. 5.6 that the segregation of particles was also observed at the level of the overflow pipe at lower feeding rates of limestone particles. However, when the feeding rate of limestone particles is increased, the mean fraction of decomposed limestone in the overflow approaches to the values in the bulk of fluidized bed. This was illustrated in Fig, 5.7, where it was revealed that any segregation of particles at the level of the overflow pipe could not be observed under these fluidizing conditions. Therefore, further inspections are made on the correlationship between the fluidizing conditions and the behavior of particles.

In the continuous process experiment of limestone particles, the flow rate of air, u, was fixed at 2.89 cm/sec which was measured at 20°C. The flow rate at the fluidized bed temperature, u*, can be calculated by,

$$u^* = u \times \frac{t_f + 273}{293} \qquad (5.31)$$

And results are illustrated in Table 5.3. The minimum fluidization velocity at the fluidized bed temperature was calculated by the following equation (18).

$$u_{mf} = \frac{(D_P \phi_P)^2}{150} \frac{\rho_P - \rho_g}{\mu} g \frac{\varepsilon_{mf}^3}{1 - \varepsilon_{mf}} \qquad (5.32)$$

In this calculation of $u_{mf}$, $\phi_p$ and $\varepsilon_{mf}$ were presumed at 0.63 (19) and 0.5 (20), respectively. $u_{mf}$ calculated by Eq. (5.32) was also listed in the same table. And the ratio of $u^*/u_{mf}$ is found to be 8.14 to 8.78.

Table 5.3 Flow rate of air

| Initial bed temperature (°C) | $u_{mf}$ (cm/sec) | $u^*$ (cm/sec) | $\frac{u^*}{u_{mf}}$ (-) |
|---|---|---|---|
| 825 | 1.35 | 10.83 | 8.14 |
| 850 | 1.31 | 11.08 | 8.46 |
| 875 | 1.29 | 11.32 | 8.78 |

Bakker and Heertjes (20) measured the vertical distribution of particle concentration across the surface of the fluidized bed. Their results are

illustrated in Fig. 5.8. In this figure, the void fraction, $\varepsilon$, instead of particle concentration, is used as the abscissa. It is seen in this figure that the particle concentration decreases abruptly across the surface of the fluidized bed at lower flow rates of air and, on the other hand, it decreases rather continuously when the flow rate of air is higher. In their work, glass beads of 175 to 200 $\mu$ diameter were used and the fluidized bed is regarded as uniform with respect to the density and the size of fluidized particles.

In the thermal decomposition of limestone particles, however, the density and the size of the particles vary along with the progress of thermal decomposition; the density becomes lower and the size is reduced when the limestone particles are being decomposed. And it is thought that the particle concentration profile in vertical direction in the thermal decomposition of limestone particles may be somewhat different from Fig. 5.8. However, Urabe et al. (19) fluidized the sand particles of wide size distribution of 20 to 1000 $\mu$ and found a similar particle concentration profile; particle concentration decreases rather abruptly across the surface of the fluidized bed at lower flow rates of gas and it decreases continuously at higher flow

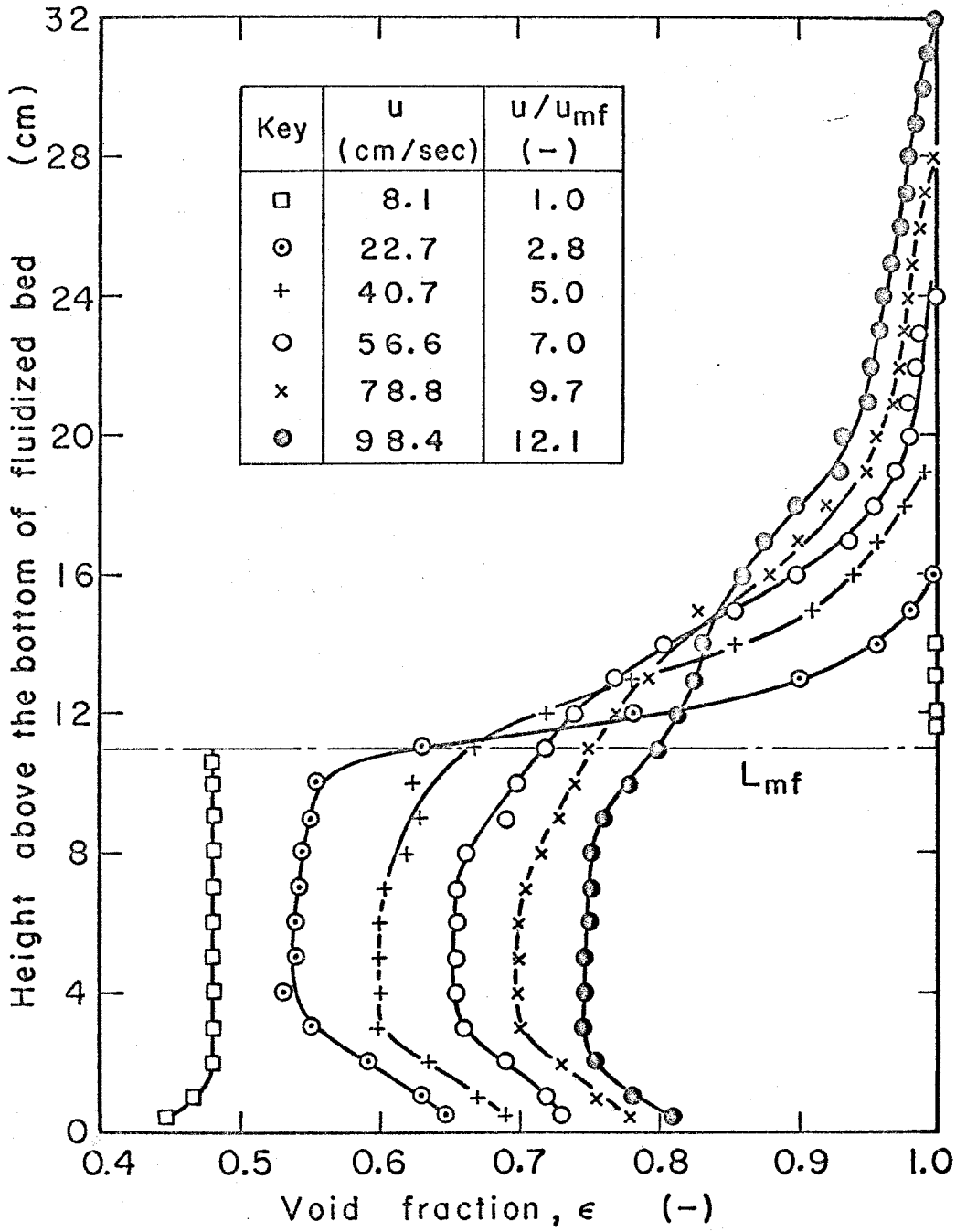


Fig.5.8 Void fraction vs. height above the bottom of fluidized bed (Bakker and Heertjes (20))

rate. It is reasonable to presume, therefore, that any significant difference may not be observed in the particle concentration profile in vertical direction in the upper part of the fluidized bed whether it is composed of uniform particles with respect to the density and the size or composed of the particles whose density and size are not uniform because of the thermal decomposition.

It is seen in Fig. 5.8 that the particle concentration decreases gradually across the surface of the fluidized bed at the flow rates of air of $u/u_{mf}$ = 7.0 to 9.7 which covers the flow rate of air adopted in this work. Consequently, it is thought that, in the steady state of fluidization, the height of the fluidized bed is elevated at higher feeding rates and that the particle concentration at the level of the overflow pipe becomes dense in order to discharge a large amount of particles which corresponds to the feeding rate. At this level of the overflow pipe, the particles are completely mixed with each other and the segregation of particles in the overflow was not observed as shown in Fig. 5.7. At lower feeding rates, on the other hand, the height of the fluidized bed sinks and the particle concentration at the level of the overflow pipe becomes dilute because of the lower overflow rate

and the segregation of decomposed limestone occurs owing to the difference in density and size at the level of the overflow pipe. And thus, the segregation of particles in the overflow at lower feeding rates shown in Fig. 5.6 can be understood. Schematic illustrations are demonstrated in Fig. 5.9 (a) and (b).

Concerning the thermal decomposition of pyrite particles described in Chapter 4, on the other hand, $u^*/u_{mf}$ was between 2.6 to 3.0 as shown in Table 4.4. It is seen from Fig. 5.8 that the particle concentration decreases rather abruptly across the surface of the fluidized bed at $u/u_{mf} = 2.8$. At this flow rate of nitrogen gas it is supposed that the particle concentration in the bulk of the fluidized bed is rather dense and that the surface of the fluidized bed is located just below the overflow pipe in order to discharge the fluidized particles. Because of the abrupt change of particle concentration across the bed surface, the variation of bed height caused by the change of feeding rate of pyrite particles is minor. This is demonstrated in Fig. 5.9 (c) schematically. The segregation of the decomposed pyrite occurs at this surface. And thus the segregation of particles at the level of of the overflow pipe which was observed at any feeding rate of pyrite particles can be understood. The

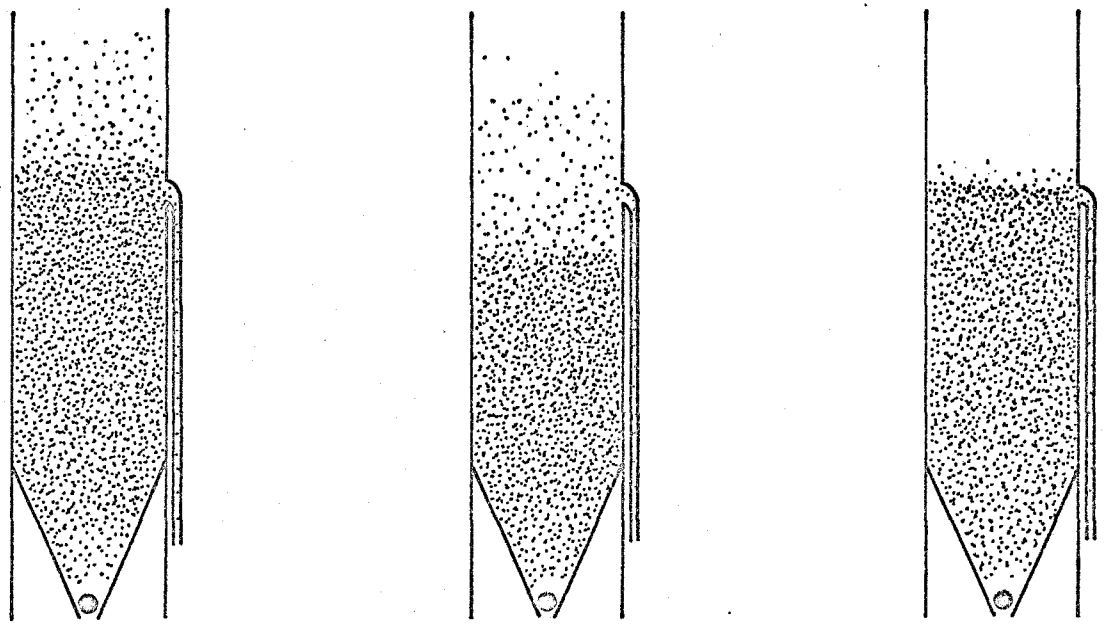

(a) higher feeding rate
higher $u^*/u_{mf}$

(b) lower feeding rate
higher $u^*/u_{mf}$

(c) lower $u^*/u_{mf}$

Fig. 5.9 Particle concentration at the upper part of fluidized bed and relationship between bed height and feeding rate

density difference between pyrite particles and their decomposed product was 2.0 $g/cm^3$ which is larger than the density difference of 0.7 $g/cm^3$ observed between limestone particles and their decomposed product. Though it is difficult to grasp quantitatively the effect of density difference on the segregation of particles at the surface of the fluidized bed, it can be mentioned that this greater difference in density may be another reason why the segregation of decomposed pyrite is always observed at the level of the overflow pipe as shown in Fig. 4.12.

It is seen in the same figure that the difference of fraction decomposed between the overflow and the bulk of the fluidized bed becomes clearer when the fraction of decomposed product is lower in the bulk of the fluidized bed. This is realized at higher feeding rates. It can be said, therefore, that the mean fraction of decomposed pyrite in the overflow deviates because of this segregation of decomposed pyrite from Eq. (4.19) whose assumption is the complete mixing of particles within the fluidized bed. It approaches to the straight lines of Eq. (4.22) which assumes the upward piston flow of particles in the fluidized bed. When the feeding rate of pyrite particles becomes lower, however, the deviation of the

mean fraction of decomposed pyrite in the overflow from Eq. (4.19) becomes minor as shown in Fig. 4.7. This is because the difference of the fraction decomposed between the overflow and the bulk of the fluidized bed is so trivial and insignificant.

Discussions on the behaviors of pyrite and limestone particles in the fluidized bed mentioned above can be summarized as follows.

1) In the bulk of the fluidized bed, the fluidized particles are completely mixed with each other.

2) At the surface of the fluidized bed where the particle concentration is fairly dilute, the segregation of particles occurs because of the difference in density and in size between feed mineral and its decomposed product.

3) In the thermal decomposition of pyrite particles where the flow rate of nitrogen gas was fixed at about 3 times larger than $u_{mf}$, the particle concentration decreases rather abruptly across the surface of the fluidized bed and the bed surface is always located just below the level of the overflow pipe. The segregation of decomposed pyrite occurs at this surface. At higher feeding rates of pyrite particles, the difference of the fraction decomposed between the bulk and the bed surface

becomes larger. Under these circumstances, the mean fraction of decomposed pyrite in the overflow deviates from the calculated value which assumes the complete mixing of particles and it approaches to the value calculated on the assumption of the upward piston flow of particles through the fluidized bed. At lower feeding rates of pyrite particles, on the other hand, this deviation becomes minor because the difference of the fraction decomposed between the bulk and the surface of the fluidized bed is trivial.

4) In the thermal decomposition of limestone particles, the flow rate of air was kept at about 8.5 times larger than $u_{mf}$. Since the change of particle concentration across the surface of the fluidized bed is rather continuous at this flow rate of air, the surface of the bed is elevated at higher feeding rates and the overflow pipe is located within the bulk of the fluidized bed where the particles are completely mixed. And thus the mean fraction of decomposed limestone in the overflow coincides with the value calculated by assuming complete mixing of particles in the bed. At lower feeding rates of limestone particles, however, the surface of the fluidized bed sinks and the segregation of particles

occurs at the level of the overflow pipe. And thus, the mean fraction of decomposed limestone in the overflow deviates from the calculated value which assumes complete mixing of particles in the fluidized bed.

As mentioned above, it may be an important feature of the continuous fluidized bed reactor that the mean fraction of decomposed product in the overflow is affected not only by the rate of thermal decomposition of mineral particles but also by the flow rate of fluidizing gas and by the difference in density and in size between the mineral particles and their decomposed products because the mean residence time of particles in the bed is affected by these factors even at a constant feeding rate of mineral particles.

## 5.5 Summary

The thermal decomposition rate of limestone particles of 60 to 100 mesh size was studied in a fluidized bed. The bed temperature was kept at 825°, 850° and 875°C. The decomposition was carried out in a batch process and in a continuous process.

From the batch process experiment, it was found

that the fraction decomposed increases linearly with the reaction time. This result satisties the linear rate equation derived in Chapter 4 which assumes that the overall reaction rate is determined by the rate of heat transfer from the reactor wall to the fluidized bed.

The overall heat transfer coefficient, $h_c$, was estimated from the rate constant. And the radiative heat transfer coefficient, $h_r$, was calculated by using the Stefan-Boltzmann's law. The film coefficient of heat transfer between the reactor wall and the fluidized bed, $h_w$, was obtained by subtracting $h_r$ from $h_c$. Any significant difference between $h_w$ thus estimated and that obtained in Chapter 3 was not found.

Thus, it was suggested that the overall thermal decomposition rate of limestone particles in a fluidized bed is determined by the rate of heat transfer from the reactor wall to the bed at the temperature of 825° 875°C. And these results seem to be somewhat different from those obtained by the previous workers. In the thermogravimetric analysis, for example, they measured the thermal decomposition rate of a small amount of limestone particles placed in a furnace at a temperature below 900°C and found that the overall reaction rate is determined by the rate of chemical

reaction occurring at the interface within particles. In order to clarify this superficial contradiction, the rate of heat transfer from the surroundings to the reaction interface within limestone particles was estimated. It was found from this calculation that a large amount of heat can easily be supplied to the interface when a small amount of limestone particles is placed in a large space within a furnace. In the fluidized bed, however, the rate of heat transfer from the reactor wall to the surface of fluidized particles is rather smaller and the resistance to heat transfer can not be neglected. And the overall decomposition rate of limestone particles in a fluidized bed is determined by the heat transfer rate at a temperature below 900°C.

On the continuous process, two rate equations of Eqs. (4.19) and (4.22) were examined which were derived in Chapter 4 on the assumption of complete mixing of particles and of upward piston flow of particles in the fluidized bed, respectively. The mean fraction of decomposed limestone in the overflow satisfies Eq. (4.19) at higher feeding rates. At lower feeding rates of limestone particles, on the other hand, the mean fraction of decomposed limestone deviates from Eq. (4.19) owing to the possible segregation of

decomposed limestone at the level of the overflow pipe and it approaches to Eq. (4.22). This correlationship between the feeding rate and the behavior of fluidized particles seems to be somewhat different from that observed in the thermal decomposition of pyrite particles described in Chapter 4.

In the thermal decomposition of limestone particles, the ratio of the flow rate of air to that of minimum fluidization is 8.14 to 8.78. At this flow rate of air, it is thought from the results obtained by Bakker and Heertjes (20) that the particle concentration decreases rather continuously across the surface of the fluidized bed. And the bed surface is located above the overflow pipe at hgiher feeding rates and thus the overflow pipe is situated within the bulk of the fluidized bed where the particles are completely mixed. It is thought, therefore, that the mean fraction of decomposed limestone in the overflow satisfies Eq. (4.19) which assumes complete mixing of particles in the fluidized bed. At lower feeding rates, on the other hand, the surface of the fluidized bed is located below the overflow pipe and the segregation of particles occurs in the overflow from the fluidized bed. This may be the reason why mean fraction of decomposed limestone in the overflow deviates from Eq. (4.19) and

it approaches to Eq. (4.22) of upward piston flow of particles at lower feeding rates.

In the thermal decomposition of pyrite particles, on the other hand, the ratio of the flow rate of nitrogen gas to the minimum fluidization velocity is 2.64 to 2.96. At this flow rate of gas, the particle concentration decreases abruptly across the surface of the fluidized bed. The surface of the fluidized bed is located just below the level of the overflow pipe and the segregation of decomposed pyrite occurs at this surface. And consequently, the deviation of the mean fraction of decomposed pyrite from Eq. (4.19) observed in the overflow is clear at higher feeding rates where the difference of the fraction of decomposed pyrite between the bulk and the surface of fluidized bed is larger. On the other hand, this deviation becomes minor when the feeding rate of pyrite particles is lower because the difference of the fraction of decomposed pyrite between the bulk and the surface of the bed is so trivial.

## Notation in Chapter 5

$h_c$ : overall heat transfer coefficient (kcal/m$^2$·hr·°C)

$h_r$ : radiative heat transfer coefficient ($kcal/m^2 \cdot hr \cdot {}^oC$)

$h_w$ : film coefficient of heat transfer ($kcal/m^2 \cdot hr \cdot {}^oC$)

$k_g$ : thermal conductivity of air ($kcal/m \cdot hr \cdot {}^oC$)

$q$ : heat transfer rate from reactor wall to fluidized bed (kcal/hr)

$q_r$ : rate of heat transfer by radiation from reactor wall to fluidized bed (kcal/hr)

$t_f$ : bed temperature (°C)

$t_w$ : temperature of reactor wall (°C)

$u$ : linear velocity of air (m/hr)

$u_{mf}$ : air velocity at minimum fluidization (m/hr)

$x$ : fraction decomposed (-)

$x_d$ : fraction decomposed at the final stage in batch process experiment (-)

$D_p$ : particle diameter (m)

$D_t$ : inner diameter of fluidization tube (m)

$F$ : feeding rate of limestone (kg/hr)

$F_c$ : heat transfer area ($m^2$)

$F_r$ : surface area through which heat is transferred by radiation ($m^2$)

$F_w$ : surface area through which heat is transferred by conduction ($m^2$)

$G$ : mass velocity of air ($kg/m^2 \cdot hr$)

$L_f$ : height of fluidized bed (m)

$Nu$ : Nusselt number (-)

| | | |
|---|---|---|
| Re | : Reynolds number | (-) |
| $T_f$ | : absolute temperature of fluidized bed | ($^oK$) |
| $T_w$ | : absolute temperature of reactor wall | ($^oK$) |
| X | : mean fraction of decomposed limestone in the overflow | (-) |
| $\varepsilon$ | : void fraction | (-) |
| $\varepsilon_{mf}$ | : void fraction at minimum fluidization | (-) |
| $\varepsilon_p$ | : emissibity of the decomposed layer of limestone particle | (-) |
| $\varepsilon_w$ | : emissibity of reactor wall | (-) |
| $\theta$ | : time | (hr) |
| $\mu$ | : viscosity of air | (kg/m·hr) |
| $\rho_g$ | : density of air | ($kg/m^3$) |
| $\rho_p$ | : density of limestone particles | ($kg/m^3$) |
| $\phi_p$ | : shape factor of limestone particles | (-) |

## Reference to Chapter 5


1) Furnas, C. C.: Ind. Eng. Chem., 1931, Vol. 23, No. 5, pp. 534-538

2) Britton, H. T. S., S. J. Gregg and G. W. Winsor: Trans. Faraday Soc., 1952, Vol. 48, pp. 63-69

3) Hashimoto, S.: Kogyo Kagaku Zasshi (Japanese), 1961, Vol. 64, No. 7, pp. 1166-1169

4) Ingraham, T. R. and P. Marier: Can. J. Chem. Eng., 1963, pp. 170-173

5) Hashimoto, S.: Kogyo Kagaku Zasshi (Japanese), 1961, Vol. 64, No. 7, pp. 1162-1166

6) Hyatt, E. P., I. B. Culter and M. E. Wadsworth: J. Am. Cer. Soc., 1958, Vol. 41, No. 1, pp. 70-74

7) Satterfield, C. N. and F. Feakes: A.I.Ch.E. Journal, 1959, Vol. 5, No. 1, pp. 115-122

8) Narsimhan, G.: Chem. Eng. Sci., 1961, Vol. 16, pp. 7-20

9) Sugiyama, Y., K. Nagasaka, H. Fukuhara and J. Miyazaki: Kagaku Kogaku (Japanese), 1961, Vol. 25, No. 4, pp. 265-273

10) Kunii, D.: "Ryudokaho" (Japanese), 1962, p. 80, Nikkan Kogyo Shinbun Co., Inc., Tokyo

11) Shirai, T.: "Ryudoso" (Japanese), 1958, p. 196, Kagaku Gijutsu Co., Inc., Kanazawa

12) Fujishige, H.: Report of the Resources Research Institute (Japan), 1965, No. 62, p. 88

13) Shiba, K.: "Butsuri Josu-hyo" (Japanese), 1949, p. 288, Iwanami Book Co., Inc., Tokyo

14) Mori, Y. and F. Yoshida: "Shoron Kagaku Kogaku" (Japanese), 1962, p. 652, Asakura Book Co., Inc., Tokyo

15) Perry, J. H.: "Chemical Engineers' Handbook",

3rd Ed., 1950, p. 461, McGraw-Hill Book Co., Inc., New York

16) Soc. Chem. Eng. (Japan): "Kagaku Kogaku Binran" (Japanese), 3rd Ed., 1968, p. 32, Maruzen Co., Inc., Tokyo

17) Weast, R. C., S. M. Selby and C. D. Hodgman: "Handbook of Chemistry and Physics", 45th Ed., 1964, p. B-242 and p. B-245, The Chemical Rubber Co., Inc., Ohio

18) Kunii, D. and O. Levenspiel: "Fluidization Engineering", 1969, p. 72, John Wiley and Sons, Inc., New York

19) Urabe, S., I. Hiraki, K. Yoshida and D. Kunii: Kagaku Kogaku (Japanese), 1965, Vol. 29, No. 11, pp. 863-867

20) Bakker, P. J. and P. M. Heertjes: Chem. Eng. Sci., 1960, Vol. 12, pp. 260-271

21) Mori, Y. and F. Yoshida: "Shoron Kagaku Kogaku" (Japanese), 1962, p. 672, Asakura Book Co., Inc., Tokyo

22) ibid., p. 577

23) Leva, M.: "Fluidization", 1959, p. 10, McGraw-Hill Book Co., Inc., New York

24) Fukuda, M.: Thesis for Master of Engineering, Kyoto University, 1968

25) Kuramasu, Y.: Graduation thesis, Kyoto University, 1969

# CHAPTER 6 SUMMARY AND CONCLUSION

It was intended in this work to study the rate of thermal decomposition of pyrite and limestone particles in a fluidized bed. When the fluidization tube is heated from the outside and the heat required for the thermal decomposition of these materials is supplied to the bed through the reactor wall, the heat transfer rate between the reactor wall and the fluidized particles plays an important role. Moreover, this rate of heat transfer is affected by the various fluidization characteristics. And prior to the thermal decomposition study of pyrite and limestone particles, the fluidization characteristics and the heat transfer rate of the fluidized bed were investigated.

In Chapter 2 of this paper, the mean of particle concentration in the fluidized bed, $\mu_c$, and the variance, $\sigma_c^2$, were measured by using a capacitance probe. In addition, the frequency, f, the vertical thickness, y, and the rise velocity, $u_b$, of bubbles in the fluidized bed were measured from the traces on the oscillograms of output signal of the probe. The peak and

valley heights of the traces on the oscillograms, $C_L$ and $C_U$, were also measured, which can be used as the measures representing the particle concentration in bubble and dense phases, respectively. These fluidization characteristics were interrelated with $\mu_c$ and $\sigma_c^2$.

In the bulk of the fluidized bed, $\mu_c$ remains at a constant value of $\bar{\mu}_{cm}$ and the latter decreases linearly with increasing excessive gas velocity above the minimum fluidization. On the other hand, $\sigma_c^2$ increases with the height above the bottom of the fluidized bed up to a considerably higher portion of the bed and it varies scarcely there. $\sigma_c^2$ was interrelated with y, f, $u_b$, $C_L$, and $C_U$ and Eq. (2.12) was derived. From statistical test on this regression equation, $\sigma_c^2$ was found to be a measure representing the nonuniformity in a fluidized bed in terms of particle concentration difference between bubble and dense phases. $\bar{\sigma}_{cm}^2$, mean of $\sigma_c^2$ in the upper portion of the fluidized bed, is mainly affected by the gas velocity and the bed height is another significant factor at higher gas velocities; it increases with the bed height at higher gas velocities.

The vertical thickness of bubbles increases with the height above the bottom of the fluidized bed at

higher gas velocities because of the coalescence of bubbles during the rise through the fluidized bed. The rise velocity of bubbles is determined mainly by the gas velocity. This is represented by Eq. (2.8).

The rate of heat transfer between the reactor wall and the fluidized bed was measured in Chapter 3 at the temperature of 500° to 800°C. Quartz and fused alumina particles were used as the fluidized materials.

The overall heat transfer coefficient, $h_c$, was measured by using Eq. (3.11) and the radiative heat transfer coefficient, $h_r$, was calculated with the Stefan-Boltzmann's law. The film coefficient of heat transfer, $h_w$, was obtained by subtracting $h_r$ from $h_c$. $h_w$ increases with gas velocity. The difference in the value of $h_w$ due to the kind of fluidized particles and to the bed temperature were scarcely found.

Measured $h_w$ were compared with those of the previous workers measured at lower temperatures where radiative heat transfer can be omitted. This comparison reveals that the film coefficient of heat transfer obtained in this work coincides fairly well with those obtained at lower temperatures. This is an interesting feature of the fluidized bed at higher temperature.

An attempt was made to correlate $h_w$ with the fluidization characteristics obtained in Chapter 2. From the inspection of the correlationship between them, it was revealed that $\bar{\sigma}_{cm}^2$ is not necessarily a useful measure of fluidization characteristics to represent the heat transfer coefficient and that $h_w$ increases with vertical thickness of bubbles ascending through the bed. Because both the vertical thickness and the rise velocity of bubbles increase with gas velocity, it was concluded that $h_w$ increases with gas velocity because of intensified particle circulation caused by the ascending bubbles. Finally, $h_w$ were correlated with the fluidizing conditions in the form of dimensionless terms, and Eq. (3.35) was derived.

In Chapters 4 and 5, the rate of thermal decomposition of pyrite and limestone particles in the fluidized bed were studied. Their particle size was 60 to 100 mesh and the bed temperature was chosen at 650° to 750°C for pyrite and at 825° to 875°C for limestone. The experimental works were composed of the batch process experiment and the continuous process experiment.

In the batch process, it was assumed that the overall reaction rate is determined by the rate of heat transfer from the reactor wall to the fluidized bed and that the resistance to heat transfer through the outer

decomposed shell within the fluidized particles can be omitted, and a zero order rate equation of Eq. (4.14) was derived. The thermal decomposition data of both pyrite and limestone particles were found to satisfy this rate equation. The film coefficient of heat transfer estimated from the rate constants of thermal decomposition coincides well with that obtained in Chapter 3. This means that the overall rate of thermal decomposition of pyrite and limestone particles in the fluidized bed is determined by the rate of heat transfer from the reactor wall to the fluidized bed. Thus, the heat transfer characteristics of fluidized bed plays an important role in the overall reaction rate. This is also of practical importance for the operation of fluidized bed.

It is of interest to note that the overall rate of thermal decomposition of limestone particles in a fluidized bed kept at 825° to 875°C was found in this work to be determined by the rate of heat transfer from the reactor wall to the fluidized bed. It was found by the previous workers, on the other hand, that the overall decomposition rate of limestone particles is determined by the interfacial reaction rate at a temperature below 900°C. They studied the rate of this reaction by using a small amount of limestone particles placed in a furnace where sufficient amount

of heat is easily supplied to the particles. In the fluidized bed, on the other hand, heat required for thermal decomposition of the particles is transferred from the reactor wall firstly to the particles in the vicinity of the reactor wall and then it is transferred again into the bulk of fluidized bed mainly by the circulating movement of the particles. And thus, only the particles in the vicinity of the reactor wall can be directly supplied with the heat from the reactor wall and the heat transfer rate per unit surface area of the particles becomes lower. This is the reason why the overall reaction rate is controlled even at these temperatures by the heat transfer rate into the fluidized bed.

For the continuous process, two rate equations of Eqs. (4.19) and (4.22) were derived on the assumption of the complete mixing and the upward piston flow of particles, respectively. In the thermal decomposition of pyrite particles, it was found that the mean fraction of decomposed pyrite in the overflow satisfies Eq. (4.22) at higher feeding rates and it approaches to Eq. (4.19) when the feeding rate of pyrite particles becomes lower. In the thermal decomposition of limestone particles, on the other hand, Eq. (4.19) was found to be satisfactory at higher feeding rates and

the mean fraction of decomposed limestone deviates from Eq. (4.19) and it approaches to Eq. (4.22) at lower feeding rates. And thus, the correlationship between the feeding rate and the behavior of particles which was observed in the thermal decomposition of pyrite seems to be somewhat different from that observed in the thermal decomposition of limestone.

In order to pursue further the possible segregation of particles in the fluidized bed, the vertical distribution of the fraction of decomposed product was measured. It was found from this measurement that the fraction of decomposed product remains almost unchanged in the bulk of fluidized bed and it increases abruptly at the surface of the fluidized bed because of the density difference between the feed particles and their decomposed product. Formation of finer particles caused by thermal decomposition may be another possible reason.

In the thermal decomposition experiment of limestone particles, the ratio of the flow rate of air to the minimum fluidization velocity was kept at 8.5. At this flow rate of air, the particle concentration decreases continuously across the surface of the fluidized bed. And at higher feeding rates of limestone particles, the height of the fluidized bed is elevated

and the overflow pipe is buried in the bulk of the fluidized bed where the particles are completely mixed with each other. This may be the reason why the mean fraction of decomposed limestone in the overflow satisfies Eq. (4.19). At lower feeding rates, on the other hand, the height of the fluidized bed sinks and the surface of the fluidized bed is located below the overflow pipe where the particle concentration is fairly dilute and the segregation was observed in the overflow. It can be understood from this inspection that the mean fraction of decomposed limestone in the overflow deviates from Eq. (4.19) at lower feeding rates and it approaches to Eq. (4.22).

In the thermal decomposition experiment of pyrite particles, on the other hand, the ratio of flow rate of nitrogen gas to the minimum fluidization velocity was kept at about 3. At this flow rate of nitrogen gas, the particle concentration decreases rather abruptly across the surface of the fluidized bed and the variation of fluidized bed height due to the feeding rate is minor. In this situation, Eq. (4.22) holds when the difference of the fraction of decomposed pyrite between the bulk and the upper part of the fluidized bed is large which is realized at higher feeding rates. On the other hand, Eq. (4.19) is valid when

this difference in the fraction of decomposed pyrite is minor which is observed at lower feeding rates. Thus, the segregation of the particles because of the differences in density and size between the feed particles and their decomposed products can occur at the surface of the fluidized bed, though the particles are completely mixed with each other in the bulk of the fluidized bed.

This behavior of the fluidized particles is indispensable to understand the characteristics of a continuous fluidized bed reactor because it has a significant effect on the overall reaction rate of the particles in the overflow. Moreover, the fluidizing conditions such as the flow rate of gas and the feeding rate of the mineral particles affect the behavior of the particles in the upper part of the fluidized bed and the roles of these fluidizing conditions also become very important.